SPIN-ORBIT TORQUES IN FERROMAGNETS AND ANTIFERROMAGNETS

A Dissertation

by

HUAWEI GAO

Submitted to the Office of Graduate and Professional Studies of
Texas A&M University
in partial fulfillment of the requirements for the degree of

DOCTOR OF PHILOSOPHY

Chair of Committee,	Alexander Finkelstein
Committee Members,	Jairo Sinova
	Glenn Agnolet
	Rusty Harris
Head of Department,	George R. Welch

August 2015

Major Subject: Physics

ABSTRACT

Spintronics is a sub-field of condensed matter physics which explores the physics of electrons involving both their charge and spin, with an emphasis on the active manipulation of the spin degree of freedom in solid state systems. In spin-based memory and storage devices, information (0 or 1) is stored based on the magnetization orientation in ferromagnets or layered magnetic structures. We study the utilization of spin-orbit torques in ferromagnets and antiferromagnets as an effective ways of magnetization switching in these nonvolatile memory devices. The method we use is linear response theory and numerical simulation. Our results show that the spin-orbit torques are effective approaches of manipulating magnetization in both ferromagnets and antiferromagnets, which can be used in the future memory device applications.

In ferromagnets, we start from a simple two dimensional electron gas ferromagnetic model with Rashba spin-orbit coupling to study the different components of spin-orbit torques and the parameter dependence. The results show the existence of these torques. Then, we study these torques in a realistic material, GaMnAs, with a complex band structure. We confirm that these torques have the same parameter dependence in GaMnAs and the simple two dimensional model. The complex band structure changes the magnitudes of the effective fields and shows more features in the results which unveils the competition between band structure and spin-orbit coupling.

In antiferromagnets, by studying the spin-orbit torques in the two dimensional antiferromagneic model and the realistic material Mn_2Au, we predict that a lateral electric current in antiferromagnets can induce non-equilibrium Neel-order fields, i.e.,

fields whose sign alternates between the spin sub lattices, which can trigger ultrafast spin-axis reorientation. Due to the two dimensional nature, the spin-orbit torques can have large magnitudes if we tune the Fermi energy to a certain level. We then extend the study to the three dimensional non-collinear antiferromagnet $IrMn_3$.

DEDICATION

To my family for their love and support.

ACKNOWLEDGEMENTS

I want to thank my advisor professor Jairo Sinova for his help and support. He helps me a lot with my study and research. He gives me flexible time to finish projects. He teaches me how to become a good researcher. He is a great advisor.

I want to thank all of my collaborators, Cirstian Cernov, Jakub, Zelezny, Hang Li, professor Tomas Jungwirth, etc. Without their help, I couldn't finish all the publications. Special thanks to Cristian Cernov for his beautiful Blender images.

I want to thank my wife. She quit her job to support my study. She encourages me to do better in my job. I couldn't say more thanks to her.

I want to thank my parents. No mater what I choose for my career, they will support me and encourage me. They are willing to live poor life in order to support my study. I owe them too much. They are the greatest parents.

I want to thank all of my friends. They make my life happy and colorful.

NOMENCLATURE

AC	Alternating Current
AFM	Antiferromagnets
BIA	Bulk Inversion Asymmetry
CIT	Current Induced Torques
DC	Direct Current
DMS	Diluted Magnetic Semiconductor
DOS	Denisty of States
FM	Ferromagnets
Γ	Spectrum Broadening
GMR	Giant Magnetoresistance
ISGE	Inverse Spin Galvanic Effect
LLG	Landau-Lifshitz-Gilbert Equation
LLGS	Landau-Lifshitz-Gilbert-Slonczewski Equation
MRAM	Magnetic Random Access Memory
SHE	Spin Hall Effect
SIA	Structural Inversion Asymmetry
SOC	Spin-Orbit Coupling
SOT	Spin-Orbit Torques
STT	Spin-Transfer Torques
2D	Two Dimensional
2DEG	Two Dimensional Electron Gas

TABLE OF CONTENTS

Page

LIST OF FIGURES

FIGURE Page

LIST OF TABLES

TABLE Page

1. INTRODUCTIONS TO CURRENT-INDUCED TORQUES

1.1 Introductions to spintronics

Spintronics is a sub-field of condensed matter physics which explores the physics of electrons involving both their charge and spin, with an emphasis on the active manipulation of the spin degree of freedom in solid state systems [1]. In our modern computers, devices using charge are mainly used for information processing, and devices using magnetism (spin) are used for information storage. The aim of spintronics is trying to understand the physics involving both the charge and the spin in order to manipulate one with the other. By doing this, we are able to build devices which combine data storage and data processing together.

Traditional electronics use the transport properties of charges. By controlling the charge transport, people are able to realize the control of current density, switching, heat generation, etc. The discovery of magnets dates back to thousands years ago. Today, they are widely used for data storage, for example magnetic tape, hard disk drives, credit, debit cards and so on. The microscopic mechanism of magnetism is given by quantum theory [2]. In quantum theory, other than the charge degree of freedom, the electron has another degree of freedom called the spin [3, 4]. Unlike the charge, the spin is a vector that corresponds to a magnetic moment. The Pauli principle forces the spins to align in the same direction in order to minimize the Coulomb interaction which gives rise to magnetic elements [2]. Exchange interactions between magnetic elements in materials result in the formation of ferromagnets and anti-ferromagnets.

In the 1980s, with the discovery of spin-dependent charge transport, in particular the discovery of giant magnetoresistance (GMR) [5, 6], spintronics emerged as an

important subfield of physics. It is growing rapidly these years with the advance of nanoscale device fabrication technology. GMR makes use of the different resistances between ferromagnetic layered structures with parallel or anti-parallel configurations. This discovery resulted in the revolution of our current hard disk technology [7]. It also made research on spin-based devices a hot topic.

In spin-based memory and storage devices, information (0 or 1) is stored based on the magnetization orientation in ferromagnets or layered structures [1, 7]. To write information, effective ways of manipulating the magnetization are needed. In early days, magnetization switching was achieved with the use of external magnetic fields. Recently, current-induced switching approaches are under intensive study in the field of nonvolatile magnetic memory devices, in order to improve device performance and efficiency [8, 9, 10, 11, 12, 13, 14, 15, 16, 17, 18, 19]. The aim of this research is to try to control the magnetization direction using electric current. To realize this, we need to understand how magnetization changes in the presence of external perturbation, i.e. magnetization dynamics.

1.2 Magnetization dynamics and spin-transfer torques

In ferromagnetic materials, the dynamics of magnetization $\vec{M}$ is described by the Landau-Lifshitz-Gilbert (LLG) equation [20, 21, 22].

$$\frac{\partial \vec{m}}{\partial t} = -\gamma \vec{m} \times \vec{H}_{eff} + \alpha \vec{m} \times \frac{\partial \vec{m}}{\partial t}, \tag{1.1}$$

where $\vec{m} = \vec{M}/|\vec{M}|$ is a unit vector along the magnetization direction, $\gamma = g\mu_B/\hbar$ is the gyromagnetic ratio and α is the Gilbert damping constant which causes the relaxation of magnetization to its equilibrium direction [22, 23, 24]. This equation gives the time evolution of the magnetization in the effective magnetic field, $\vec{H}_{eff}$, determined by the external magnetic field, exchange field, anisotropic field, etc. [22]

This first term in the right side of this equation leads to the precession of magnetization around the effective field and the second term is the damping term which forces the magnetization relax to this field. From this equation, we see that we are able to control the magnetization dynamics by changing the effective field using external magnetic field.

Are there any other ways of changing the LLG equation? If we analyze the units of both sides of this equation, we see that they have the units of torque. In 1996, Slonczewski and Berger [8, 9] proposed to use spin polarized current to manipulate the magnetization. The physical picture can be easily understood by using the angular momentum conservation [22]. When the direction of the spin polarization is non-collinear with the magnetization, the spins of carriers will trend to align with the magnetization due to exchange interactions. Reversely, the carrier spins will exert torques on the magnetization itself, because of angular momentum conservation, to ultimately switch the magnetization direction. These spin current-induced torques are called spin-transfer torques (STT) [8, 9, 12, 13].

The LLG equation with STT is called Landau-Lifshitz-Gilbert-Slonczewski (LLGS) equation, which is written as [22]

$$\frac{\partial \vec{m}}{\partial t} = -\gamma \vec{m} \times \vec{H}_{eff} + \alpha \vec{m} \times \frac{\partial \vec{m}}{\partial t} + \vec{\tau}, \tag{1.2}$$

where $\vec{\tau}$ denotes the spin-transfer torques. Later, people realize that two types of terms are allowed in STT in the asymmetric layered system based on symmetry arguments. One is called Slonczewski torque which has form

$$\vec{\tau}_s \propto \vec{m} \times (\vec{m} \times \vec{J}_s), \tag{1.3}$$

where $\vec{J}_s$ is the spin current. The other term is called a field-like torque which can be written as

$$\vec{\tau}_{s\beta} \propto \beta \vec{m} \times \vec{J}_s, \tag{1.4}$$

where β gives the relative strength with respect to the Slonczewski torque.

With the discovery of STT, current-induced magnetization manipulation is under intensive study recently. People are able to build new spin-based devices using STT, one of the examples is spin-transfer-torque magnetic random access memories (STT-MRAM) [22], which are ideal for integrating data storage and data processing in a single device. Information is stored in MRAM using layers of ferromagnets which are stable even without power supply. This makes the instant data accessing and processing possible when we turn on the computer. However, the disadvantage of STT-MRAM is the requirement of a polarized current and a large current density which causes heating problems. If we can find other ways of manipulating magnetization in which to overcome these issues, MRAM will be a promising future information technology. This is the reason we are going to study spin-orbit torques [27, 28, 29, 30, 31, 32, 33, 34].

1.3 Spin-orbit troques

Before introducing the details of spin-orbit torques, let's have a look at the LLG equation. As mentioned before, the effective field includes external magnetic field, dipole field, exchange interaction, anisotropic field, etc. Can we add some sort of effective fields by electric current, so that we can control the magnetization? The answer is yes. Inverse spin galvanic effect (ISGE) [25, 26] says that in electronic systems lacking inversion symmetry, electric current will result in non-equilibrium spin polarizations. If we consider this effect in ferromagnets, these non-equilibrium spin polarization will be exchange-coupled with magnetization and act as effective

fields [34]. The question is whether ISGE really exists in ferromagnetic materials.

Recent observations of in-plane current-induced magnetization switching at ferromagnet and normal-conductor interfaces [18, 19], suggests that we may use unpolarized current to realize magnetization manipulation. The explanation of these experiments is based on either spin Hall effect (SHE) [35, 36, 37, 38] plus STT across the surface [19, 39], or the spin-dependent scattering of carriers which gives rise to a relativistic anti-damping spin-orbit torque (SOT) [18, 27, 28, 33]. The SOT effect was initially observed in epilayers of (Ga,Mn)As diluted magnetic semiconductors with bulk inversion asymmetry in their strained zinc-blende crystal [40, 41]. This effect was soon widely confirmed in metallic bilayers with structural inversion symmetry breaking [42, 43, 44, 45, 46, 47, 48, 49, 50, 51]. Later experiments on bulk (Ga,Mn)As, which eliminates the surface effects, show similar effects demonstrating that SOT causes the unpolarized current inducing magnetization switching [34].

As discussed in the previous paragraphs, SOT is the inverse spin galvanic effect in magnets. To understand the physics of ISGE, spin-orbit coupling and symmetry must be considered. Spin-orbit coupling is the interaction between spin and momentum of electron which comes from the relativistic Dirac equation [3]. Usually, a simple physical picture using semiclassical electrodynamics can gives us some hint. In atoms, an electron moves around the nucleus. In the rest frame of this electron, the nucleus is moving around this electron. As we know, moving charges will generate magnetic field. So, the spin of the electron will interact with the magnetic field generated by the moving nucleus. This is the origin of spin-orbit coupling which can be generated to electrons moving in any potential $V(\vec{r})$. A more rigorous result can be obtained from the Dirac equation.

$$H_{soc} = \frac{\hbar}{4m_0^2c^2}(\vec{\sigma} \times \nabla V) \cdot \vec{p}, \tag{1.5}$$

where $\vec{\sigma}$ is the Pauli matrix vector. Equation (1.5) is the most general form of spin-orbit coupling. However, in solid state systems, the potential V is usually hard to determine. People use some symmetry arguments and phenomenological parameters to describe the spin-orbit coupling which can be compared with experimental observations. Due to the crystal symmetry of solid state materials, the form of spin-orbit couping can be simplified. The two most commonly used forms of spin-orbit coupling in solids are Dresselhaus [52] spin-orbit coupling and Rashba [53] spin-orbit coupling. The Dresselhaus spin-orbit coupling is from the bulk inversion asymmetry

$$H_D = \beta(k_x\sigma_x - k_y\sigma_y), \tag{1.6}$$

and the Rashba spin-orbit coupling is from the structural inversion asymmetry

$$H_R = \alpha(k_y\sigma_x - k_x\sigma_y), \tag{1.7}$$

where β, α are the corresponding coupling strengths.

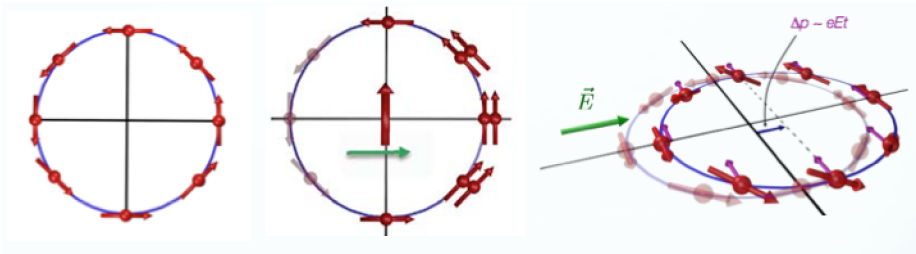

Figure 1.1: ISGE in 2D electron gas model with Rashba SOC.

After understanding the spin-orbit coupling in solids, we can give a physical picture of ISGE. As shown in Figure 1.1, the Rashba spin-orbit coupling aligns the spins

of carriers on the Fermi surface to a certain configuration. By adding an external electric field (current), the Fermi surface is shifted in k space. The spin expectation value will give rise to non-equilibrium spin polarizations which correspond to the intra band contributions [34, 54]. On the other hand, carrier spins will precess around the effective spin-orbit field, as shown in the right panel of figure 1.1, which correspond to the inter band contributions [34, 54].

In magnets, the non-equilibrium spin polarizations generated by ISGE will interact with the magnetic order which correspond to effective magnetic fields. As discussed, these effective magnetic fields correspond to torques in the LLG equation.

$$\delta\vec{H}_{eff} = -\frac{J_{sd}}{g\mu_B}\delta\vec{s}, \tag{1.8}$$

where $\delta\vec{s}$ is the non-equilibrium spin polarization, J_{sd} is the exchange constant between carrier spins and magnetization, g is the g-factor, and μ_B denotes Bohr magneton. This is exactly what we need in order to manipulate the magnetic order by current. Due to the spin-orbit coupling origin of these torque, they are called spin-orbit torques.

So far, we have only discussed the SOT in ferromagnets. The physical picture is very clear. However, the majority of magnetic materials are antiferromangets which are also widely used in spintronics. Do we have similar SOT effects in antiferromagnets? The answer is yes. In antiferromagnet, sub lattice magnetizations cancel with each other and the total magnetization is zero. It seems that SOT have no effects on the magnetic order. But the SOT are local effects meaning that we can project these torques onto sub lattices. With careful choice of crystal asymmetry or structural asymmetry, SOT can be used to manipulate the Neel order in antiferromagnets [55].

This report is organized as follows. Chapter 2 is the methods of our SOT simu-

lation where two approaches and their equivalence will be discussed. Chapter 3 to 6 contain the SOT studies in 2D Rashba model, GaMnAs ferromagnetic semiconductors and anti-ferromagnets. Chapter 7 is our conclusions.

2. SEMICLASSICAL APPROACH AND KUBO FORMULA

2.1 Introductions

In this chapter, we will discuss the simulation methods for the spin-orbit torques. As mentioned in the first chapter, we need to compute the non-equilibrium spin polarization $\delta\vec{s}$ when a unpolarized electric current is driven through the system. Current is related to the electric field across the system by the conductivity. For later convenience, we will use the electric field vector $\vec{E}$ as external perturbation. Linear response is assumed in our system. The Hamiltonian can be written as

$$H = H_0 + H_1, \tag{2.1}$$

where H_0 is the Hamiltonian of the system without perturbation and H_1 is the perturbation. Linear response theory says that the response of the system can be written as [56]

$$X(\vec{r}, t) = \int d\vec{r}' \int dt' \chi(\vec{r}, \vec{r}'; t - t') H_1(\vec{r}', t'), \tag{2.2}$$

where χ is called the response function, which we will calculate. For some cases, the response function can be integrated to give a proportional constant between response and perturbation. There are two main approaches, the semiclassical Boltzmann [57, 58] approach and Kubo formula [56, 57]. In the next sections, we'll discussion these two approaches and the links between them.

2.2 Semiclassical approach

In the semiclassical Boltzmann approach, the ground state of the system is described by an equilibrium distribution function f_0. In fermion system, f_0 is nothing

but Fermi-Dirac distribution function. Perturbation will change the equilibrium distribution function to some unknown distribution f. What we need to do is calculate this unknown distribution. In our case, the equilibrium spin expectation value is given by

$$\vec{s}_0 = \frac{1}{V}\sum_{\vec{k},a} \langle \vec{s} \rangle f_0, \tag{2.3}$$

where a denotes different bands, $\vec{s}$ is the spin operator vector which is $\vec{\sigma}/2$ for free electron, and

$$\langle \vec{s} \rangle = \left\langle \vec{k}, a \left| \vec{s} \right| \vec{k}, a \right\rangle \tag{2.4}$$

is the spin expectation value for quasiparticle. When we introduce the external electric field $\vec{E}$ as a perturbation, both the distribution function and the quasiparticle wave function will change [59]. It is natural to divide the resulting non-equilibrium spin expectation value into two parts. We call these two parts intra band and inter band. The reason will become clearer later. So we have

$$\delta\vec{s} = \delta\vec{s}^{intra} + \delta\vec{s}^{inter} = \frac{1}{V}\sum_{\vec{k},a} \langle \vec{s} \rangle \delta f + \frac{1}{V}\sum_{\vec{k},a} \langle \delta\vec{s} \rangle f_0, \tag{2.5}$$

where $\delta f = f - f_0$, and we have ignored the higher order term. The first term corresponds to the redistribution of electrons on the Fermi surface, and the second term corresponds to the modification of electronic wave functions cause by the external electric field. Next, we'll derive these two terms separately.

In the framework of relaxation time approximation, if we consider an electronic system in a uniform external electric field, we have

$$\frac{q\vec{E}}{\hbar}\frac{\partial f_{\vec{k},a}}{\partial \vec{k}} = -\frac{\delta f_{\vec{k},a}}{\tau}, \tag{2.6}$$

where τ is the relaxation time, and q is the charge of carrier. Here we write out f explicitly which depends on $(\vec{k}, a)$. Since we consider a steady current state and a uniform system, so

$$\begin{aligned} \frac{\partial f}{\partial t} &= 0 \\ \frac{\partial f}{\partial \vec{r}} &= 0. \end{aligned} \tag{2.7}$$

We have the relation

$$\frac{1}{\hbar}\frac{\partial f_{\vec{k},a}}{\partial \vec{k}} = \frac{1}{\hbar}\frac{\partial E_{\vec{k},a}}{\partial \vec{k}}\frac{\partial f_{\vec{k},a}}{\partial E_{\vec{k},a}} = \vec{v}_{\vec{k},a}\frac{\partial f_{\vec{k},a}}{\partial E_{\vec{k},a}}, \tag{2.8}$$

where $E_{\vec{k},a}$ is the band structure and $\vec{v}_{\vec{k},a}$ is the velocity operator. In the linear response and zero temperature limit, $f_{\vec{k},a}$ is very close to the Fermi-Dirac distribution. We have

$$\frac{\partial f_{\vec{k},a}}{\partial E_{\vec{k},a}} \approx -\delta(E_{\vec{k},a} - E_F). \tag{2.9}$$

So, we have

$$\delta f_{\vec{k},a} = \tau(q\vec{E}\cdot\vec{v})_a\delta(E_{\vec{k},a} - E_F). \tag{2.10}$$

Here, we have used the notation

$$(\ldots)_a = \langle\ldots\rangle_a = \left\langle \vec{k}, a \,|\ldots|\, \vec{k}, a \right\rangle. \tag{2.11}$$

for later convenience. Plugging into equation (2.5), we get the non-equilibrium spin polarization

$$\delta\vec{s}^{intra} = \frac{1}{V}\sum_{\vec{k},a}\frac{\hbar}{2\Gamma}(\vec{s})_a(q\vec{E}\cdot\vec{v})_a\delta(E_{\vec{k},a} - E_F), \tag{2.12}$$

where $\Gamma = \hbar/2\tau$ is the spectral broadening. This term is called the intra band contribution because the average of the spin and velocity operators is within the same band. Then, contributions from different bands are added together.

To derive the inter band contribution, we use quantum mechanics perturbation theory [4]. We start from the Hamiltonian of the system in an AC electric field

$$H = H_0 + \frac{i}{\omega}(q\vec{E} \cdot \vec{v})e^{-i\omega t} + \text{c.c}, \tag{2.13}$$

where ω is the frequency of the field. Later, we'll take the DC limit. The eigenvectors for the unperturbed Hamiltonian H_0 is denoted by $|\vec{k}, a>$, and

$$H_0|\vec{k}, a >= E_{\vec{k},a}|\vec{k}, a> . \tag{2.14}$$

The time dependent wave function for the unperturbed system can be written as

$$|\phi_0(t) >= \sum_{\vec{k},a} e^{-\frac{i}{\hbar}E_{\vec{k},a}t}|\vec{k}, a> . \tag{2.15}$$

Following the standard time dependent perturbation theory, the perturbed wave function can be written as

$$|\phi(t) >= \sum_{\vec{k},a} c_{\vec{k},a}(t)e^{-\frac{i}{\hbar}E_{\vec{k},a}t}|\vec{k}, a>, \tag{2.16}$$

where $c_{\vec{k},a}(t)$ are the time dependent expansion coefficients. Then, we expand these coefficients into a perturbative series

$$c_{\vec{k},a}(t) = c^{(0)}_{\vec{k},a}(t) + c^{(1)}_{\vec{k},a}(t) + \ldots \tag{2.17}$$

Within the linear response limit, we only need to calculate $c^{(1)}_{\vec{k},a}(t)$. On the other hand, the perturbed wave function can be written as

$$|\phi(t)>=\sum_{\vec{k},a} e^{-\frac{i}{\hbar}E_{\vec{k},a}t}(|\vec{k},a>+\delta|\vec{k},a>), \tag{2.18}$$

where $\delta|\vec{k},a>$ is the correction to the unperturbed wave function $|\vec{k},a>$ due to the perturbation. Using the standard expression for $c^{(1)}_{\vec{k},a}(t)$ and comparing with equation (2.18), we obtain

$$\delta|\vec{k},a>=\frac{e^{-i\omega t}}{-i\omega}\sum_{b}\frac{(q\vec{E}\cdot\vec{v})_{ba}}{E_{\vec{k},a}-E_{\vec{k},b}+\hbar\omega}|\vec{k},b>+\text{c.c}, \tag{2.19}$$

where similar notation is used here

$$(\ldots)_{ab}=\left\langle \vec{k},a\left|\ldots\right|\vec{k},b\right\rangle . \tag{2.20}$$

And the non-equilibrium spin polarization can be obtained as

$$\delta\vec{s}^{inter}=\frac{1}{V}\sum_{\vec{k},a}\left[\left\langle \vec{k},a\left|\vec{s}(\delta\right|\vec{k},b\right\rangle)+\text{c.c}\right]f_{\vec{k},a}. \tag{2.21}$$

Putting the expression of $\delta|\vec{k},a>$ into this formula, we get

$$\delta\vec{s}^{inter}=\frac{i}{\omega V}\sum_{\vec{k},a\neq b}\frac{(\vec{s})_{ab}(q\vec{E}\cdot\vec{v})_{ba}}{E_{\vec{k},a}-E_{\vec{k},b}+\hbar\omega+i\Gamma}\left(f_{\vec{k},a}-f_{\vec{k},b}\right), \tag{2.22}$$

where the spectral broadening Γ must be smaller than the average eigen energy difference.

In the next steps, we should take the DC limit by setting $\omega\to 0$. We will use a

trick here. If the limit

$$\lim_{\omega\to 0}\frac{f(\omega)}{\omega} \tag{2.23}$$

exists for some function of $f(\omega)$, $f(0)$ must be 0. So, we have

$$\lim_{\omega\to 0}\frac{f(\omega)}{\omega}=\lim_{\omega\to 0}\frac{f(\omega)-f(0)}{\omega}. \tag{2.24}$$

Using this relation in our expression of the inter band contribution, we obtain

$$\delta\vec{s}^{inter}=\frac{i}{\omega V}\sum_{\vec{k},a\neq b}\left[\frac{(\vec{s})_{ab}(q\vec{E}\cdot\vec{v})_{ba}}{E_{\vec{k},a}-E_{\vec{k},b}+\hbar\omega+i\Gamma}-\frac{(\vec{s})_{ab}(q\vec{E}\cdot\vec{v})_{ba}}{E_{\vec{k},a}-E_{\vec{k},b}+i\Gamma}\right]\left(f_{\vec{k},a}-f_{\vec{k},b}\right). \tag{2.25}$$

Then, after working out this limit and taking the real part only, we have two terms

$$\delta\vec{s}^{inter}=\delta\vec{s}^{(1)}+\delta\vec{s}^{(2)}, \tag{2.26}$$

with

$$\delta\vec{s}^{(1)}=-\frac{\hbar}{V}\sum_{\vec{k},a\neq b}2\mathrm{Re}[(\vec{s})_{ab}(q\vec{E}\cdot\vec{v})_{ba}]\frac{\Gamma(E_{\vec{k},a}-E_{\vec{k},b})}{[(E_{\vec{k},a}-E_{\vec{k},b})^2+\Gamma^2]^2}\left(f_{\vec{k},a}-f_{\vec{k},b}\right);$$
$$\delta\vec{s}^{(2)}=-\frac{\hbar}{V}\sum_{\vec{k},a\neq b}\mathrm{Im}[(\vec{s})_{ab}(q\vec{E}\cdot\vec{v})_{ba}]\frac{\Gamma^2-(E_{\vec{k},a}-E_{\vec{k},b})^2}{[(E_{\vec{k},a}-E_{\vec{k},b})^2+\Gamma^2]^2}\left(f_{\vec{k},a}-f_{\vec{k},b}\right).$$

These formulae are the final expressions for the inter band contributions. They are called inter band because the summation is over $a\neq b$, which involve transitions between different bands. One important point we should keep in mind is that these formulae only work for small Γ.

2.3 Kubo formula

In this part, we will give a brief derivation of the non-equilibrium spin polarization using Kubo linear response theory. This part is covered by most standard many body textbooks, the book by Mahan [56] for example. Just like the semiclassical derivation, we consider a AC field of form $\vec{E}e^{i(\vec{q}\cdot\vec{r}-\omega t)}$ first. Then, we take the limits $\vec{q}\to 0$ and $\omega\to 0$. The Hamiltonian for a particle in electric field can be written by vector potential $\vec{A}$ by making substitution $\vec{p}\to\vec{p}-q\vec{A}$. By expanding the Hamiltonian to the first order of $\vec{A}$ with Coulomb gauge $\nabla\cdot\vec{A}=0$, we obtain the standard expression

$$H = H_0 - \int \vec{j}(\vec{r})\cdot\vec{A}(\vec{r},t)\mathrm{d}\vec{r}, \tag{2.27}$$

where $\vec{j}(\vec{r})$ is the current density operator and the vector potential depends on position and time. In linear response, the spin response can be written as

$$\delta s_\alpha(\vec{r},t) = \int \mathrm{d}\vec{r'}\mathrm{d}t'\chi_{\alpha\beta}(\vec{r}-\vec{r'},t-t')A_\beta(\vec{r'},t'), \tag{2.28}$$

where $\chi_{\alpha\beta}(\vec{r}-\vec{r'},t-t')$ is the retarded response function, α,β are the coordinate indices x,y,z, and summation over repeated indices is assumed. This expression is in real space. After the Fourier transformation, we obtain the equation in momentum space

$$\delta s_\alpha(\vec{q},\omega) = -\frac{i}{\omega}\chi_{\alpha\beta}(\vec{q},\omega)E_\beta(\vec{q},\omega), \tag{2.29}$$

where $E_\beta(t)=-\partial A_\beta/\partial t$ is the external electric field component. We'll use imaginary time methods to calculate the response function. By replacing it by τ_B, The response function is

$$\chi_{\alpha\beta}(\vec{r}-\vec{r'},\tau_B-\tau_B') =< \mathcal{T}s_\alpha^I(\vec{r},\tau_B), j_\beta^I(\vec{r'},\tau_B') >, \tag{2.30}$$

where the thermal average of an operator is defined as $< O >= \mathrm{Tr}\{e^{-\beta_B H} O\}$, $\beta_B = 1/k_B T$ and $\mathcal{T}$ is the time ordering operator. The operators in equation (2.30) are in the interaction representation. Then, we calculate the Fourier transform

$$\chi_{\alpha\beta}(\vec{q}, i\omega_n) = \int \mathrm{d}\vec{r} \int_0^{\beta_B} \mathrm{d}\tau_B e^{-i(\vec{q}\cdot\vec{r} - \omega_n \tau_B)} \chi_{\alpha\beta}(\vec{r}, \tau_B), \tag{2.31}$$

where $\hbar\omega_n = 2n\pi/\beta_B$ with integer n, is the Matsubara frequency corresponding to the external field. So,

$$\chi_{\alpha\beta}(\vec{q}, i\omega_n) =< s_\alpha(\vec{q}, \omega_n) j_\beta(-\vec{q}, -\omega_n) > . \tag{2.32}$$

The spin polarization in momentum space can be written as

$$s_\alpha(\vec{q}, i\omega_n) = \frac{1}{\beta_B} \sum_{\vec{k},a,b,m} \psi^\dagger_{\vec{k},a}(i\omega_m)(s_\alpha)_{ab} \psi_{\vec{k}+\vec{q},b}(i\omega_m + i\omega_n), \tag{2.33}$$

where $\hbar\omega_m = (2m+1)\pi/\beta_B$ is the fermionic Matsubara frequency. $\psi_{\vec{k},a}(i\omega_m)$ is the Fourier transform of the imaginary time field operator that annihilates a carrier with momentum $\vec{k}$ and band index a. For the Fourier transform of the current, we have a similar expression

$$j_\alpha(\vec{q}, i\omega_n) = \frac{1}{\beta_B} \sum_{\vec{k},a,b,m} \psi^\dagger_{\vec{k},a}(i\omega_m)(j_\alpha)_{ab} \psi_{\vec{k}+\vec{q},b}(i\omega_m + i\omega_n) + j^{dia}_\alpha. \tag{2.34}$$

The term j^{dia}_α represents the diamagnetic contribution to the current which cancels the zero-frequency part of the response function. We define the matrix element of the current operator as

$$(j_\alpha)_{ab} = \frac{q}{\hbar} \left\langle \vec{k}, a \left| \frac{\partial H}{\partial k_\alpha} \right| \vec{k}, b \right\rangle . \tag{2.35}$$

The response function can be written as

$$\chi_{\alpha\beta}(\vec{q}, i\omega_n) = -\frac{\hbar}{\beta_B}\sum_m \sum_{\vec{k},a,b} (s_\alpha)_{ab}(j_\beta)_{ba} G_{\vec{k},a}(i\omega_m) G_{\vec{k}+\vec{q},b}(i\omega_n + i\omega_m). \tag{2.36}$$

The Green's functions in this formula are the propagators for the carriers in the disordered carrier system. We consider the Green's functions in the presence of disorder

$$G_{\vec{k},a}(i\omega_m) = \frac{1}{i\hbar\omega_m - (E_{\vec{k},a} - E_F) + \frac{i\hbar}{2\tau}\mathrm{sgn}(\omega_m)}. \tag{2.37}$$

Equation (2.36) has ignored the vertex corrections. We can calculate the response function by using the Matsubara sum. Let's consider the integration

$$\frac{1}{\beta_B}\sum_m F(i\omega_m) = \frac{1}{2\pi i}\int_{\mathcal{C}} \mathrm{d}z f(z) F(z). \tag{2.38}$$

where $f(z) = 1/(e^{-\beta_B z+1})$ is the Fermi function in the complex plane and the contour $\mathcal{C}$ is the sum of all the counter-clockwise contours around the poles and branch cuts of the function $F(z)$. The function $F(z)$ is

$$F(z) = -\sum_{\vec{k},a,b} (s_\alpha)_{ab}(j_\beta)_{ba} G_{\vec{k},a}(z) G_{\vec{k}+\vec{q},b}(z + i\omega_n). \tag{2.39}$$

We define the retarded and advanced Green's function in complex domain as

$$G^{R(A)}_{\vec{k},a}(z) = \frac{1}{z - (E_{\vec{k},a} - E_F) \pm \frac{i\hbar}{2\tau}}. \tag{2.40}$$

By working out the complex integral in the $\vec{q} \to 0$ limit and using analytical continuation $i\omega_n \to \omega + i0_+$, we obtain

$$\chi_{\alpha\beta}(\vec{q}=0,\omega) = \frac{i\omega\hbar}{2\pi} \sum_{\vec{k},a,b} \mathrm{Re}[(s_\alpha)_{ab}(j_\beta)_{ba}(G^A_{\vec{k},a}G^R_{\vec{k},b} - G^R_{\vec{k},a}G^R_{\vec{k},b})]. \tag{2.41}$$

Plugging into equation (2.29), we have

$$\delta s_\alpha(\vec{q}=0,\omega) = \frac{\hbar}{2\pi} \sum_{\vec{k},a,b} \mathrm{Re}[(s_\alpha)_{ab}(q\vec{v}\cdot\vec{E}(\vec{q}=0,\omega))_{ba}(G^A_{\vec{k},a}G^R_{\vec{k},b} - G^R_{\vec{k},a}G^R_{\vec{k},b})], \tag{2.42}$$

where we have used relation $\vec{j} = q\vec{v}$. In an almost uniform electric field, the spin response from $\vec{q} \neq 0$ is quite small, $\delta s_\alpha(\vec{q}=0) \gg \delta s_\alpha(\vec{q} \neq 0)$. We will ignore the non-uniform spin response. The real space spin polarization is $\delta s_\alpha(\vec{r}) \approx \delta s_\alpha(\vec{q}=0)/V$. So, by taking $\omega \to 0$ limit, finally we have the expression for the average spin polarization from Kubo linear response theory

$$\delta\vec{s} = \frac{\hbar}{2\pi V} \sum_{\vec{k},a,b} \mathrm{Re}[(\vec{s})_{ab}(q\vec{v}\cdot\vec{E})_{ba}(G^A_{\vec{k},a}G^R_{\vec{k},b} - G^R_{\vec{k},a}G^R_{\vec{k},b})], \tag{2.43}$$

where the Green's function in energy domain is

$$G^R_{\vec{k},a}(E)|_{E=E_F} \equiv G^R_{\vec{k},a} = \frac{1}{(E_F - E_{\vec{k},a} + i\Gamma)}, \tag{2.44}$$

with the property $G^A_{\vec{k},a} = \left(G^R_{\vec{k},a}\right)^*$, and $\Gamma = \hbar/2\tau$ is the spectral broadening. Equation (2.43) can be divided into two parts with summation $a = b$, and $a \neq b$, which correspond to intra band and inter band contributions respectively.

2.4 Equivalence between Semiclassical approach and Kubo

In the last two sections, we have derived the non-equilibrium spin polarization using two different approaches. The two sets of formulae look quite different from each other. In this part, we will show that these two sets of formulae are actually equivalent to each other within the small Γ limit (weak disorder) [54, 59]. But for large Γ, they are different, even a sign difference. So we will limit our study in the clean sample limit with $\Gamma \to 0$. When considering disorder samples, more realistic treatment of disorder is needed. However, our method can give a good approximation when Γ is not too large. We will start from the Kubo formula, and arrive at the semiclassical expressions.

First, we will consider the intra band term. From equation (2.43), we have

$$\delta\vec{s}^{intra} = \frac{\hbar}{2\pi V}\sum_{\vec{k},a}\mathrm{Re}[(\vec{s})_a(q\vec{v}\cdot\vec{E})_a(G^A_{\vec{k},a}G^R_{\vec{k},a} - G^R_{\vec{k},a}G^R_{\vec{k},a})]. \tag{2.45}$$

For simplicity, we label $x = E_F - E_{\vec{k},a}$, and $\mathcal{G} = \mathrm{Re}[G^A_{\vec{k},a}G^R_{\vec{k},a} - G^R_{\vec{k},a}G^R_{\vec{k},a}]$. So

$$\mathcal{G}(x) = \frac{2\Gamma^2}{(x^2+\Gamma^2)^2} \tag{2.46}$$

This expression can be further written as

$$\mathcal{G}(x) = 2\pi^2\delta^2_\Gamma(x), \tag{2.47}$$

with $\delta_\Gamma(x) = (\Gamma/\pi)/(x^2+\Gamma^2)$. When $\Gamma \to 0$, we have $\delta_\Gamma(x)$ approaches Dirac δ function with properties $\delta_\Gamma(x) \to 0$ for any $x \neq 0$ and $\int_{-\infty}^{\infty}\delta_\Gamma(x)\mathrm{d}x$ converges to 1. In the same manner, we can show that $2\pi\Gamma\delta^2_\Gamma(x)$ approaches the Dirac δ function.

So we have

$$\mathcal{G}(x) = \frac{\pi}{\Gamma}\delta(x). \tag{2.48}$$

Putting this relation into equation (2.45), we get

$$\delta\vec{s}^{intra} = \frac{\hbar}{2\Gamma V}\sum_{\vec{k},a}(\vec{s})_a(q\vec{v}\cdot\vec{E})_a\delta(E_F - E_{\vec{k},a}). \tag{2.49}$$

This expression is indeed the same as the one obtained from the semiclassical approach.

Then, we will study the inter band term. Instead of starting from equation (2.43), it is easier to start from the Kubo formula for spin response function

$$\delta s_\alpha(\vec{q}=0,\omega) = -\frac{i}{\omega}\chi_{\alpha\beta}(\omega)E_\beta(\omega) \tag{2.50}$$

where

$$\chi_{\alpha\beta}(\vec{q}, i\omega_n) = -\frac{\hbar}{\beta_B}\sum_m\sum_{\vec{k},a,b}(s_\alpha)_{ab}(j_\beta)_{ba}F(i\omega_m), \tag{2.51}$$

with the function

$$F(z) = \frac{1}{z - E_{\vec{k},a}}\frac{1}{z + i\hbar\omega_n - E_{\vec{k},b}}. \tag{2.52}$$

This function $F(z)$ has two poles, and we can perform the Matsubara sum with the aid of integration (2.38) to get

$$\frac{1}{\beta_B}\sum_m F(i\omega_m) = \frac{f_{\vec{k},a} - f_{\vec{k},b}}{E_{\vec{k},a} - E_{\vec{k},b} + i\hbar\omega_n}. \tag{2.53}$$

Putting this relation into the response function equation (2.51), and making the

analytical continuation $i\omega_n \to \omega + i0_+$, we obtain the average spin polarization

$$\delta\vec{s}^{inter} = \frac{i}{\omega V}\sum_{\vec{k},a\neq b}\frac{(\vec{s})_{ab}(q\vec{E}\cdot\vec{v})_{ba}}{E_{\vec{k},a}-E_{\vec{k},b}+\hbar\omega+i\Gamma}\left(f_{\vec{k},a}-f_{\vec{k},b}\right), \tag{2.54}$$

where we have made substitution $0_+ \to \Gamma$. This expression is exactly the same as the AC results obtained from semiclassical approach. By performing the same trick to take the DC limit, we get the same results as equation (2.26).

2.5 Summary

In this chapter, we have used two approaches to derive the non-equilibrium spin polarization for a system in the presence of electric field. The two approaches give equivalent results in the weak disorder limit. From semiclassical approach, we have

$$\delta\vec{s}^{intra} = \frac{1}{V}\sum_{\vec{k},a}\frac{\hbar}{2\Gamma}(\vec{s})_a(q\vec{E}\cdot\vec{v})_a\delta(E_{\vec{k},a}-E_F); \tag{2.55}$$

and

$$\delta\vec{s}^{inter} = \delta\vec{s}^{(1)} + \delta\vec{s}^{(2)}, \tag{2.56}$$

with

$$\delta\vec{s}^{(1)} = -\frac{\hbar}{V}\sum_{\vec{k},a\neq b}2\mathrm{Re}[(\vec{s})_{ab}(q\vec{E}\cdot\vec{v})_{ba}]\frac{\Gamma(E_{\vec{k},a}-E_{\vec{k},b})}{[(E_{\vec{k},a}-E_{\vec{k},b})^2+\Gamma^2]^2}\left(f_{\vec{k},a}-f_{\vec{k},b}\right);$$
$$\delta\vec{s}^{(2)} = -\frac{\hbar}{V}\sum_{\vec{k},a\neq b}\mathrm{Im}[(\vec{s})_{ab}(q\vec{E}\cdot\vec{v})_{ba}]\frac{\Gamma^2-(E_{\vec{k},a}-E_{\vec{k},b})^2}{[(E_{\vec{k},a}-E_{\vec{k},b})^2+\Gamma^2]^2}\left(f_{\vec{k},a}-f_{\vec{k},b}\right).$$

$\Gamma = \hbar/2\tau$ is the spectral broadening. From Kubo linear response theory, we get Kubo formula

$$\delta\vec{s} = \frac{\hbar}{2\pi V}\sum_{\vec{k},a,b}\mathrm{Re}[(\vec{s})_{ab}(q\vec{v}\cdot\vec{E})_{ba}(G^A_{\vec{k},a}G^R_{\vec{k},b} - G^R_{\vec{k},a}G^R_{\vec{k},b})], \tag{2.57}$$

where

$$G^R_{\vec{k},a}(E)|_{E=E_F} \equiv G^R_{\vec{k},a} = \frac{1}{(E_F - E_{\vec{k},a} + i\Gamma)}, \tag{2.58}$$

with the property $G^A_{\vec{k},a} = \left(G^R_{\vec{k},a}\right)^*$, and $\Gamma = \hbar/2\tau$ is the spectral broadening. Summations over $a = b$, and $a \neq b$ correspond to intra band and inter band contributions respectively.

The choice of these two sets of formulae is personal preference. In the numerical simulation, we do see some differences, especially when we use finite values of Γ. To be consistent, we usually compare the results from the two sets of formulae for a specific system. Then, we will decide which set of formula is more suitable for that system.

3. SPIN-ORBIT TORQUES IN 2D FERROMAGNETIC SYSTEM

3.1 Introductions

The simplest model to study the SOT effects is the two dimensional electron gas (2DEG) with ferromagnetism and spin-orbit coupling [54]. In this model, we assume the ferromagnetic order is embedded in the 2DEG. The electrons are described using parabolic approximation. The spins of electrons interact with the ferromagnetic order semi-classically. This model can be integrated analytically in certain limits which can be compared with numerical results. Also, from these analytical results, we are able to obtain the parameter dependence which will be used to test the results from a more realistic model, for example, the GaMnAs model in chapter 4. The rest of this chapter includes the Hamiltonian of this model, SOT in small and large exchange limits, and the comparison with numerical results.

3.2 2DEG ferromagnetic model

In parabolic approximation, the Hamiltonian of a 2DEG ferromagnet with Rashba spin-orbit coupling can be written as

$$H = \frac{\hbar^2}{2m^*}(k_x^2 + k_y^2) + \alpha(k_y\sigma_x - k_x\sigma_y) + J_{sd}\vec{M}\cdot\vec{\sigma} \tag{3.1}$$

where m^* is the effective mass, α is the Rashba spin-orbit coupling constant, σ are the Pauli matrices, and J_{sd} is the exchange interaction constant. For simplicity, we assume that the external electric field is in the x direction,

$$\vec{E} = E_x\hat{x} \tag{3.2}$$

and the magnetization is in plane.

$$\vec{M} = (\cos\theta_m, \sin\theta_m) \tag{3.3}$$

gives the direction of the magnetization, and θ_m is the angle between the magnetization and electric current (electric field). The setup of this system is shown in figure 3.1. The effective magnetic field is what we need to calculate next.

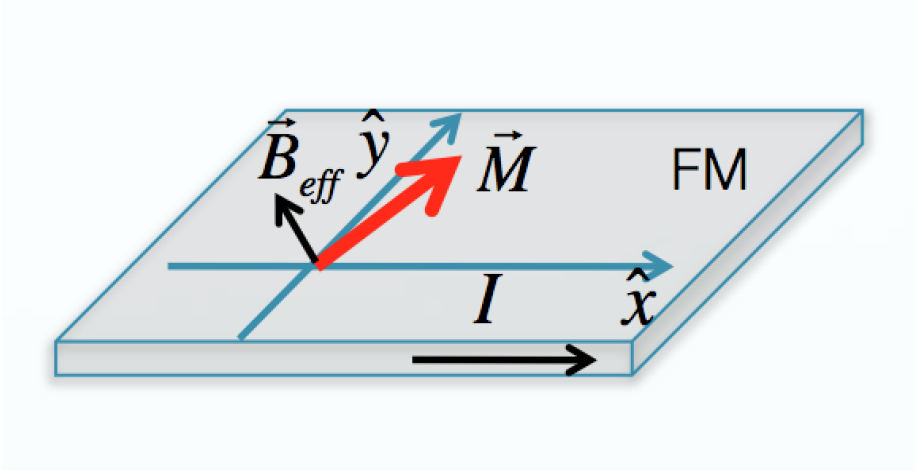

Figure 3.1: Simulation setup of SOT in 2DEG FM model with Rashba SOC.

3.3 SOT in 2DEG FM

This Hamiltonian mentioned in the previous part can be diagonalized directly. The eigenvalues as a function of $\vec{k}$ are given by:

$$E_{\vec{k}\pm} = \frac{\hbar^2}{2m^*}(k_x^2 + k_y^2) \pm \sqrt{(J_{sd}\cos\theta_m + \alpha k_y)^2 + (J_{sd}\sin\theta_m - \alpha k_x)^2}. \tag{3.4}$$

To simplify this expression, we denote:

$$\begin{aligned}\Delta_{\vec{k}} &= J_{sd}\cos\theta_m + \alpha k_y + i(-J_{sd}\sin\theta_m + \alpha k_x) \\ &\equiv |\Delta_{\vec{k}}|e^{i\phi_{\vec{k}}} \end{aligned} \tag{3.5}$$

where

$$\phi_{\vec{k}} = \tan^{-1}\left(\frac{-J_{sd}\sin\theta_m + \alpha k_x}{J_{sd}\cos\theta_m + \alpha k_y}\right). \tag{3.6}$$

So, the eigenvalues are

$$E_{\vec{k}\pm} = \frac{\hbar^2}{2m^*}(k_x^2 + k_y^2) \pm |\Delta_{\vec{k}}|, \tag{3.7}$$

and the eigenvectors are given by

$$\lambda_{\vec{k}\pm} = \frac{e^{i\vec{k}\cdot\vec{r}}}{\sqrt{2L^2}}\begin{pmatrix} \pm e^{i\phi_{\vec{k}}} \\ 1 \end{pmatrix}, \tag{3.8}$$

where the factor $e^{i\vec{k}\cdot\vec{r}}/\sqrt{L^2}$ is added by hand to represent the wave function for carriers. The velocity operators for this Hamiltonian are

$$\begin{aligned} v_x &= \frac{\hbar k_x}{m^*} - \frac{\alpha}{\hbar}\sigma_y \\ v_y &= \frac{\hbar k_y}{m^*} + \frac{\alpha}{\hbar}\sigma_x \end{aligned} \tag{3.9}$$

and the spin operator are Pauli matrices. So we have

$$\begin{aligned} \langle\lambda_{\vec{k}+}|v_x|\lambda_{\vec{k}+}\rangle &= \frac{\hbar k_x}{m^*} + \frac{\alpha}{\hbar}\sin\phi_{\vec{k}} \\ \langle\lambda_{\vec{k}-}|v_x|\lambda_{\vec{k}-}\rangle &= \frac{\hbar k_x}{m^*} - \frac{\alpha}{\hbar}\sin\phi_{\vec{k}} \\ \langle\lambda_{\vec{k}+}|v_x|\lambda_{\vec{k}-}\rangle &= \frac{i\alpha}{\hbar}\cos\phi_{\vec{k}} \end{aligned}$$

$$\langle\lambda_{\vec{k}+}|v_y|\lambda_{\vec{k}+}\rangle = \frac{\hbar k_y}{m^*} + \frac{\alpha}{\hbar}\cos\phi_{\vec{k}}$$
$$\langle\lambda_{\vec{k}-}|v_y|\lambda_{\vec{k}-}\rangle = \frac{\hbar k_y}{m^*} - \frac{\alpha}{\hbar}\cos\phi_{\vec{k}}$$
$$\langle\lambda_{\vec{k}+}|v_y|\lambda_{\vec{k}-}\rangle = -\frac{i\alpha}{\hbar}\sin\phi_{\vec{k}}$$
$$\langle\lambda_{\vec{k}\pm}|v_z|\lambda_{\vec{k}\pm}\rangle = 0 \tag{3.10}$$

and for the spin operator

$$\langle\lambda_{\vec{k}+}|\sigma_x|\lambda_{\vec{k}+}\rangle = \cos\phi_{\vec{k}}$$
$$\langle\lambda_{\vec{k}-}|\sigma_x|\lambda_{\vec{k}-}\rangle = -\cos\phi_{\vec{k}}$$
$$\langle\lambda_{\vec{k}+}|\sigma_x|\lambda_{\vec{k}-}\rangle = -i\sin\phi_{\vec{k}}$$
$$\langle\lambda_{\vec{k}+}|\sigma_y|\lambda_{\vec{k}+}\rangle = -\sin\phi_{\vec{k}}$$
$$\langle\lambda_{\vec{k}-}|\sigma_y|\lambda_{\vec{k}-}\rangle = \sin\phi_{\vec{k}}$$
$$\langle\lambda_{\vec{k}+}|\sigma_y|\lambda_{\vec{k}-}\rangle = -i\cos\phi_{\vec{k}}$$
$$\langle\lambda_{\vec{k}+}|\sigma_z|\lambda_{\vec{k}+}\rangle = 0$$
$$\langle\lambda_{\vec{k}-}|\sigma_z|\lambda_{\vec{k}-}\rangle = 0$$
$$\langle\lambda_{\vec{k}+}|\sigma_z|\lambda_{\vec{k}-}\rangle = -1. \tag{3.11}$$

Using above relations, we can calculate the current induced spin polarization using the Kubo formula.

3.3.1 Intra band term

The Kubo formula for the intra band contribution is given by

$$\delta\vec{s}^{intra} = \frac{1}{L^2}\sum_{\vec{k}a}\frac{\hbar}{2\Gamma}(\vec{s})_{\vec{k}a}(q\vec{E}\cdot\vec{v})_{\vec{k}a}\delta(E_{\vec{k}a} - E_F). \tag{3.12}$$

Here Γ is the spectrum broadening, and $\vec{s} = \vec{\sigma}$. We need to multiply a factor of $\frac{1}{2}$ in the final result if we consider spin $\frac{1}{2}$ electrons. In our two-band model with the electric field in the x direction, we have

$$\begin{aligned}
\langle\lambda_{\vec{k}+}|\sigma_x|\lambda_{\vec{k}+}\rangle\langle\lambda_{\vec{k}+}|v_x|\lambda_{\vec{k}+}\rangle &= \frac{\hbar k_x}{m^*}\cos\phi_{\vec{k}} + \frac{\alpha}{\hbar}\sin\phi_{\vec{k}}\cos\phi_{\vec{k}} \\
\langle\lambda_{\vec{k}+}|\sigma_y|\lambda_{\vec{k}+}\rangle\langle\lambda_{\vec{k}+}|v_x|\lambda_{\vec{k}+}\rangle &= -\frac{\hbar k_x}{m^*}\sin\phi_{\vec{k}} - \frac{\alpha}{\hbar}\sin^2\phi_{\vec{k}} \\
\langle\lambda_{\vec{k}+}|\sigma_z|\lambda_{\vec{k}+}\rangle\langle\lambda_{\vec{k}+}|v_x|\lambda_{\vec{k}+}\rangle &= 0
\end{aligned} \tag{3.13}$$

and

$$\begin{aligned}
\langle\lambda_{\vec{k}-}|\sigma_x|\lambda_{\vec{k}-}\rangle\langle\lambda_{\vec{k}-}|v_x|\lambda_{\vec{k}-}\rangle &= -\frac{\hbar k_x}{m^*}\cos\phi_{\vec{k}} + \frac{\alpha}{\hbar}\sin\phi_{\vec{k}}\cos\phi_{\vec{k}} \\
\langle\lambda_{\vec{k}-}|\sigma_y|\lambda_{\vec{k}-}\rangle\langle\lambda_{\vec{k}-}|v_x|\lambda_{\vec{k}-}\rangle &= \frac{\hbar k_x}{m^*}\sin\phi_{\vec{k}} - \frac{\alpha}{\hbar}\sin^2\phi_{\vec{k}} \\
\langle\lambda_{\vec{k}-}|\sigma_z|\lambda_{\vec{k}-}\rangle\langle\lambda_{\vec{k}-}|v_x|\lambda_{\vec{k}-}\rangle &= 0.
\end{aligned} \tag{3.14}$$

So the current induced spin polarization can be calculated as follows

$$\begin{aligned}
\delta s_x^{intra} &= \frac{1}{L^2}\frac{L^2}{(2\pi)^2}\frac{qE_x\hbar}{2\Gamma}\int d^2k\left[\left(\frac{\hbar k_x}{m^*}\cos\phi_{\vec{k}} + \frac{\alpha}{\hbar}\sin\phi_{\vec{k}}\cos\phi_{\vec{k}}\right)\delta(E_{\vec{k}+} - E_F)\right. \\
&\quad \left. + \left(-\frac{\hbar k_x}{m^*}\cos\phi_{\vec{k}} + \frac{\alpha}{\hbar}\sin\phi_{\vec{k}}\cos\phi_{\vec{k}}\right)\delta(E_{\vec{k}-} - E_F)\right] \\
&= \frac{qE_x\hbar}{8\pi^2\Gamma}\int kdkd\theta\left[\left(\frac{\hbar k}{m^*}\cos\theta\cos\phi_{\vec{k}} + \frac{\alpha}{\hbar}\sin\phi_{\vec{k}}\cos\phi_{\vec{k}}\right)\delta(E_{\vec{k}+} - E_F)\right. \\
&\quad \left. + \left(-\frac{\hbar k}{m^*}\cos\theta\cos\phi_{\vec{k}} + \frac{\alpha}{\hbar}\sin\phi_{\vec{k}}\cos\phi_{\vec{k}}\right)\delta(E_{\vec{k}-} - E_F)\right],
\end{aligned} \tag{3.15}$$

$$\delta s_y^{intra} = \frac{qE_x\hbar}{8\pi^2\Gamma}\int kdkd\theta\left[\left(-\frac{\hbar k}{m^*}\cos\theta\sin\phi_{\vec{k}} - \frac{\alpha}{\hbar}\sin^2\phi_{\vec{k}}\right)\delta(E_{\vec{k}+} - E_F)\right.$$

$$+\left(\frac{\hbar k}{m^*}\cos\theta\sin\phi_{\vec{k}}-\frac{\alpha}{\hbar}\sin^2\phi_{\vec{k}}\right)\delta(E_{\vec{k}-}-E_F)\Bigg], \tag{3.16}$$

and

$$\delta s_z^{intra}=0. \tag{3.17}$$

We have changed the integrations to polar coordinates for simplicity. These integrals are difficult to treat exactly. So we'll test different limits.

3.3.1.1 Small exchange limit

In the small exchange limit $J_{sd}\to 0$ or $J_{sd}/\alpha k_F \ll 1$, where k_F is the Fermi wave vector, we can expand expressions up to the first order of J_{sd}

$$\begin{aligned}\frac{1}{|\Delta_{\vec{k}}|} &= [J_{sd}^2+2J_{sd}\alpha(k_y\cos\theta_m-k_x\sin\theta_m)+\alpha^2(k_x^2+k_y^2)]^{-1/2}\\ &= \frac{1}{\alpha k}\left[1+\frac{2J_{sd}}{\alpha k}(\sin\theta\cos\theta_m-\cos\theta\sin\theta_m)+\frac{J_{sd}^2}{\alpha^2}\right]^{-1/2}\\ &\sim \frac{1}{\alpha k}-\frac{J_{sd}}{\alpha^2k^2}(\sin\theta\cos\theta_m-\cos\theta\sin\theta_m).\end{aligned} \tag{3.18}$$

and

$$\begin{aligned}\sin\phi_{\vec{k}} &\sim \cos\theta-\frac{J_{sd}}{\alpha k}(\sin\theta_m+\sin\theta\cos\theta\cos\theta_m-\cos^2\theta\sin\theta_m)\\ \cos\phi_{\vec{k}} &\sim \sin\theta+\frac{J_{sd}}{\alpha k}(\cos\theta_m-\sin^2\theta\cos\theta_m+\sin\theta\cos\theta\sin\theta_m).\end{aligned} \tag{3.19}$$

Then the integrand can be expressed as

$$\begin{aligned}&\frac{\hbar k}{m^*}\cos\theta\cos\phi_{\vec{k}}+\frac{\alpha}{\hbar}\sin\phi_{\vec{k}}\cos\phi_{\vec{k}}\\ \sim\ &\frac{\hbar k}{m^*}\sin\theta\cos\theta+\frac{\hbar J_{sd}}{m^*\alpha}(\cos\theta\cos\theta_m-\sin^2\theta\cos\theta\cos\theta_m+\sin\theta\cos^2\theta\sin\theta_m)\\ &-\frac{\alpha}{\hbar}\sin\theta\cos\theta+\frac{J_{sd}}{\hbar k}(\cos\theta\cos\theta_m-\sin^2\theta\cos\theta\cos\theta_m+\sin\theta\cos^2\theta\sin\theta_m)\end{aligned}$$

$$-\frac{J_{sd}}{\hbar k}(\sin\theta\sin\theta_m+\sin^2\theta\cos\theta\cos\theta_m-\sin\theta\cos^2\theta\sin\theta_m), \tag{3.20}$$

and

$$\begin{aligned} & -\frac{\hbar k}{m^*}\cos\theta\sin\phi_{\vec{k}}-\frac{\alpha}{\hbar}\sin^2\phi_{\vec{k}} \\ \sim\ & -\frac{\hbar k}{m^*}\cos^2\theta+\frac{\hbar J_{sd}}{m^*\alpha}(\cos\theta\sin\theta_m+\sin\theta\cos^2\theta\cos\theta_m-\cos^3\theta\sin\theta_m) \\ & -\frac{\alpha}{\hbar}\cos^2\theta+\frac{2J_{sd}}{\hbar k}(\cos\theta\sin\theta_m+\sin\theta\cos^2\theta\cos\theta_m-\cos^3\theta\sin\theta_m), \end{aligned} \tag{3.21}$$

where we have only kept terms up to the first order of J_{sd}. The Fermi surface (lines in 2D) is given by equation

$$\frac{\hbar^2k^2}{2m^*}\pm\sqrt{(J_{sd}\cos\theta_m+\alpha k_y)^2+(J_{sd}\sin\theta_m-\alpha k_x)^2}=E_F \tag{3.22}$$

In the small exchange limit, we have

$$\frac{\hbar^2k^2}{2m^*}\pm\alpha k\pm J_{sd}(\sin\theta\cos\theta_m-\cos\theta\sin\theta_m)=E_F \tag{3.23}$$

For simplicity, we denote

$$\Theta=\sin\theta\cos\theta_m-\cos\theta\sin\theta_m. \tag{3.24}$$

as the angle dependence of the Fermi surface. Then

$$\frac{\hbar^2k^2}{2m^*}\pm\alpha k\pm J_{sd}\Theta=E_F. \tag{3.25}$$

The solutions give the Fermi surface as a function of θ. Here we assume both bands are occupied. So we have only one acceptable solution for each band

$$k_{\pm} = \mp\frac{m^*\alpha}{\hbar^2} + \sqrt{\frac{m^{*2}\alpha^2}{\hbar^4} + \frac{2m^*}{\hbar^2}(E_F \mp J_{sd}\Theta)}. \tag{3.26}$$

Here $k_{\pm}$ correspond to the Fermi surface for the upper and lower bands respectively. Then, we'll do the integration. One thing we'll keep in mind is that we only keep terms up to the first order of the small parameter and the integration of some combinations of $\sin\theta$ and $\cos\theta$ from 0 to 2π are zero. First we have

$$\int kdkd\theta\frac{\hbar k}{m^*}[\delta(E_{\vec{k}+} - E_F) - \delta(E_{\vec{k}-} - E_F)]\sin\theta\cos\theta \sim 0 \tag{3.27}$$

because the k integration will give the J_{sd} independent term and first order of $J_{sd}\Theta$ term, and the later θ integrations will both be zero. We can do the same arguments to the other terms in the δs_x^{intra} integration. All of these terms are zero. So we have

$$\delta s_x^{intra} \sim 0 \tag{3.28}$$

And for the δs_y^{intra} integration, we have non-zero terms

$$\begin{aligned} & -\int kdkd\theta\frac{\hbar k}{m^*}\cos^2\theta[\delta(E_{\vec{k}+} - E_F) - \delta(E_{\vec{k}-} - E_F)] \\ = \; & -\frac{\hbar}{m^*}\int dkd\theta\cos^2\theta[k^2\delta(E_{\vec{k}+} - E_F) - k^2\delta(E_{\vec{k}-} - E_F)], \end{aligned} \tag{3.29}$$

$$\begin{aligned} & -\int kdkd\theta\frac{\alpha}{\hbar}\cos^2\theta[\delta(E_{\vec{k}+} - E_F) + \delta(E_{\vec{k}-} - E_F)] \\ = \; & -\frac{\alpha}{\hbar}\int dkd\theta\cos^2\theta[k\delta(E_{\vec{k}+} - E_F) + k\delta(E_{\vec{k}-} - E_F)], \end{aligned} \tag{3.30}$$

and all other terms are zero. So

$$\begin{aligned}
\delta s_y^{intra} &\sim \frac{qE_x\hbar}{8\pi^2\Gamma}\int d\theta\cos^2\theta\int dk\left[\left(-\frac{\hbar k^2}{m^*}-\frac{\alpha k}{\hbar}\right)\delta(E_{\vec{k}+}-E_F)\right. \\
&\quad \left.+\left(\frac{\hbar k^2}{m^*}-\frac{\alpha k}{\hbar}\right)\delta(E_{\vec{k}-}-E_F)\right] \\
&\sim \frac{qE_x\hbar}{8\pi^2\Gamma}\int d\theta\cos^2\theta\left[\left(-\frac{\hbar k_+^2}{m^*}-\frac{\alpha k_+}{\hbar}\right)\frac{1}{\left|\frac{\hbar^2 k_+}{m^*}+\alpha\right|}\right. \\
&\quad \left.+\left(\frac{\hbar k_-^2}{m^*}-\frac{\alpha k_-}{\hbar}\right)\frac{1}{\left|\frac{\hbar^2 k_-}{m^*}-\alpha\right|}\right] \\
&\sim \frac{qE_x\hbar}{8\pi^2\Gamma}\int d\theta\cos^2\theta\frac{1}{\hbar}(k_- - k_+) \\
&= \frac{qE_x\alpha m^*}{4\pi\hbar^2\Gamma}
\end{aligned} \tag{3.31}$$

where we have used the relation

$$\delta(f(x)) = \sum_{x_0}\frac{\delta(x-x_0)}{|f'(x_0)|}. \tag{3.32}$$

The final results in these limits are

$$\delta\vec{s}^{intra} = 0\hat{x} + \hat{y}\frac{qE_x\alpha m^*}{4\pi\hbar^2\Gamma} + 0\hat{z}. \tag{3.33}$$

These results indicate that in the small exchange limit, the non-equilibrium spin polarization is independent of the angle θ_m, and is inversely proportional to Γ. We can actually numerically integrate the polarization. The numerical results match with analytical result very well. As show in figure 3.2, intra band SOT in the small exchange limit is indeed inversely proportional to Γ.

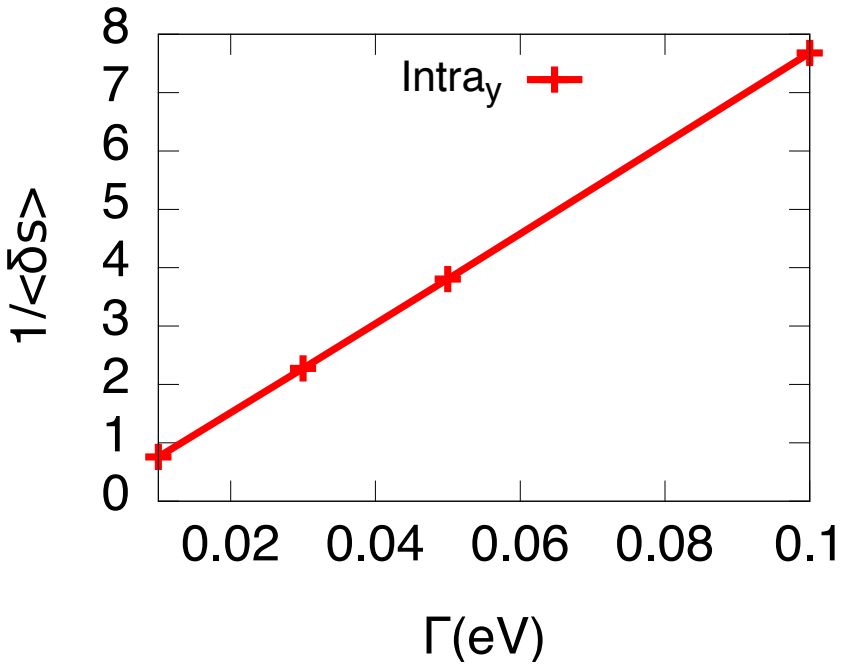

Figure 3.2: Intra band SOT as a function of Γ for small exchange interaction.

3.3.1.2 Large exchange limit

On the other hand, in the large J_{sd} limit, $J_{sd} \gg \alpha k_F, J_{sd} \gg \Gamma$, keeping up to the first order of α/J_{sd}, we have

$$\begin{aligned}
\frac{1}{|\Delta_{\vec{k}}|} &= [J_{sd}^2 + 2J_{sd}\alpha(k_y \cos\theta_m - k_x \sin\theta_m) + \alpha^2(k_x^2 + k_y^2)]^{-1/2} \\
&= \frac{1}{J_{sd}}\left[1 + \frac{2\alpha k}{J_{sd}}(\sin\theta\cos\theta_m - \cos\theta\sin\theta_m) + \frac{\alpha^2}{J_{sd}^2}\right]^{-1/2} \\
&\sim \frac{1}{J_{sd}} - \frac{\alpha k}{J_{sd}^2}(\sin\theta\cos\theta_m - \cos\theta\sin\theta_m). \qquad (3.34)
\end{aligned}$$

then

$$\sin\phi_{\vec{k}} \sim -\sin\theta_m + \frac{\alpha k}{J_{sd}}(\cos\theta + \sin\theta\sin\theta_m\cos\theta_m - \cos\theta\sin^2\theta_m)$$
$$\cos\phi_{\vec{k}} \sim \cos\theta_m + \frac{\alpha k}{J_{sd}}(\sin\theta - \sin\theta\cos^2\theta_m + \cos\theta\sin\theta_m\cos\theta_m). \quad (3.35)$$

So, in this limit, the integrand can be written as

$$\begin{aligned} & \frac{\hbar k}{m^*}\cos\theta\cos\phi_{\vec{k}} + \frac{\alpha}{\hbar}\sin\phi_{\vec{k}}\cos\phi_{\vec{k}} \\ \sim\ & \frac{\hbar k}{m^*}\cos\theta\cos\theta_m + \frac{\alpha\hbar k^2}{m^* J_{sd}}(\sin\theta\cos\theta - \sin\theta\cos\theta\cos^2\theta_m + \cos^2\theta\sin\theta_m\cos\theta_m) \\ & -\frac{\alpha}{\hbar}\sin\theta_m\cos\theta_m \end{aligned} \quad (3.36)$$

and

$$\begin{aligned} & -\frac{\hbar k}{m^*}\cos\theta\sin\phi_{\vec{k}} - \frac{\alpha}{\hbar}\sin^2\phi_{\vec{k}} \\ \sim\ & \frac{\hbar k}{m^*}\cos\theta\sin\theta_m - \frac{\alpha\hbar k^2}{m^* J_{sd}}(\cos^2\theta + \sin\theta\cos\theta\sin\theta_m\cos\theta_m - \cos^2\theta\sin^2\theta_m) \\ & -\frac{\alpha}{\hbar}\sin^2\theta_m \end{aligned} \quad (3.37)$$

where we have only kept terms up to first order of α/J_{sd}. Then we'll do the integration term by term. We'll do the k integration first. The Fermi surface (lines in 2D) is given by equation

$$\frac{\hbar^2 k^2}{2m^*} \pm \sqrt{(J_{sd}\cos\theta_m + \alpha k_y)^2 + (J_{sd}\sin\theta_m - \alpha k_x)^2} = E_F \quad (3.38)$$

In the large exchange limit, we have

$$\frac{\hbar^2 k^2}{2m^*} \pm J_{sd} \pm \alpha k(\sin\theta\cos\theta_m - \cos\theta\sin\theta_m) = E_F \quad (3.39)$$

Again, we denote

$$\Theta = \sin\theta\cos\theta_m - \cos\theta\sin\theta_m. \tag{3.40}$$

as the angular dependence of the Fermi surface. Then

$$\frac{\hbar^2 k^2}{2m^*} \pm J_{sd} \pm \alpha k\Theta = E_F. \tag{3.41}$$

The solutions give the Fermi surface as a function of θ. Here we assume both bands are occupied.

$$k_\pm = \mp\frac{m^*\alpha\Theta}{\hbar^2} + \sqrt{\frac{m^{*2}\alpha^2\Theta^2}{\hbar^4} + \frac{2m^*}{\hbar^2}(E_F \mp J_{sd})}. \tag{3.42}$$

We can ignore the first term in the square root.

$$k_\pm = \mp\frac{m^*\alpha\Theta}{\hbar^2} + \sqrt{\frac{2m^*}{\hbar^2}(E_F \mp J_{sd})}. \tag{3.43}$$

Here $k_\pm$ correspond to the Fermi surface for the upper and lower bands respectively. Two useful relations can be obtained

$$\begin{aligned} k_+k_- \sim \quad & \sqrt{\frac{2m^*}{\hbar^2}(E_F + J_{sd})}\sqrt{\frac{2m^*}{\hbar^2}(E_F - J_{sd})} \\ & + \frac{m^*\alpha\Theta}{\hbar^2}\left(\sqrt{\frac{2m^*}{\hbar^2}(E_F - J_{sd})} - \sqrt{\frac{2m^*}{\hbar^2}(E_F + J_{sd})}\right), \\ k_- - k_+ \sim \quad & \frac{2m^*\alpha\Theta}{\hbar^2} + \left(\sqrt{\frac{2m^*}{\hbar^2}(E_F + J_{sd})} - \sqrt{\frac{2m^*}{\hbar^2}(E_F - J_{sd})}\right). \end{aligned} \tag{3.44}$$

Then we write

$$\delta s_x^{intra} = \frac{qE_x\hbar}{8\pi^2\Gamma}(A_1 + A_2 + A_3) \tag{3.45}$$

The first term has form

$$A_1 = \int k dk d\theta \frac{\hbar k}{m^*} \cos\theta \cos\theta_m [\delta(E_{\vec{k}+} - E_F) - \delta(E_{\vec{k}-} - E_F)]. \tag{3.46}$$

By integrating over k, we only keep terms with first order of α, because the α independent term will be zero when integrating over θ later.

$$\begin{aligned}
& \int dk \left(k^2 \delta(E_{\vec{k}+} - E_F) - k^2 \delta(E_{\vec{k}-} - E_F) \right) \\
\sim & \frac{k_+^2}{\left| \frac{\hbar^2 k_+}{m^*} + \alpha\Theta \right|} - \frac{k_-^2}{\left| \frac{\hbar^2 k_-}{m^*} - \alpha\Theta \right|} \\
\sim & \frac{m^* \hbar^2 k_+ k_- (k_+ - k_-) - m^{*2} \alpha\Theta (k_+^2 + k_-^2)}{\hbar^4 k_+ k_- + m^* \hbar^2 \alpha\Theta (k_- - k_+)} \\
\sim & \frac{-4m^{*2}\alpha\Theta \left(\sqrt{\frac{2m^*}{\hbar^2}(E_F + J_{sd})} \sqrt{\frac{2m^*}{\hbar^2}(E_F - J_{sd})} \right)}{\hbar^4 \left(\sqrt{\frac{2m^*}{\hbar^2}(E_F + J_{sd})} \sqrt{\frac{2m^*}{\hbar^2}(E_F - J_{sd})} \right)} \\
\sim & -\frac{4m^{*2}\alpha\Theta}{\hbar^4}
\end{aligned} \tag{3.47}$$

So,

$$\begin{aligned}
A_1 &= -\int d\theta \frac{4m^*\alpha\Theta}{\hbar^3} \cos\theta \cos\theta_m \\
&= -\frac{4m^*\alpha}{\hbar^3} \cos\theta_m \int d\theta \cos\theta (\sin\theta \cos\theta_m - \cos\theta \sin\theta_m) \\
&= \frac{4m^*\pi\alpha}{\hbar^3} \sin\theta_m \cos\theta_m.
\end{aligned} \tag{3.48}$$

The second term has form

$$\begin{aligned}
A_2 = & \int k dk d\theta \frac{\alpha\hbar k^2}{m^* J_{sd}} (\sin\theta\cos\theta - \sin\theta\cos\theta\cos^2\theta_m + \cos^2\theta \sin\theta_m \cos\theta_m) \times \\
& [\delta(E_{\vec{k}+} - E_F) - \delta(E_{\vec{k}-} - E_F)].
\end{aligned} \tag{3.49}$$

By integrating over k, we only keep the α independent term.

$$\begin{aligned}
& \int dk \left(k^3\delta(E_{\vec{k}+}-E_F)-k^3\delta(E_{\vec{k}-}-E_F)\right) \\
\sim & \frac{k_+^3}{\left|\frac{\hbar^2 k_+}{m^*}+\alpha\Theta\right|}-\frac{k_-^3}{\left|\frac{\hbar^2 k_-}{m^*}-\alpha\Theta\right|} \\
\sim & \frac{m^*\hbar^2 k_+ k_-(k_+^2-k_-^2)}{\hbar^4 k_+ k_-} \\
\sim & -\frac{4m^{*2}J_{sd}}{\hbar^4}
\end{aligned} \tag{3.50}$$

So,

$$\begin{aligned}
A_2 \sim & -\frac{4m^{*2}J_{sd}}{\hbar^4}\int d\theta \frac{\alpha\hbar}{m^*J_{sd}}(\sin\theta\cos\theta-\sin\theta\cos\theta\cos^2\theta_m+\cos^2\theta\sin\theta_m\cos\theta_m) \\
\sim & -\frac{4m^*\alpha}{\hbar^3}\int d\theta(\sin\theta\cos\theta-\sin\theta\cos\theta\cos^2\theta_m+\cos^2\theta\sin\theta_m\cos\theta_m) \\
\sim & -\frac{4m^*\pi\alpha}{\hbar^3}\sin\theta_m\cos\theta_m.
\end{aligned} \tag{3.51}$$

And the third term is

$$A_3=-\int kdkd\theta\frac{\alpha}{\hbar}\sin\theta_m\cos\theta_m[\delta(E_{\vec{k}+}-E_F)+\delta(E_{\vec{k}-}-E_F)] \tag{3.52}$$

Again, we only keep the α independent term when integrating over k

$$\begin{aligned}
& \int dk \left(k\delta(E_{\vec{k}+}-E_F)+k\delta(E_{\vec{k}-}-E_F)\right) \\
\sim & \frac{k_+}{\left|\frac{\hbar^2 k_+}{m^*}+\alpha\Theta\right|}+\frac{k_-}{\left|\frac{\hbar^2 k_-}{m^*}-\alpha\Theta\right|} \\
\sim & \frac{2m^*}{\hbar^2}
\end{aligned} \tag{3.53}$$

and

$$A_3 = -\frac{4m^*\pi\alpha}{\hbar^3}\sin\theta_m\cos\theta_m \tag{3.54}$$

So, the final result is

$$\begin{aligned}
\delta s_x^{intra} &= \frac{qE_x\hbar}{8\pi^2\Gamma}(A_1+A_2+A_3) \\
&\sim \frac{qE_x\hbar}{8\pi^2\Gamma}(-\frac{4m^*\pi\alpha}{\hbar^3}\sin\theta_m\cos\theta_m) \\
&\sim -\frac{qE_x\alpha m^*}{2\pi\hbar^2\Gamma}\sin\theta_m\cos\theta_m.
\end{aligned} \tag{3.55}$$

We'll do similar derivations for the y component

$$\delta s_y^{intra} = \frac{qE_x\hbar}{8\pi^2\Gamma}(B_1+B_2+B_3) \tag{3.56}$$

where

$$\begin{aligned}
B_1 &\sim -\int d\theta \frac{4m^*\alpha\Theta}{\hbar^3}\cos\theta\sin\theta_m \\
&\sim -\frac{4m^*\alpha}{\hbar^3}\sin\theta_m\int d\theta\cos\theta(\sin\theta\cos\theta_m-\cos\theta\sin\theta_m) \\
&\sim \frac{4m^*\pi\alpha}{\hbar^3}\sin^2\theta_m,
\end{aligned} \tag{3.57}$$

$$\begin{aligned}
B_2 &\sim \frac{4m^{*2}J_{sd}}{\hbar^4}\int d\theta\frac{\alpha\hbar}{m^*J_{sd}}(\cos^2\theta+\sin\theta\cos\theta\sin\theta_m\cos\theta_m-\cos^2\theta\sin^2\theta_m) \\
&\sim \frac{4m^*\alpha}{\hbar^3}\int d\theta(\cos^2\theta+\sin\theta\cos\theta\sin\theta_m\cos\theta_m-\cos^2\theta\sin^2\theta_m) \\
&\sim \frac{4m^*\pi\alpha}{\hbar^3}(1-\sin^2\theta_m),
\end{aligned} \tag{3.58}$$

and

$$B_3 = -\frac{4m^*\pi\alpha}{\hbar^3}\sin^2\theta_m. \tag{3.59}$$

The final result is

$$\begin{aligned} \delta s_y^{intra} &\sim \frac{qE_x\hbar}{8\pi^2\Gamma}\frac{4m^*\pi\alpha}{\hbar^3}(1-\sin^2\theta_m) \\ &= \frac{qE_x\alpha m^*}{2\pi\hbar^2\Gamma}\cos^2\theta_m. \end{aligned} \tag{3.60}$$

So, the final results in this limit are

$$\delta\vec{s}^{intra} = \frac{qE_x\alpha m^*}{2\pi\hbar^2\Gamma}(-\hat{x}\sin\theta_m\cos\theta_m + \hat{y}\cos^2\theta_m) + 0\hat{z}. \tag{3.61}$$

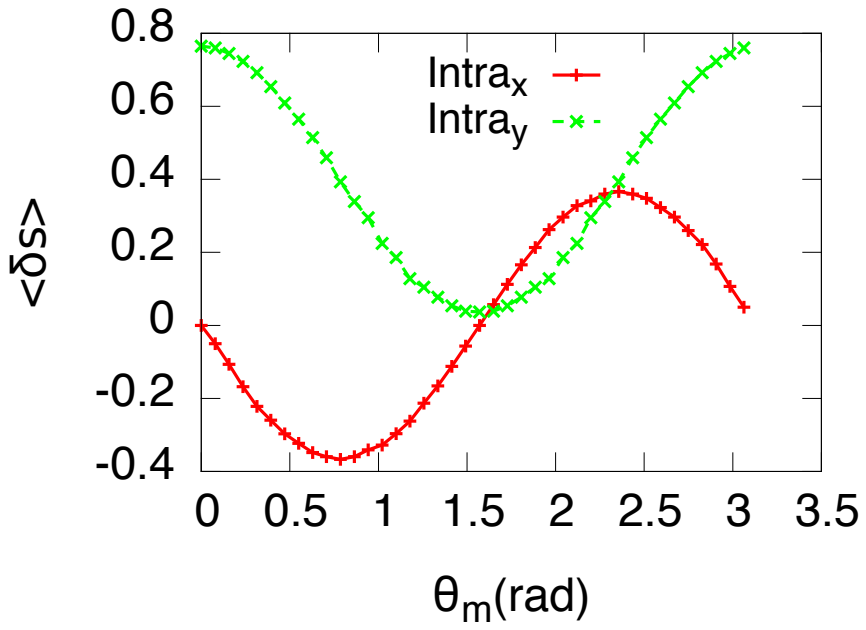

Figure 3.3: Intra band SOT as a function of θ_m for large exchange interaction.

As shown in figure 3.3, the numerical results match with analytical results. In

this limit, the results are still inversely proportional to Γ. So, in both limits, the intra band SOT have this inverse proportionality.

3.3.2 Inter band term

The Kubo formula for the inter band contribution is given by two terms

$$\delta\vec{s}^{inter} = \delta\vec{s}^{(1)} + \delta\vec{s}^{(2)}, \tag{3.62}$$

with

$$\begin{aligned}
\delta\vec{s}^{(1)} &= -\frac{\hbar}{L^2}\sum_{\vec{k}a\neq b} 2\mathrm{Re}[(\vec{s})_{ab}(q\vec{E}\cdot\vec{v})_{ba}]\frac{\Gamma(E_{\vec{k}a}-E_{\vec{k}b})}{[(E_{\vec{k}a}-E_{\vec{k}b})^2+\Gamma^2]^2}(f_{\vec{k}a}-f_{\vec{k}b}) \\
\delta\vec{s}^{(2)} &= -\frac{\hbar}{L^2}\sum_{\vec{k}a\neq b} \mathrm{Im}[(\vec{s})_{ab}(q\vec{E}\cdot\vec{v})_{ba}]\frac{\Gamma^2-(E_{\vec{k}a}-E_{\vec{k}b})^2}{[(E_{\vec{k}a}-E_{\vec{k}b})^2+\Gamma^2]^2}(f_{\vec{k}a}-f_{\vec{k}b}).
\end{aligned}$$

As in the intra band term, Γ is the spectrum broadening, $\vec{s}=\vec{\sigma}$, and $f_{\vec{k}}$ is the Fermi-Dirac distribution function. In our two-band model with electric field in the x direction, we have

$$\begin{aligned}
\langle\lambda_{\vec{k}+}|\sigma_x|\lambda_{\vec{k}-}\rangle\langle\lambda_{\vec{k}-}|v_x|\lambda_{\vec{k}+}\rangle &= -\frac{\alpha}{\hbar}\sin\phi_{\vec{k}}\cos\phi_{\vec{k}} \\
\langle\lambda_{\vec{k}+}|\sigma_y|\lambda_{\vec{k}-}\rangle\langle\lambda_{\vec{k}-}|v_x|\lambda_{\vec{k}+}\rangle &= -\frac{\alpha}{\hbar}\cos^2\phi_{\vec{k}} \\
\langle\lambda_{\vec{k}+}|\sigma_z|\lambda_{\vec{k}-}\rangle\langle\lambda_{\vec{k}-}|v_x|\lambda_{\vec{k}+}\rangle &= \frac{i\alpha}{\hbar}\cos\phi_{\vec{k}}
\end{aligned} \tag{3.63}$$

and

$$\begin{aligned}
\langle\lambda_{\vec{k}-}|\sigma_x|\lambda_{\vec{k}+}\rangle\langle\lambda_{\vec{k}+}|v_x|\lambda_{\vec{k}-}\rangle &= -\frac{\alpha}{\hbar}\sin\phi_{\vec{k}}\cos\phi_{\vec{k}} \\
\langle\lambda_{\vec{k}-}|\sigma_y|\lambda_{\vec{k}+}\rangle\langle\lambda_{\vec{k}+}|v_x|\lambda_{\vec{k}-}\rangle &= -\frac{\alpha}{\hbar}\cos^2\phi_{\vec{k}} \\
\langle\lambda_{\vec{k}-}|\sigma_z|\lambda_{\vec{k}+}\rangle\langle\lambda_{\vec{k}+}|v_x|\lambda_{\vec{k}-}\rangle &= -\frac{i\alpha}{\hbar}\cos\phi_{\vec{k}}.
\end{aligned} \tag{3.64}$$

So the non-equilibrium spin polarization can be calculated as follows

$$\begin{aligned}
\delta s_x^{(1)} &= \frac{\hbar q E_x}{L^2}\frac{2\alpha}{\hbar}\sum_{\vec{k}}\sin\phi_{\vec{k}}\cos\phi_{\vec{k}}\left[\frac{\Gamma(E_{\vec{k}+}-E_{\vec{k}-})}{[(E_{\vec{k}+}-E_{\vec{k}-})^2+\Gamma^2]^2}(f_{\vec{k}+}-f_{\vec{k}-})\right. \\
&\quad \left.+\frac{\Gamma(E_{\vec{k}-}-E_{\vec{k}+})}{[(E_{\vec{k}-}-E_{\vec{k}+})^2+\Gamma^2]^2}(f_{\vec{k}-}-f_{\vec{k}+})\right] \\
&= \frac{2qE_x\alpha}{L^2}\frac{L^2}{(2\pi)^2}\int d^2k\frac{2\Gamma(E_{\vec{k}+}-E_{\vec{k}-})\sin\phi_{\vec{k}}\cos\phi_{\vec{k}}}{[(E_{\vec{k}+}-E_{\vec{k}-})^2+\Gamma^2]^2}(f_{\vec{k}+}-f_{\vec{k}-}) \\
&= \frac{qE_x\alpha\Gamma}{\pi^2}\int d^2k\frac{2|\Delta_{\vec{k}}|\sin\phi_{\vec{k}}\cos\phi_{\vec{k}}}{(4|\Delta_{\vec{k}}|^2+\Gamma^2)^2}(f_{\vec{k}+}-f_{\vec{k}-}) \\
&= \frac{2qE_x\alpha\Gamma}{\pi^2}\int d^2k\frac{|\Delta_{\vec{k}}|\sin\phi_{\vec{k}}\cos\phi_{\vec{k}}}{(4|\Delta_{\vec{k}}|^2+\Gamma^2)^2}(f_{\vec{k}+}-f_{\vec{k}-}), \qquad (3.65)
\end{aligned}$$

$$\begin{aligned}
\delta s_y^{(1)} &= \frac{\hbar q E_x}{L^2}\frac{2\alpha}{\hbar}\sum_{\vec{k}}\cos^2\phi_{\vec{k}}\left[\frac{\Gamma(E_{\vec{k}+}-E_{\vec{k}-})}{[(E_{\vec{k}+}-E_{\vec{k}-})^2+\Gamma^2]^2}(f_{\vec{k}+}-f_{\vec{k}-})\right. \\
&\quad \left.+\frac{\Gamma(E_{\vec{k}-}-E_{\vec{k}+})}{[(E_{\vec{k}-}-E_{\vec{k}+})^2+\Gamma^2]^2}(f_{\vec{k}-}-f_{\vec{k}+})\right] \\
&= \frac{2qE_x\alpha}{L^2}\frac{L^2}{(2\pi)^2}\int d^2k\frac{2\Gamma(E_{\vec{k}+}-E_{\vec{k}-})\cos^2\phi_{\vec{k}}}{[(E_{\vec{k}+}-E_{\vec{k}-})^2+\Gamma^2]^2}(f_{\vec{k}+}-f_{\vec{k}-}) \\
&= \frac{2qE_x\alpha\Gamma}{\pi^2}\int d^2k\frac{|\Delta_{\vec{k}}|\cos^2\phi_{\vec{k}}}{(4|\Delta_{\vec{k}}|^2+\Gamma^2)^2}(f_{\vec{k}+}-f_{\vec{k}-}), \qquad (3.66)
\end{aligned}$$

and

$$\begin{aligned}
\delta s_z^{(2)} &= -\frac{\hbar q E_x}{L^2}\frac{\alpha}{\hbar}\sum_{\vec{k}}\cos\phi_{\vec{k}}\left[\frac{\Gamma^2-(E_{\vec{k}+}-E_{\vec{k}-})^2}{[(E_{\vec{k}+}-E_{\vec{k}-})^2+\Gamma^2]^2}(f_{\vec{k}+}-f_{\vec{k}-})\right. \\
&\quad \left.-\frac{\Gamma^2-(E_{\vec{k}-}-E_{\vec{k}+})^2}{[(E_{\vec{k}-}-E_{\vec{k}+})^2+\Gamma^2]^2}(f_{\vec{k}-}-f_{\vec{k}+})\right] \\
&= -\frac{2qE_x\alpha}{L^2}\frac{L^2}{(2\pi)^2}\int d^2k\cos\phi_{\vec{k}}\frac{\Gamma^2-(E_{\vec{k}+}-E_{\vec{k}-})^2}{[(E_{\vec{k}+}-E_{\vec{k}-})^2+\Gamma^2]^2}(f_{\vec{k}+}-f_{\vec{k}-}) \\
&= -\frac{qE_x\alpha}{2\pi^2}\int d^2k\frac{(\Gamma^2-4|\Delta_{\vec{k}}|^2)\cos\phi_{\vec{k}}}{(4|\Delta_{\vec{k}}|^2+\Gamma^2)^2}(f_{\vec{k}+}-f_{\vec{k}-}). \qquad (3.67)
\end{aligned}$$

Again, these integrals are difficult to treat exactly. We'll test the different limits.

3.3.2.1 Small exchange limit

In the small exchange limit $J_{sd} \to 0$ or $J_{sd}/\alpha k_F \ll 1$, we have

$$\begin{aligned} |\Delta_{\vec{k}}| &= [J_{sd}^2 + 2J_{sd}\alpha(k_y \cos\theta_m - k_x \sin\theta_m) + \alpha^2(k_x^2 + k_y^2)]^{1/2} \\ &= \alpha k \left[1 + \frac{2J_{sd}}{\alpha k}(\sin\theta\cos\theta_m - \cos\theta\sin\theta_m) + \frac{J_{sd}^2}{\alpha^2}\right]^{1/2} \\ &\sim \alpha k + J_{sd}(\sin\theta\cos\theta_m - \cos\theta\sin\theta_m). \end{aligned} \tag{3.68}$$

$$\begin{aligned} \frac{1}{|\Delta_{\vec{k}}|} &= [J_{sd}^2 + 2J_{sd}\alpha(k_y \cos\theta_m - k_x \sin\theta_m) + \alpha^2(k_x^2 + k_y^2)]^{-1/2} \\ &= \frac{1}{\alpha k}\left[1 + \frac{2J_{sd}}{\alpha k}(\sin\theta\cos\theta_m - \cos\theta\sin\theta_m) + \frac{J_{sd}^2}{\alpha^2}\right]^{-1/2} \\ &\sim \frac{1}{\alpha k} - \frac{J_{sd}}{\alpha^2 k^2}(\sin\theta\cos\theta_m - \cos\theta\sin\theta_m). \end{aligned} \tag{3.69}$$

and

$$\begin{aligned} \sin\phi_{\vec{k}} &\sim \cos\theta - \frac{J_{sd}}{\alpha k}(\sin\theta_m + \sin\theta\cos\theta\cos\theta_m - \cos^2\theta\sin\theta_m) \\ \cos\phi_{\vec{k}} &\sim \sin\theta + \frac{J_{sd}}{\alpha k}(\cos\theta_m - \sin^2\theta\cos\theta_m + \sin\theta\cos\theta\sin\theta_m). \end{aligned} \tag{3.70}$$

So we have

$$\begin{aligned} & \sin\phi_{\vec{k}}\cos\phi_{\vec{k}} \\ \sim\ & \sin\theta\cos\theta + \frac{J_{sd}}{\alpha k}(\cos\theta\cos\theta_m - \sin^2\theta\cos\theta\cos\theta_m + \sin\theta\cos^2\theta\sin\theta_m) \\ & -\frac{J_{sd}}{\alpha k}(\sin\theta\sin\theta_m + \sin^2\theta\cos\theta\cos\theta_m - \sin\theta\cos^2\theta\sin\theta_m), \end{aligned} \tag{3.71}$$

and

$$\begin{aligned} & \cos^2\phi_{\vec{k}} \\ \sim\ & \sin^2\theta + \frac{2J_{sd}}{\alpha k}(\sin\theta\cos\theta_m - \sin^3\theta\cos\theta_m + \sin^2\theta\cos\theta\sin\theta_m). \end{aligned} \tag{3.72}$$

The k integration boundaries are given by the roots

$$k_\pm = \mp\frac{m^*\alpha}{\hbar^2} + \sqrt{\frac{m^{*2}\alpha^2}{\hbar^4} + \frac{2m^*}{\hbar^2}(E_F \mp J_{sd}\Theta)}. \tag{3.73}$$

Again, we only need results up to the first order of small parameter. For the $\delta s_x^{(1)}$ integration, we have terms like

$$\begin{aligned} & \frac{2qE_x\alpha\Gamma}{\pi^2}\int kdkd\theta\frac{(\alpha k + J_{sd}\Theta)\sin\theta\cos\theta}{[4(\alpha k + J_{sd}\Theta)^2 + \Gamma^2]^2}(f_{\vec{k}+} - f_{\vec{k}-}) \\ \sim\ & \frac{2qE_x\alpha\Gamma}{16\pi^2}\int kdkd\theta\frac{(\alpha k - J_{sd}\Theta)\sin\theta\cos\theta}{\alpha^4k^4}(f_{\vec{k}+} - f_{\vec{k}-}) \\ \sim\ & 0 \end{aligned} \tag{3.74}$$

because after integrating over k, the θ integration will be zero for any combinations here. And it is the same for other terms in $\delta s_x^{(1)}$. So

$$\delta s_x^{(1)} \sim 0 \tag{3.75}$$

For the same reason, the only non-zero term in $\delta s_y^{(1)}$ is given by

$$\begin{aligned} \delta s_y^{(1)} \ \sim\ & \frac{2qE_x\alpha\Gamma}{\pi^2}\int kdkd\theta\frac{(\alpha k + J_{sd}\Theta)\sin^2\theta}{[4(\alpha k + J_{sd}\Theta)^2 + \Gamma^2]^2}(f_{\vec{k}+} - f_{\vec{k}-}) \\ \sim\ & \frac{2qE_x\alpha\Gamma}{\pi^2}\int d\theta\sin^2\theta\int kdk\frac{\alpha k}{16\alpha^4k^4}(f_{\vec{k}+} - f_{\vec{k}-}) \\ \sim\ & \frac{qE_x\Gamma}{8\pi^2\alpha^2}\int d\theta\sin^2\theta\int dk\frac{1}{k^2}(f_{\vec{k}+} - f_{\vec{k}-}) \end{aligned}$$

$$\begin{aligned} &\sim \frac{qE_x\Gamma}{8\pi^2\alpha^2}\int d\theta \sin^2\theta\left(\frac{1}{k_-}-\frac{1}{k_+}\right) \\ &\sim -\frac{qE_x\Gamma}{8\pi\alpha E_F} \end{aligned} \tag{3.76}$$

Here in the k integration, we only keep the Θ independent term because, otherwise, the θ integration will be zero. And we have two non-zero terms in $\delta s_z^{(2)}$

$$\begin{aligned} Z_1 = &\sim -\frac{qE_x\alpha}{2\pi^2}\int kdkd\theta\frac{[\Gamma^2-4(\alpha k+J_{sd}\Theta)^2]\sin\theta}{[4(\alpha k+J_{sd}\Theta)^2+\Gamma^2]^2}(f_{\vec{k}+}-f_{\vec{k}-}) \\ &\sim \frac{qE_x\alpha}{8\pi^2}\int dkd\theta\frac{k\sin\theta}{(\alpha k+J_{sd}\Theta)^2}(f_{\vec{k}+}-f_{\vec{k}-}) \\ &\sim \frac{qE_x\alpha}{8\pi^2}\int dkd\theta\sin\theta\left(\frac{1}{\alpha^2 k}-\frac{2J_{sd}\Theta}{\alpha^3k^2}\right)(f_{\vec{k}+}-f_{\vec{k}-}) \\ &\sim -\frac{qE_xJ_{sd}}{8\pi\alpha E_F}\cos\theta_m+\frac{qE_xJ_{sd}}{4\pi\alpha E_F}\cos\theta_m \\ &\sim \frac{qE_xJ_{sd}}{8\pi\alpha E_F}\cos\theta_m. \end{aligned} \tag{3.77}$$

$$\begin{aligned} Z_2 = &\sim -\frac{qE_x\alpha}{2\pi^2}\int kdkd\theta\frac{[\Gamma^2-4(\alpha k+J_{sd}\Theta)^2]J_{sd}(1-\sin^2\theta)\cos\theta_m}{[4(\alpha k+J_{sd}\Theta)^2+\Gamma^2]^2\alpha k}(f_{\vec{k}+}-f_{\vec{k}-}) \\ &\sim \frac{qE_xJ_{sd}\cos\theta_m}{8\pi^2\alpha^2}\int dkd\theta\frac{\cos^2\theta}{k^2}(f_{\vec{k}+}-f_{\vec{k}-}) \\ &\sim -\frac{qE_xJ_{sd}}{8\pi\alpha E_F}\cos\theta_m. \end{aligned} \tag{3.78}$$

So

$$\delta s_z^{(2)} = Z_1 + Z_2 \sim 0. \tag{3.79}$$

Here we assume $\alpha \gg \Gamma$. E_F is the Fermi energy. So, the final results in this limits are

$$\delta\vec{s}^{inter} = 0\hat{x} - \hat{y}\frac{qE_x\Gamma}{8\pi\alpha E_F} + 0\hat{z}. \tag{3.80}$$

Comparing with the intra band SOT, the inter band SOT is also independent of

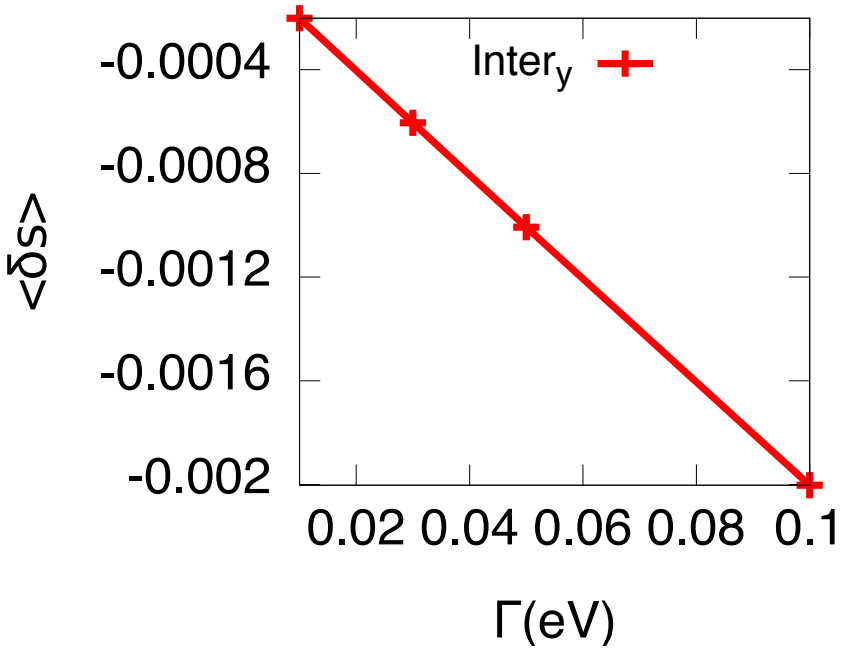

Figure 3.4: Inter band SOT as a function of Γ for small exchange interaction.

θ_m, but is proportional to Γ, which is shown in figure 3.4 from numerical simulation.

3.3.2.2 Large exchange limit

On the other hand, in the large J_{sd} limit, $J_{sd} \gg \alpha k_F, J_{sd} \gg \Gamma$, keeping up to the first order of α/J_{sd}, we have

$$\begin{aligned} |\Delta_{\vec{k}}| &= [J_{sd}^2 + 2J_{sd}\alpha(k_y \cos\theta_m - k_x \sin\theta_m) + \alpha^2(k_x^2 + k_y^2)]^{1/2} \\ &= J_{sd}\left[1 + \frac{2\alpha k}{J_{sd}}(\sin\theta\cos\theta_m - \cos\theta\sin\theta_m) + \frac{\alpha^2}{J_{sd}^2}\right]^{1/2} \\ &\sim J_{sd} + \alpha k(\sin\theta\cos\theta_m - \cos\theta\sin\theta_m). \end{aligned} \tag{3.81}$$

and

$$\begin{aligned}\frac{1}{|\Delta_{\vec{k}}|} &= [J_{sd}^2 + 2J_{sd}\alpha(k_y\cos\theta_m - k_x\sin\theta_m) + \alpha^2(k_x^2+k_y^2)]^{-1/2} \\ &= \frac{1}{J_{sd}}\left[1 + \frac{2\alpha k}{J_{sd}}(\sin\theta\cos\theta_m - \cos\theta\sin\theta_m) + \frac{\alpha^2}{J_{sd}^2}\right]^{-1/2} \\ &\sim \frac{1}{J_{sd}} - \frac{\alpha k}{J_{sd}^2}(\sin\theta\cos\theta_m - \cos\theta\sin\theta_m). \end{aligned} \tag{3.82}$$

then

$$\begin{aligned}\sin\phi_{\vec{k}} &\sim -\sin\theta_m + \frac{\alpha k}{J_{sd}}(\cos\theta + \sin\theta\sin\theta_m\cos\theta_m - \cos\theta\sin^2\theta_m) \\ \cos\phi_{\vec{k}} &\sim \cos\theta_m + \frac{\alpha k}{J_{sd}}(\sin\theta - \sin\theta\cos^2\theta_m + \cos\theta\sin\theta_m\cos\theta_m). \end{aligned} \tag{3.83}$$

The angular dependence in the integrands are given by

$$\begin{aligned}&\sin\phi_{\vec{k}}\cos\phi_{\vec{k}} \\ \sim\ & -\sin\theta_m\cos\theta_m + \frac{\alpha k}{J_{sd}}(\cos\theta\cos\theta_m + \sin\theta\sin\theta_m\cos^2\theta_m - \cos\theta\sin^2\theta_m\cos\theta_m) \\ & -\frac{\alpha k}{J_{sd}}(\sin\theta\sin\theta_m - \sin\theta\cos^2\theta_m\sin\theta_m + \cos\theta\sin^2\theta_m\cos\theta_m) \end{aligned} \tag{3.84}$$

and

$$\begin{aligned}&\cos^2\phi_{\vec{k}} \\ \sim\ & \cos^2\theta_m + \frac{2\alpha k}{J_{sd}}(\sin\theta\cos\theta_m - \sin\theta\cos^3\theta_m + \cos\theta\sin\theta_m\cos^2\theta_m). \end{aligned} \tag{3.85}$$

When both bands are occupied, the integration boundaries are given by

$$k_\pm = \mp\frac{m^*\alpha\Theta}{\hbar^2} + \sqrt{\frac{m^{*2}\alpha^2\Theta^2}{\hbar^4} + \frac{2m^*}{\hbar^2}(E_F \mp J_{sd})}. \tag{3.86}$$

where E_F is the Fermi energy. Then, we have

$$\begin{aligned}
\delta s_x^{(1)} &= \frac{2qE_x\alpha\Gamma}{\pi^2}\int d^2k\frac{|\Delta_{\vec{k}}|\sin\phi_{\vec{k}}\cos\phi_{\vec{k}}}{(4|\Delta_{\vec{k}}|^2+\Gamma^2)^2}(f_{\vec{k}+}-f_{\vec{k}-}) \\
&\sim -\frac{2qE_x\alpha\Gamma}{\pi^2}\int kdkd\theta\frac{(J_{sd}+\alpha k\Theta)\sin\theta_m\cos\theta_m}{[4(J_{sd}+\alpha k\Theta)^2+\Gamma^2]^2}(f_{\vec{k}+}-f_{\vec{k}-}) \\
&\sim -\frac{qE_x\alpha\Gamma\sin\theta_m\cos\theta_m}{8J_{sd}^3\pi^2}\int kdkd\theta(f_{\vec{k}+}-f_{\vec{k}-}) \\
&\sim \frac{qE_x\alpha\Gamma\sin\theta_m\cos\theta_m}{8J_{sd}^3\pi^2}\int d\theta\left(\frac{k^2}{2}\right)\Big|_{k_+}^{k_-} \\
&\sim \frac{qE_x\alpha\Gamma\sin\theta_m\cos\theta_m}{8J_{sd}^3\pi^2}\frac{4\pi mJ_{sd}}{\hbar^2} \\
&\sim \frac{qE_x\alpha m^*\Gamma}{2\pi\hbar^2J_{sd}^2}\sin\theta_m\cos\theta_m
\end{aligned} \tag{3.87}$$

$$\begin{aligned}
\delta s_y^{(1)} &= \frac{2qE_x\alpha\Gamma}{\pi^2}\int d^2k\frac{|\Delta_{\vec{k}}|\cos^2\phi_{\vec{k}}}{(4|\Delta_{\vec{k}}|^2+\Gamma^2)^2}(f_{\vec{k}+}-f_{\vec{k}-}) \\
&\sim \frac{2qE_x\alpha\Gamma}{\pi^2}\int kdkd\theta\frac{(J_{sd}+\alpha k\Theta)\cos^2\theta_m}{[4(J_{sd}+\alpha k\Theta)^2+\Gamma^2]^2}(f_{\vec{k}+}-f_{\vec{k}-}) \\
&\sim \frac{qE_x\alpha\Gamma\cos^2\theta_m}{8J_{sd}^3\pi^2}\int kdkd\theta(f_{\vec{k}+}-f_{\vec{k}-}) \\
&\sim -\frac{qE_x\alpha m^*\Gamma}{2\pi\hbar^2J_{sd}^2}\cos^2\theta_m
\end{aligned} \tag{3.88}$$

and

$$\begin{aligned}
\delta s_z^{(2)} &= -\frac{qE_x\alpha}{2\pi^2}\int d^2k\frac{(\Gamma^2-4|\Delta_{\vec{k}}|^2)\cos\phi_{\vec{k}}}{(4|\Delta_{\vec{k}}|^2+\Gamma^2)^2}(f_{\vec{k}+}-f_{\vec{k}-}). \\
&\sim -\frac{qE_x\alpha}{2\pi^2}\int kdkd\theta\frac{[\Gamma^2-4(J_{sd}+\alpha k\Theta)^2]\cos\theta_m}{[4(J_{sd}+\alpha k\Theta)^2+\Gamma^2]^2}(f_{\vec{k}+}-f_{\vec{k}-}) \\
&\sim \frac{qE_x\alpha\cos\theta_m}{8\pi^2J_{sd}^2}\int kdkd\theta(f_{\vec{k}+}-f_{\vec{k}-}) \\
&\sim -\frac{qE_x\alpha m^*}{2\pi\hbar^2J_{sd}}\cos\theta_m.
\end{aligned} \tag{3.89}$$

So, the final results are:

$$\delta\vec{s}^{inter} = \frac{qE_x\alpha m^*\Gamma}{2\pi\hbar^2 J_{sd}^2}(\hat{x}\sin\theta_m\cos\theta_m - \hat{y}\cos^2\theta_m) - \hat{z}\frac{qE_x\alpha m^*}{2\pi\hbar^2 J_{sd}}\cos\theta_m. \tag{3.90}$$

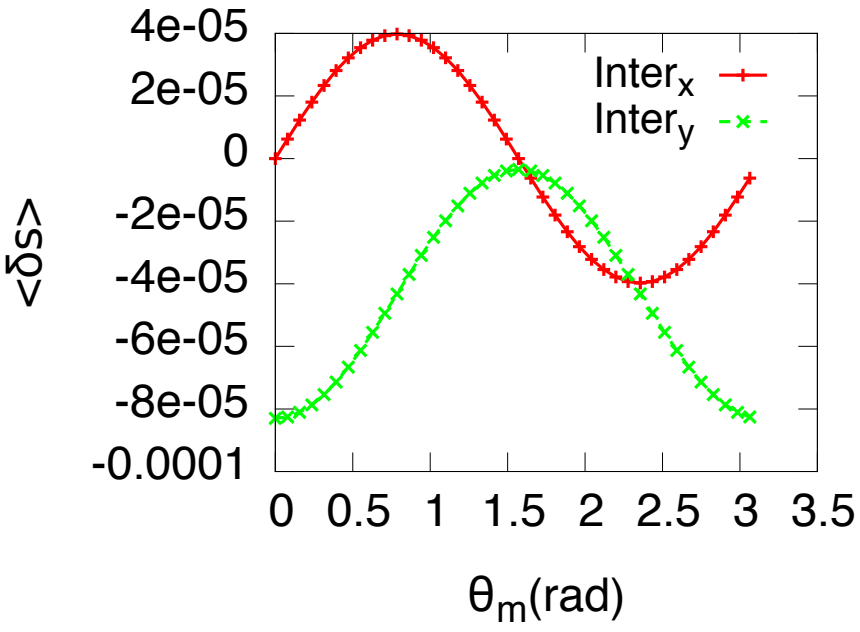

Figure 3.5: Inter band SOT as a function of θ_m for large exchange interaction.

Again, these results can be compared with the numerical integrations. As shown in figure 3.5 and 3.6, numerical results match with analytical results exactly. One important observation is that the out-of-plane SOT is independent of Γ, which means this is an intrinsic contribution. As shown in figure 3.7, this term is independent of Γ whenever Γ is small. The importance of this term is that it will induce in-plane magnetization switching.

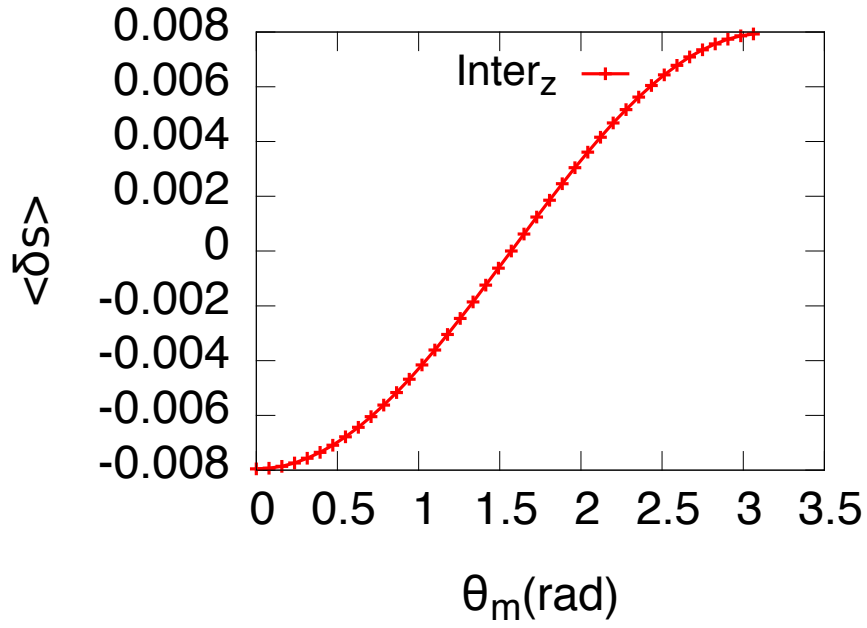

Figure 3.6: Inter band out-of-plane SOT as a function of θ_m for large exchange interaction.

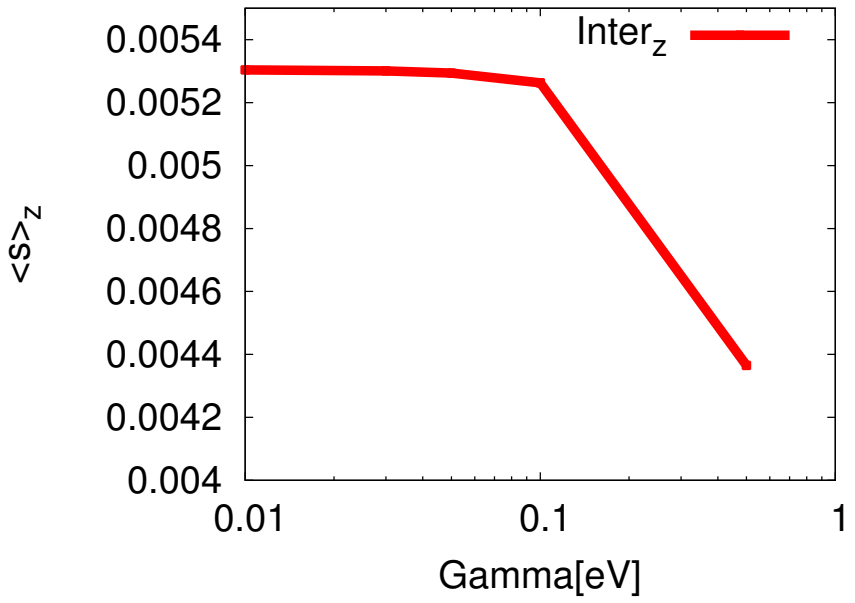

Figure 3.7: Inter band out-of-plane SOT as a function of Γ for large exchange interaction.

3.4 Summary

A brief summary of this chapter will be given in this part. The Hamiltonian of this system is

$$H = \frac{\hbar^2}{2m^*}(k_x^2 + k_y^2) + \alpha(k_y\sigma_x - k_x\sigma_y) + J_{sd}\vec{M}\cdot\vec{\sigma} \tag{3.91}$$

The external electric field is

$$\vec{E} = E_x\hat{x} \tag{3.92}$$

The magnetization is given by

$$\vec{M} = (\cos\theta_m, \sin\theta_m), \tag{3.93}$$

where θ_m is the angle between the magnetization and the external electric current, which is along the x-axis in our case. Base on this simulation setup, in the small J_{sd} limit ($J_{sd} \to 0$ or $J_{sd}/\alpha k_F \ll 1$) and $\alpha \gg \Gamma$, current induced spin polarization is given by

$$\begin{aligned} \delta\vec{s}^{intra} &= 0\hat{x} + \hat{y}\frac{qE_x\alpha m^*}{4\pi\hbar^2\Gamma} + 0\hat{z} \\ \delta\vec{s}^{inter} &= 0\hat{x} - \hat{y}\frac{qE_x\Gamma}{8\pi\alpha E_F} + 0\hat{z}. \end{aligned} \tag{3.94}$$

In the large J_{sd} limit, ($J_{sd} \gg \alpha k_F, J_{sd} \gg \Gamma$), current induced spin polarization is given by

$$\delta\vec{s}^{intra} = \frac{qE_x\alpha m^*}{2\pi\hbar^2\Gamma}(-\hat{x}\sin\theta_m\cos\theta_m + \hat{y}\cos^2\theta_m) + 0\hat{z} \tag{3.95}$$

$$\delta\vec{s}^{inter} = \frac{qE_x\alpha m^*\Gamma}{2\pi\hbar^2 J_{sd}^2}(\hat{x}\sin\theta_m\cos\theta_m - \hat{y}\cos^2\theta_m) - \hat{z}\frac{qE_x\alpha m^*}{2\pi\hbar^2 J_{sd}}\cos\theta_m. \tag{3.96}$$

All these results are confirmed by the numerical simulations. With this minimal model, we are able to derive the form of SOT as well as the parameter dependence analytically in certain limits. In the next chapter, we will study how the complicated band structure will affect the results of SOT using numerical simulations.

4. SPIN-ORBIT TORQUES IN $Ga_{1-x}Mn_xAs$*

4.1 Introductions to GaAs and $Ga_{1-x}Mn_xAs$

GaAs is a typical III-V semiconductor with the Zinc-blende crystal structure [60], as shown in figure 4.1. The lattice constant is 0.56535 nm. Figure 5.3 illustrates the band structure near Γ point [60, 61]. GaAs is direct gap semiconductor with a band gap of 1.424 eV at 300K. The valence band is 6 fold degenerate with the symmetry similar that of an angular moment $l = 1$. Due to spin-orbit coupling, this band splits into three 2-fold degenerate bands: two heavy hole bands, two light hole bands and two spin split-off bands. The gap between the heavy hole and split-off band at the Γ point is 0.34 eV. GaAs is widely used in the semiconductor industries.

When doping Manganeses (Mn) into GaAs, the Mn will take the cations of Ga to form substitutional dopants [62]. This doping is referred to as hole doping because there are two valance electrons for Mn whereas there are three for Ga. And also, Mn will introduce magnetic moments into this material. (see figure 4.3) When the doping rate is high enough, ferromagnetism happens due to hole mediated ferromagnetic interactions between Mn moments.

A ferromagnetic semiconductor [62] is the magnetic system in which ferromagnetism is primarily due to the coupling between the magnetic element moments that are mediated by conducting carriers. $Ga_{1-x}Mn_xAs$ is an example of a ferromagnetic semiconductor. Since the doping rate of Mn is usually less than 10%, $Ga_{1-x}Mn_xAs$ is called a diluted ferromagnetic semiconductor(DMS). This material is ideal to study the spin-obit torque effects, because of the relatively simple band structures, large

*Reprinted with permission from Hang Li, H. Gao, Liviu P. Zarbo, K. Vyborny, Xuhui Wang, Ion Garate, Fatih Dogan, A. Cejchan, Jairo Sinova, T. Jungwirth, and Aurelien Manchon, Phys. Rev. B **91,** 134402 (2015). Copyright 2015 by the American Physical Society.

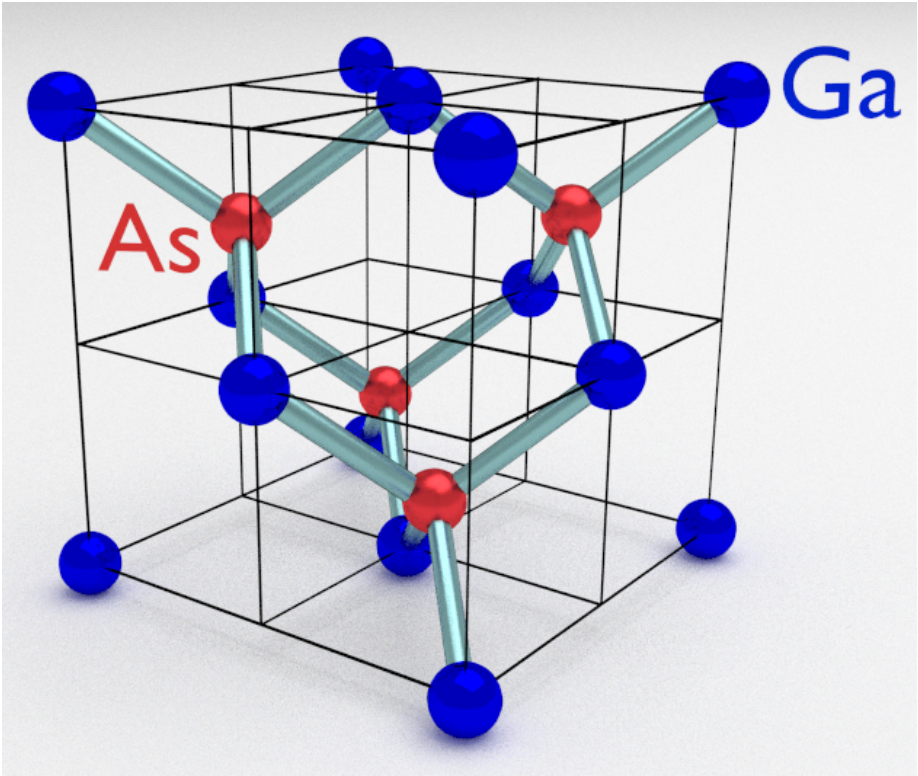

Figure 4.1: Lattice structure of GaAs.

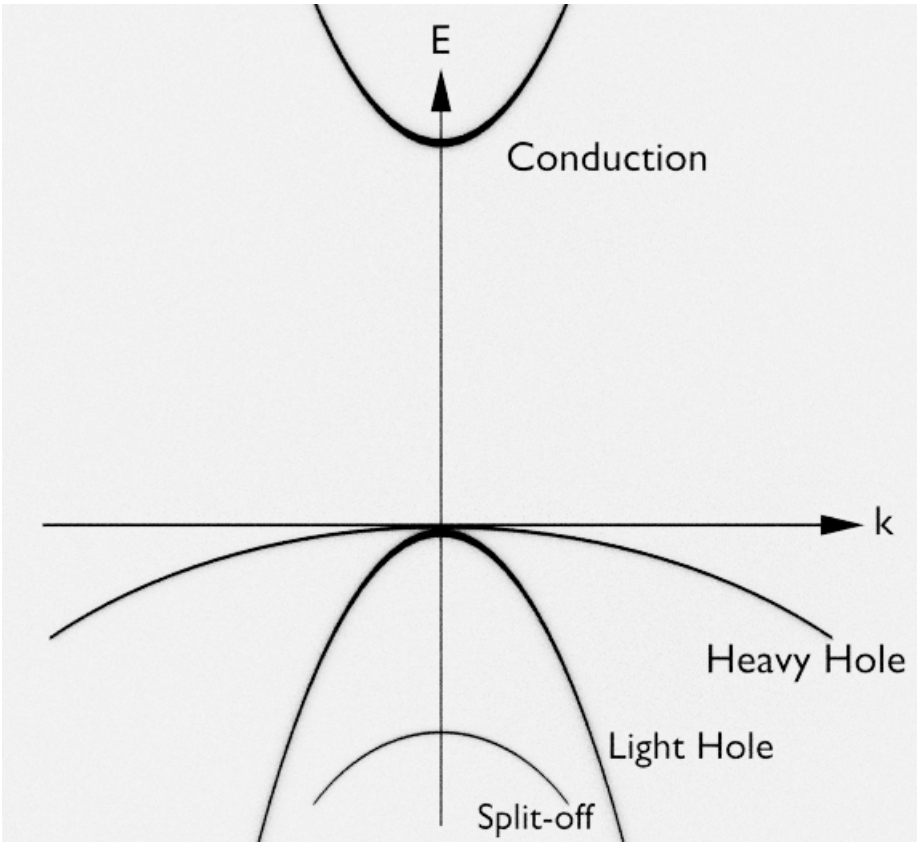

Figure 4.2: Band structure of GaAs near the Γ point.

spin-orbit coupling, and strain induced spin-orbit coupling [34, 61, 63, 64].

After an introduction of the $Ga_{1-x}Mn_xAs$ simulation model, we will study the spin-orbit torques and the impact of band structure on spin-orbit torques. Compared with the simple 2DEG Rashba model, we see that the spin-orbit torques in $Ga_{1-x}Mn_xAs$ follow similar parameter dependence, and the more complicated band structures affect the magnitudes of the results.

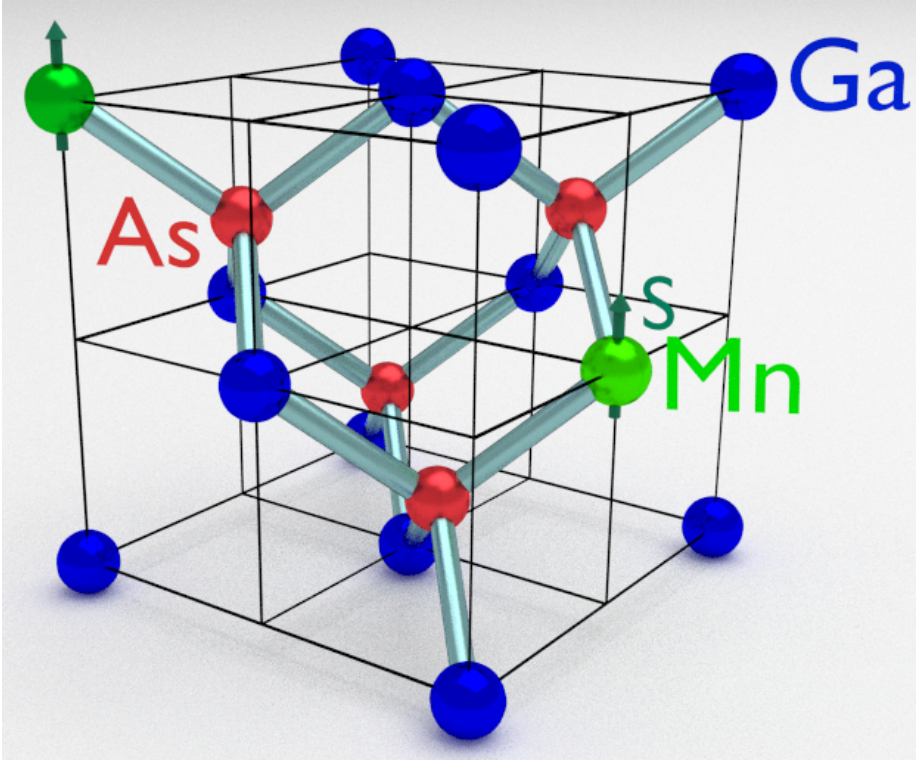

Figure 4.3: Dope Mn into GaAs to form $Ga_{1-x}Mn_xAs$. S denotes spin.

4.2 Model to simulate $Ga_{1-x}Mn_xAs$

To calculate the band structures of a crystal, there are three main methods [57], tight-binding, $\vec{k}\cdot\vec{p}$, and density functional theory. In this project, we use $\vec{k}\cdot\vec{p}$ method

to describe $Ga_{1-x}Mn_xAs$, because this method can make use of the symmetry of band structures and greatly simplify the calculation [64, 65]. Also, the spin-orbit coupling is embedded naturally in this method. We also consider strain-induced spin-orbit coupling which is important in nano-scale thin film geometry.

4.2.1 Introduction to the $\vec{k} \cdot \vec{p}$ method

The $\vec{k} \cdot \vec{p}$ method is used to calculate the band structure near a specific $\vec{k}_0$ point if we know the eigen energies and wave functions for each bands at that $\vec{k}_0$ point. For GaAs we choose $\vec{k}_0 = 0$ because this is the top of the valence band and is highly symmetric. As we know, in crystals, the periodic potential V_0 satisfies:

$$V_0(\vec{r} + \vec{R}_l) = V_0(\vec{r}) \tag{4.1}$$

where $\vec{R}_l$ is the lattice vector. Then we have the time-independent Schrödinger equation:

$$\left(\frac{\vec{p}^2}{2m_0} + V_0 \right) |\phi_{n\vec{k}}\rangle = \epsilon_{n\vec{k}} |\phi_{n\vec{k}}\rangle \tag{4.2}$$

where n is the band index, and $\vec{k}$ is the wavevector.

Using Bloch theorem [57], the solution of this equation can be written as:

$$\langle \vec{r} | \phi_{n\vec{k}} \rangle = e^{i\vec{k}\cdot\vec{r}} u_{n\vec{k}}(\vec{r}) \tag{4.3}$$

where $u_{n\vec{k}}(\vec{r})$ has the periodicity of the lattice vector. Plugging equation (4.3) into equation (4.2), we get the equation for $u_{n\vec{k}}(\vec{r})$:

$$\left(\frac{\vec{p}^2}{2m_0} + V_0 + \frac{\hbar}{m_0} \vec{k} \cdot \vec{p} \right) u_{n\vec{k}}(\vec{r}) = \left(\epsilon_{n\vec{k}} - \frac{\hbar^2 \vec{k}^2}{2m_0} \right) u_{n\vec{k}}(\vec{r}) \tag{4.4}$$

If we choose the reference point as $\vec{k} = 0$, for $\vec{k}$ near $\vec{k} = 0$, we can treat the

term $\frac{\hbar}{m_0}\vec{k}\cdot\vec{p}$ as a perturbation. That is why it is called the $\vec{k}\cdot\vec{p}$ model. When the valence bands are degenerate, we have to use degenerate perturbation theory to calculate the band structure. See chapter 6 of S. Chow [61]. After doing the perturbation expansion, we will get a polynomial of k_x, k_y, k_z to describe the band structure near the reference k point. This Hamiltonian is called Kohn-Luttinger Hamiltonian [65, 66, 67].

4.2.2 Hamiltonian of $Ga_{1-x}Mn_xAs$

To describe $Ga_{1-x}Mn_xAs$, we need the band structures of the valence band of the host GaAs, the exchange interaction between holes and local magnetic moments, and the spin-orbit coupling induced by strain. So the Hamiltonian can be written as: [34, 54]

$$H = H_{KL} + H_{exch} + H_{strain}. \tag{4.5}$$

where H_{KL} is the Kohn-Luttinger Hamiltonian for GaAs. In our simulation, we choose the four band model to describe the valence band of GaAs, which includes two heavy hole bands and two light hole bands.

$$\begin{aligned} H_{KL} &= \frac{\hbar^2 k^2}{2m_0}\left(\gamma_1 + \frac{5}{2}\gamma_2\right) I_4 - \frac{\hbar^2}{m_0}\gamma_3(\vec{k}\cdot\vec{J})^2 \\ &\quad + \frac{\hbar^2}{m_0}(\gamma_3 - \gamma_2)(k_x^2 J_x^2 + k_y^2 J_y^2 + k_z^2 J_z^2). \end{aligned} \tag{4.6}$$

Here m_0 is the electron mass, $\gamma_1 = 6.98, \gamma_2 = 2.06, \gamma_3 = 2.93$ are the Luttinger parameters for GaAs, I_4 is 4×4 identity matrix, and $\vec{J} = (J_x, J_y, J_z)$ are the 4×4

angular momentum matrices. One choice of $\vec{J}$ is given by: [65]

$$J_x = \begin{pmatrix} 0 & 0 & \frac{\sqrt{3}}{2} & 0 \\ 0 & 0 & 1 & \frac{\sqrt{3}}{2} \\ \frac{\sqrt{3}}{2} & 1 & 0 & 0 \\ 0 & \frac{\sqrt{3}}{2} & 0 & 0 \end{pmatrix} \tag{4.7}$$

$$J_y = i \begin{pmatrix} 0 & 0 & -\frac{\sqrt{3}}{2} & 0 \\ 0 & 0 & 1 & -\frac{\sqrt{3}}{2} \\ \frac{\sqrt{3}}{2} & -1 & 0 & 0 \\ 0 & \frac{\sqrt{3}}{2} & 0 & 0 \end{pmatrix} \tag{4.8}$$

$$J_z = \begin{pmatrix} \frac{3}{2} & 0 & 0 & 0 \\ 0 & -\frac{1}{2} & 0 & 0 \\ 0 & 0 & \frac{1}{2} & 0 \\ 0 & 0 & 0 & -\frac{3}{2} \end{pmatrix} \tag{4.9}$$

So the KL Hamiltonian can also be written in the matrix form [68]

$$H_{KL} = \begin{pmatrix} \mathcal{H}_{hh} & -c & -b & 0 \\ -c^* & \mathcal{H}_{lh} & 0 & b \\ -b^* & 0 & \mathcal{H}_{lh} & -c \\ 0 & b^* & -c^* & \mathcal{H}_{hh} \end{pmatrix} \tag{4.10}$$

where

$$\mathcal{H}_{hh} = \frac{\hbar^2}{2m}[(\gamma_1 + \gamma_2)(k_x^2 + k_y^2) + (\gamma_1 - 2\gamma_2)k_z^2], \tag{4.11}$$

$$\mathcal{H}_{lh} = \frac{\hbar^2}{2m}[(\gamma_1 - \gamma_2)(k_x^2 + k_y^2) + (\gamma_1 + 2\gamma_2)k_z^2], \tag{4.12}$$

$$b = \frac{\sqrt{3}\hbar^2}{m}\gamma_3 k_z(k_x - ik_y), \tag{4.13}$$

$$c = \frac{\sqrt{3}\hbar^2}{2m}[\gamma_2(k_x^2 - k_y^2) - 2i\gamma_3 k_x k_y]. \tag{4.14}$$

One thing that should be mentioned here is that we are working in the hole picture. It means that the zero energy is on the top of the valence band, and the positive energy goes into the valence band side.

The exchange coupling between holes and the Mn local moments is given by [62, 69]

$$H_{exch} = J_{pd} S_{Mn} c_{Mn} \vec{M} \cdot \vec{s} \tag{4.15}$$

where J_{pd}=55 meV nm^3, $S_{Mn} = 5/2$, c_{Mn} is the Mn density, $\vec{M}$ is the unit direction of magnetization, and $\vec{s} = \vec{J}/3$ is the spin operator of the holes. The matrix form is easy to obtain as

$$H_{exch} = J_{pd} S_{Mn} c_{Mn} \begin{pmatrix} \frac{M_z}{2} & 0 & \frac{M_x - iM_y}{2\sqrt{3}} & 0 \\ 0 & -\frac{M_z}{6} & \frac{M_x + iM_y}{3} & \frac{M_x - iM_y}{2\sqrt{3}} \\ \frac{M_x + iM_y}{2\sqrt{3}} & \frac{M_x - iM_y}{3} & \frac{M_z}{6} & 0 \\ 0 & \frac{M_x + iM_y}{2\sqrt{3}} & 0 & -\frac{M_z}{2} \end{pmatrix} \tag{4.16}$$

Our later simulations always assume that magnetization is in-plane. So, there is no M_z component.

The strain Hamiltonian in the hole picture is [61, 68, 70]

$$\begin{aligned} H_{strain} &= b\left[\left(J_x^2 - \frac{\vec{J}^2}{3}\right)\epsilon_{xx} + c.p.\right] + \frac{d}{\sqrt{3}}\left[2\left\{J_x, J_y\right\}\epsilon_{xy} + c.p.\right] \\ &\quad -C_4\left[J_x(\epsilon_{yy} - \epsilon_{zz})k_x + c.p.\right] \end{aligned}$$

$$-C_5\left[\epsilon_{xy}(k_yJ_x - k_xJ_y) + c.p.\right] \tag{4.17}$$

Here, $b = -2.0$ eV and $d = -4.8$ eV [70] are the deformation potentials. C_4 and C_5 are the strength of the momentum dependent Dresselhaus-symmetric [52, 71] and Rashba-symmetric [53, 72] strain terms respectively. In our calculation, we use $C_4 = 5.0$ eV$\mathring{A}$ calculated from first principles [63] and $C_5 = C_4$ [33, 40]. We assume $\epsilon_{xz} = \epsilon_{yz} = 0$ and $\epsilon_{xx} = \epsilon_{yy}$. So the b term is given by

$$b\begin{pmatrix} Q & 0 & 0 & 0 \\ 0 & -Q & 0 & 0 \\ 0 & 0 & -Q & 0 \\ 0 & 0 & 0 & Q \end{pmatrix} \tag{4.18}$$

where

$$Q = \epsilon_{zz} - \frac{1}{2}(\epsilon_{xx} + \epsilon_{yy}). \tag{4.19}$$

And we have one more relation

$$\epsilon_{zz} = -\frac{(\epsilon_{xx} + \epsilon_{yy})C_{12}}{C_{11}}. \tag{4.20}$$

For GaAs, $C_{11} = 122.1$ GPa, $C_{12} = 56.6$ GPa. Then using relation

$$\begin{aligned} \{J_x, J_y\} &= \frac{1}{2}(J_xJ_y + J_yJ_x) \\ &= \frac{1}{2}\begin{pmatrix} 0 & -i\sqrt{3} & 0 & 0 \\ i\sqrt{3} & 0 & 0 & 0 \\ 0 & 0 & 0 & -i\sqrt{3} \\ 0 & 0 & i\sqrt{3} & 0 \end{pmatrix}, \end{aligned} \tag{4.21}$$

the d term can be written as

$$\begin{pmatrix} 0 & -id\epsilon_{xy} & 0 & 0 \\ id\epsilon_{xy} & 0 & 0 & 0 \\ 0 & 0 & 0 & -id\epsilon_{xy} \\ 0 & 0 & id\epsilon_{xy} & 0 \end{pmatrix}. \tag{4.22}$$

And C_4, C_5 terms are

$$-C_4(\epsilon_{xx} - \epsilon_{zz}) \begin{pmatrix} 0 & 0 & \frac{\sqrt{3}(k_x+ik_y)}{2} & 0 \\ 0 & 0 & k_x - ik_y & \frac{\sqrt{3}(k_x+ik_y)}{2} \\ \frac{\sqrt{3}(k_x-ik_y)}{2} & k_x + ik_y & 0 & 0 \\ 0 & \frac{\sqrt{3}(k_x-ik_y)}{2} & 0 & 0 \end{pmatrix}, \tag{4.23}$$

and

$$-C_5\epsilon_{xy} \begin{pmatrix} 0 & 0 & \frac{\sqrt{3}(k_y+ik_x)}{2} & 0 \\ 0 & 0 & k_y - ik_x & \frac{\sqrt{3}(k_y+ik_x)}{2} \\ \frac{\sqrt{3}(k_y-ik_x)}{2} & k_y + ik_x & 0 & 0 \\ 0 & \frac{\sqrt{3}(k_y-ik_x)}{2} & 0 & 0 \end{pmatrix}. \tag{4.24}$$

Adding all terms together, the matrix form of the strain Hamiltonian is obtained.

Since all the details of our simulation Hamiltonian have been given, we are able to diagonalize the Hamiltonian and calculate the SOT. The out-of-plane SOT study has been reported earlier to explain the experimental observation on $Ga_{1-x}Mn_xAs$ [34]. They primarily focus on the inter band term. We are going to study SOT systematically in this project to understand the parameter dependence, impact of complex band structure, and the analogy with the 2DEG Rashba model [54].

4.3 Numerical results

Here we use a slightly different notation since we are dealing with a 3D sample. We decompose the SOT effective fields into components parallel to the magnetization $\vec{M}$, and components perpendicular to $\vec{M}$. So the effective field $\vec{h}$ can be written as

$$\vec{h} = h_m \vec{M} + h_{\parallel} \hat{e}_{\parallel} + h_{\perp} \hat{e}_{\perp}, \tag{4.25}$$

where $\hat{e}_{\parallel}, \hat{e}_{\perp}$ are the unit vectors perpendicular to $\vec{M}$, $\hat{e}_{\parallel}$ is within the sample plane, and $\hat{e}_{\perp}$ is perpendicular to the sample plane. The h_m component has no contribution to the torques. So we don't consider this component in our calculation. For all the following simulation, we assume an electric field of $E = 0.02$ V/nm along the x axis. The hole concentration is between 0.3 and 1 nm^{-3}, and the Fermi energy is determined by the corresponding hole density.

4.3.1 Intrinsic versus extrinsic SOT: disorder effect

As seen in the 2DEG FM model, we have an out-of-plane intrinsic SOT, which means it is independent of disorder. For the in-plane components, the intra band and inter band have $1/\Gamma$ and Γ dependence respectively for both small and large exchange limits. These components are called extrinsic because they depend on the disorder broadening. Do we have similar Γ dependence in $Ga_{1-x}Mn_xAs$?

Figure 4.4 shows the SOT as a function of the energy broadening Γ. Although Γ is on the order of hundreds of meV in realistic $Ga_{1-x}Mn_xAs$, we choose $\Gamma < 10$ meV in order to compare with the analytical result in the 2DEG FM model. The intra band contribution to the SOT field, $h_{\parallel}^{intra}$, is inversely proportional to Γ for all hole densities as is seen in figure 4.4(a), which agrees with the the Rashba 2DEG FM. The inset of figure 4.4(a) shows that this relation works well for large Γ. As in the 2DEG

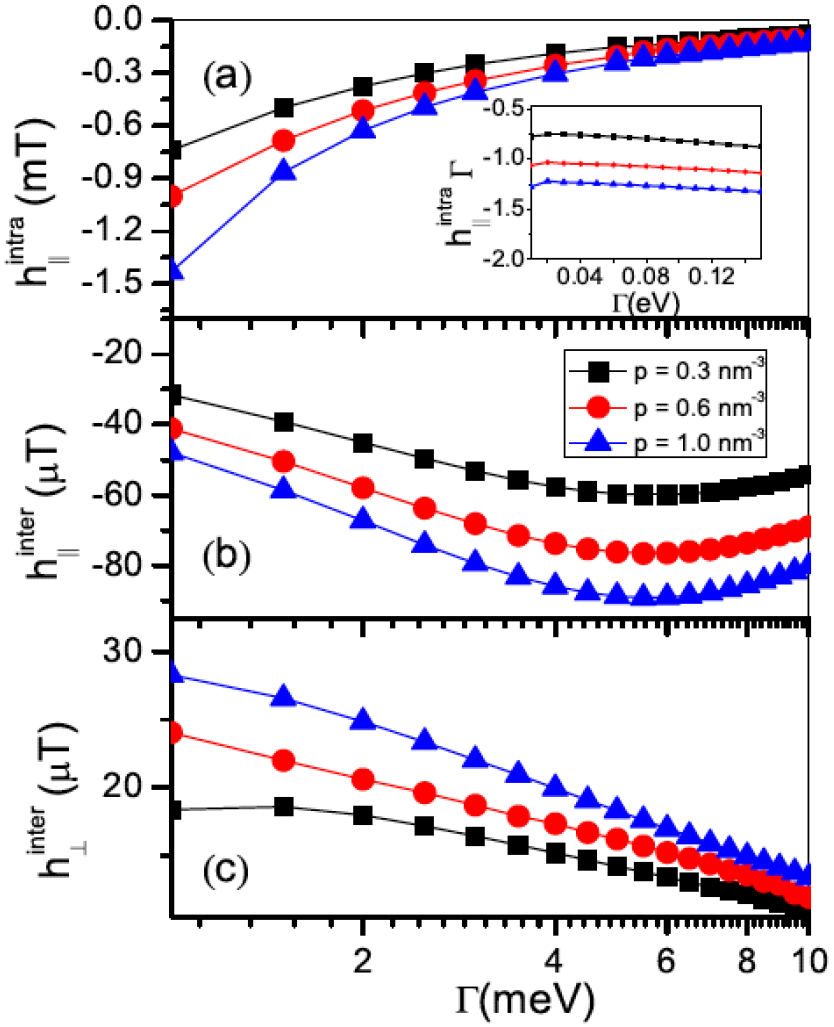

Figure 4.4: (a) Intra band and (b), (c) inter band SOT effective fields as a function of Γ.

FM, no $h_{\perp}^{intra}$ component exists. On the other hand, the inter band contributes to both $h_{\parallel}^{intra}$ and $h_{\perp}^{intra}$, which is shown in figure 4.4(b) and 4.4(c). The former scales as $h_{\parallel}^{inter} \propto \Gamma$ in the weak scattering limit which is consistent with the 2DEG FM.The out-of plane component $h_{\perp}^{inter}$ converges to a finite value when Γ vanishes, indicating the intrinsic character of this component. All these results are consistent with the analytical solutions obtained in in the Rashba 2DEG FM model and weak scattering limit.

From these results, we see that the complex band structure of $Ga_{1-x}Mn_xAs$ doesn't affect the SOT qualitatively. The intrinsic out-of-plane SOT is consistent with previous studies [34].

4.3.2 Impact of the band structure

The Hamiltonian to describe the GaAs is Kohn-Luttinger Hamiltonian. As shown in equation 4.6, this Hamiltonian has centrosymmetric and noncentrosymmetric components. The first term in the right hand side of equation 4.6 has parabolic form. The second term has spherical symmetry. And the third term is noncentrosymmetric. By tuning the Luttinger parameters $\gamma_1, \gamma_2, \gamma_3$, we are able to study the effects of these three terms separately.

Table 4.1: Symmetry of the Hamiltonian

Symmetry	Parameters
Parabolic	$\gamma_1 = 2.00, \gamma_2 = 0.00, \gamma_3 = 0.00$
Spherical	$\gamma_1 = 6.98, \gamma_2 = 2.50, \gamma_3 = 2.50$
Diamond	$\gamma_1 = 6.98, \gamma_2 = 2.06, \gamma_3 = 2.93$

As shown in table 4.1, we model three cases: (i) the parabolic band approximation where no centrosymmetric spin-orbit coupling is present, (ii) the spherical

approximation where the cenrosymmetric spin-orbit coupling is turned on but only contains the spherical symmetric part, and (iii) the diamond crystal where the original Luttinger parameters are used. The reason we call it the diamond crystal is because we have ignored the cubic Dresselhaus spin-orbit coupling due to bulk inversion asymmetry. There is no experimental indication that this cubic term contributes significantly to the SOT. So the Kohn-Luttinger Hamiltonian has bulk inversion symmetry as in the diamond crystal case. Figure 4.5 shows the angular dependence of the SOT in the approximation of (i)-(iii). The magnetization is in the (x, y) plane $\theta = \pi/2$, and its direction is given by angle ϕ. We have changed the magnitudes to similar order.

As shown in this figure, all three approximations have roughly $\sin\phi$ dependence for these three components. The parabolic approximation gives perfect $\sin\phi$ dependence. In the spherical approximation, the inter band component deviates from this dependence, while the intra band term remains unaffected. Furthermore, the magnitudes of intra band and inter band SOT strongly decrease, which manifests the competition between the strain-induced spin-orbit coupling and the centrosymmetric Luttinger spin-orbit coupling terms. When the spherical approximation is lifted, the band structures become warped. This results in an increase of the inter band SOT and an additional angular dependence on top of the $\sin\phi$ dependence.

4.4 Summary

In this chapter, we have discussed the spin-orbit torques in $Ga_{1-x}Mn_xAs$ ferromagnetic semiconductor. We have studied the parameter dependence and the impact of complex band structures. The SOT results in the more realistic model following the same qualitative trends as in the case of the simple Rashba 2D FM model. The impact of complex band structures give rise to more feathers in the SOT results. The

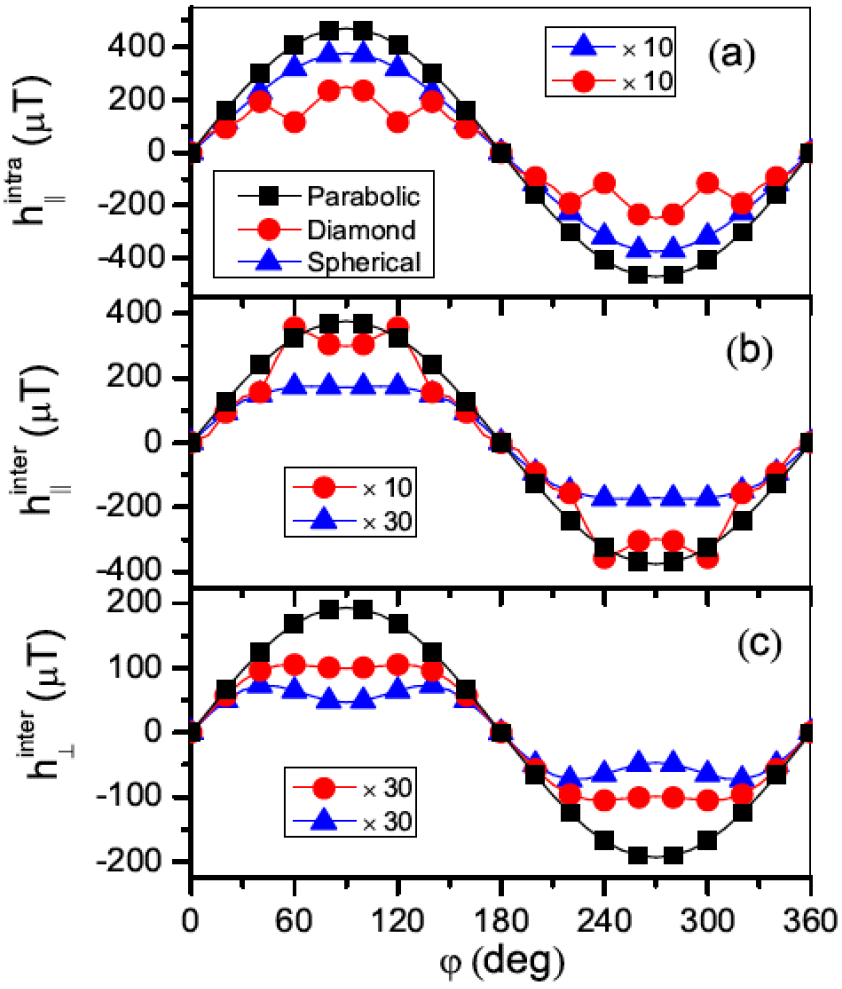

Figure 4.5: (a) Intra band and (b), (c) inter band SOT effective fields as a function of the magnetization direction using different approximations.

change of the magnitudes of the SOT unveils the competition between band structure and spin-orbit coupling with different symmetries. To conclude, SOT effects exist in this realistic material and can be used for current-induced magnetization switching.

5. SPIN-ORBIT TORQUES IN 2D ANTIFERROMAGNETIC SYSTEM*

5.1 Introductions to antiferrogmantes

We have studied the spin-orbit torque effects in ferromagnets systematically in the previous chapters. As we know, there is another category of magnetic materials called antiferromagnets. Antiferromagnets (AFM) are attractive building blocks of spintronics devices because they are insensitive to magnetic field perturbation, produce no perturbing stray fields, and are readily compatible with metal, semiconductor, or insulator electronic structure. They can also act as magnetic memory because they can generate large magneto transport effects [73, 74, 75, 76]. A natural question is whether we have similar effects in AFM. Experiments on the Mn_2Au AFM show that a field-like spin-orbit torque exists in this system [77, 78]. Unlike ferromagnets, AFM usually have more than one sub lattice magnetization which add up to zero total magnetization [79, 80, 81]. Although the simple picture for SOT in ferromagnets doesn't work in this case, if we project the SOT into sub lattices, we expect meaningful results [55].

To describe AFM, we consider the simplest case with two sub lattices. $\vec{m}_A, \vec{m}_B$ represent the sub lattice magnetizations. And we have two relations

$$\vec{M} = \vec{m}_A + \vec{m}_B \approx 0, \tag{5.1}$$

and

$$\vec{n} = \vec{m}_A - \vec{m}_B \approx 2\vec{m}_A, \tag{5.2}$$

*Reprinted with permission from J. Zelezny, H. Gao, K. Vyborny, J. Zemen, J. Masek, Aurelien Manchon, J. Wunderlich, Jairo Sinova, and T. Jungwirth, Phys. Rev. Lett. **113,** 157201 (2014). Copyright 2014 by the American Physical Society.

where $\vec{M}$ is called the magnetization and $\vec{n}$ is called the Neel vector. The dynamics of these parameters are coupled differential equations [82].

The AFM Neel vector direction can be controlled indirectly by a magnetic field via an attached exchanged-coupled FM [74, 75] or, without the auxiliary FM, by techniques analogous to heat-assisted magnetic recording [76]. However, as with heat-assisted FM MRAMs [83, 84], the speed and energy efficiency of this method are limited. The SOT effects provide us a novel mechanism for AFM spin-arid reorientation by a lateral electrical current via Neel-order SOT fields, i.e., via non-equilibrium fields that alternate in sign between the two spin sub lattices [55],

In this chapter, we will study the static SOT effects in the AFM with a 2D model. The systematic study of dynamics will be left for further research.

5.2 Hamiltonian of the 2D AFM: Four bands model

We start with a simple model by assuming that the underlying lattice is a 2D square lattice with local moments on each lattice sites. As shown in figure 5.1, these local moments interact with each other antiferromagnetically to form sub lattice magnetization which is treated as static background since we only consider the static effective field. The carriers are treated by using tight-binding model. We consider the nearest and next nearest neighbor hopping and the exchange interaction between carrier spins and local moments. Also, we'll incorporate the Rashba spin orbit interaction in this 2D system. The total Hamiltonian reads:

$$H = \sum_{<ij>} J_{dd}\vec{S_i} \cdot \vec{S_j} + H^{tb} + \sum_i J_{sd}\vec{s} \cdot \vec{S_i} + H_R, \tag{5.3}$$

where J_{dd} and J_{sd} are the exchange constants, H^{tb} is the tight-binding Hamiltonian for the carriers with both nearest and next nearest neighbor hopping, and H_R is the

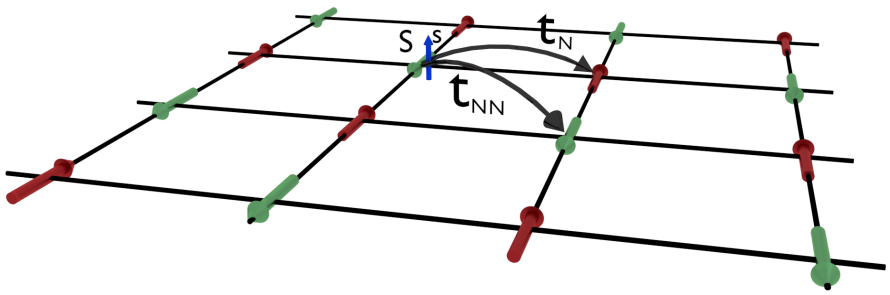

Figure 5.1: 2D antiferromagnetic square lattice structure.

Rashba spin-orbit interaction in 2D system. It is given by formula

$$H_R = \frac{\alpha}{\hbar}(\sigma_x p_y - \sigma_y p_x) \tag{5.4}$$

where α is the strength of the Rashba spin-orbit coupling. The antiferromagnetic background can be ignored and the *sd* exchange interaction are treated as onsite energies. In the tight-binding scheme, H^{tb} is given by:

$$H^{tb} = -t_N \sum_{<ij>_N \sigma} c^\dagger_{i\sigma} c_{j\sigma} - t_{NN} \sum_{<ij>_{NN} \sigma} c^\dagger_{i\sigma} c_{j\sigma}, \tag{5.5}$$

where t_N and t_{NN} are the nearest and next nearest neighbor hopping parameters respectively, and σ is spin index. The onsite energy is written as

$$H_{sd} = \sum_{i\sigma\sigma'} \frac{1}{2} J_{sd} \vec{S}_i \cdot (\vec{\sigma})_{\sigma\sigma'} c^\dagger_{i\sigma} c_{i\sigma'}, \tag{5.6}$$

where $\vec{\sigma}$ is the Pauli matrices vector, carrier spin is $\vec{s} = \frac{1}{2}\vec{\sigma}$ ($\hbar$ is absorbed in J_{sd}), and the $\vec{S_i}$ change sign if they are on nearest neighbors which capture the antiferromagnetism in the system. The Rashba spin-orbit interaction in 2D system is given by [85], (see also Appendix B)

$$H_R = V_{SO}\sum_i[(c^\dagger_{i\uparrow}c_{i+\delta_x\downarrow} - c^\dagger_{i\downarrow}c_{i+\delta_x\uparrow}) - i(c^\dagger_{i\uparrow}c_{i+\delta_y\downarrow} + c^\dagger_{i\downarrow}c_{i+\delta_y\uparrow}) + \text{H.c.}]. \tag{5.7}$$

Here, $V_{SO} = \alpha/2a$ represents the spin-orbit coupling strength, and δ_x,δ_y are the nearest neighbors in the x and y direction. So, the total Hamiltonian is

$$\begin{aligned} H &= \sum_i \frac{1}{2}J_{sd}\vec{S_i}\cdot(\vec{\sigma})_{\sigma\sigma'}c^\dagger_{i\sigma}c_{i\sigma'} - t_N\sum_{<ij>_N\sigma} c^\dagger_{i\sigma}c_{j\sigma} - t_{NN}\sum_{<ij>_{NN}\sigma} c^\dagger_{i\sigma}c_{j\sigma} \\ &\quad + V_{SO}\sum_i[(c^\dagger_{i\uparrow}c_{i+\delta_x\downarrow} - c^\dagger_{i\downarrow}c_{i+\delta_x\uparrow}) - i(c^\dagger_{i\uparrow}c_{i+\delta_y\downarrow} + c^\dagger_{i\downarrow}c_{i+\delta_y\uparrow}) + \text{H.c.}]. \end{aligned} \tag{5.8}$$

This model can be studied by either finite-size supercell method or Bloch theory. In the case without disorder, this model is treated in the frame of the Bloch energy band theory. The unit vector is defined as $\vec{a}_1 = (a, -a)$ and $\vec{a}_2 = (a, a)$. See figure 5.2. For later convenience, we change our coordinates such that $\vec{a}_1 \equiv \sqrt{2}a\hat{x}, \vec{a}_2 \equiv \sqrt{2}a\hat{y}$. There are two atoms in each unit cell, which are denoted by A and B with positions $\vec{r}_A = (0,0)$ and $\vec{r}_B = \frac{a}{\sqrt{2}}(1,1)$ within the unit cell. We label the creation and annihilation operator on atom A by $(c^\dagger, c)$, and on atom B by $(d^\dagger, d)$ respectively. The Hamiltonian can be written as

$$\begin{aligned} H &= \sum_i \frac{1}{2}J_{sd}\vec{S_{i_A}}\cdot(\vec{\sigma})_{\sigma\sigma'}c^\dagger_{i\sigma}c_{i\sigma'} + \sum_i \frac{1}{2}J_{sd}\vec{S_{i_B}}\cdot(\vec{\sigma})_{\sigma\sigma'}d^\dagger_{i\sigma}d_{i\sigma'} \\ &\quad -t_N\sum_{<ij>_N\sigma} c^\dagger_{i\sigma}d_{j\sigma} - t_N\sum_{<ij>_N\sigma} d^\dagger_{i\sigma}c_{j\sigma} \end{aligned} \tag{5.9}$$

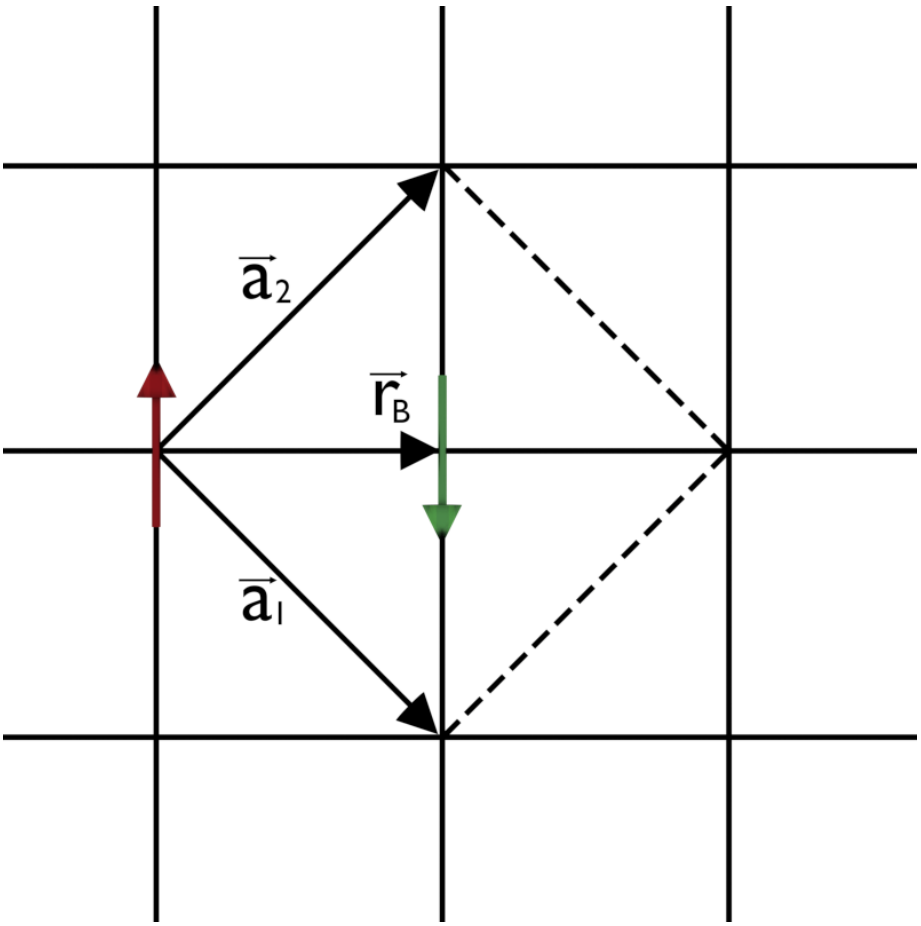

Figure 5.2: Unit vectors and unit cell of the 2D antiferromagnetic square lattice structure.

$$
\begin{aligned}
&-t_{NN}\sum_{<ij>_{NN}\sigma} c^{\dagger}_{i\sigma}c_{j\sigma} - t_{NN}\sum_{<ij>_{NN}\sigma} d^{\dagger}_{i\sigma}d_{j\sigma} \\
&+ V_{SO}\sum_{i}\{(c^{\dagger}_{i\uparrow}d_{i\downarrow} - c^{\dagger}_{i\downarrow}d_{i\uparrow}) - i(c^{\dagger}_{i\uparrow}d_{i-\delta_x\downarrow} + c^{\dagger}_{i\downarrow}d_{i-\delta_x\uparrow}) \\
&\qquad + (-c^{\dagger}_{i\uparrow}d_{i-\delta_x-\delta_y\downarrow} + c^{\dagger}_{i\downarrow}d_{i-\delta_x-\delta_y\uparrow}) + i(c^{\dagger}_{i\uparrow}d_{i-\delta_y\downarrow} + c^{\dagger}_{i\downarrow}d_{i-\delta_y\uparrow})\} \\
&+ V_{SO}\sum_{i}\{c \leftrightarrow d\}
\end{aligned}
$$

where the summation i is over the unit cell. Then, we do the transformation

$$
c_{i\sigma} = \frac{1}{\sqrt{N}}\sum_{\vec{k}} e^{i\vec{k}\cdot\vec{R}_i}c_{\vec{k}\sigma} \tag{5.10}
$$

and

$$
d_{i\sigma} = \frac{1}{\sqrt{N}}\sum_{\vec{k}} e^{i\vec{k}\cdot(\vec{R}_i+\vec{r}_B)}d_{\vec{k}\sigma} \tag{5.11}
$$

Here, we don't write out $\vec{r}_A = (0,0)$ explicitly. Using the relation

$$
\frac{1}{N}\sum_{\vec{R}_i} e^{i(\vec{k}-\vec{k}')\cdot\vec{R}_i} = \delta_{\vec{k}\vec{k}'}, \tag{5.12}
$$

the Hamiltonian can be written as:

$$
\begin{aligned}
H \;=\; & \sum_{\vec{k}}\frac{1}{2}J_{sd}\vec{S}\cdot(\vec{\sigma})_{\sigma\sigma'}c^{\dagger}_{\vec{k}\sigma}c_{\vec{k}\sigma'} - \sum_{\vec{k}}\frac{1}{2}J_{sd}\vec{S}\cdot(\vec{\sigma})_{\sigma\sigma'}d^{\dagger}_{\vec{k}\sigma}d_{\vec{k}\sigma'} \\
& -t_N\sum_{\vec{k}\sigma} 4\cos(\frac{k_xa}{\sqrt{2}})\cos(\frac{k_ya}{\sqrt{2}})(c^{\dagger}_{\vec{k}\sigma}d_{\vec{k}\sigma} + d^{\dagger}_{\vec{k}\sigma}c_{\vec{k}\sigma}) \\
& -t_{NN}\sum_{\vec{k}\sigma} 2[\cos(\sqrt{2}k_xa) + \cos(\sqrt{2}k_ya)](c^{\dagger}_{\vec{k}\sigma}c_{\vec{k}\sigma} + d^{\dagger}_{\vec{k}\sigma}d_{\vec{k}\sigma}) \\
& + V_{SO}\sum_{\vec{k}}\{2[\sin(\frac{-k_xa}{\sqrt{2}} + \frac{k_ya}{\sqrt{2}}) + i\sin(\frac{k_xa}{\sqrt{2}} + \frac{k_ya}{\sqrt{2}})]c^{\dagger}_{\vec{k}\uparrow}d_{\vec{k}\downarrow} \\
& \qquad + 2[\sin(\frac{-k_xa}{\sqrt{2}} + \frac{k_ya}{\sqrt{2}}) - i\sin(\frac{k_xa}{\sqrt{2}} + \frac{k_ya}{\sqrt{2}})]c^{\dagger}_{\vec{k}\downarrow}d_{\vec{k}\uparrow} + \text{H.c.}\}
\end{aligned} \tag{5.13}
$$

where we have considered the direction of magnetization for sub-lattices explicitly.

This Hamiltonian can be written in the form of a matrix. We define a vector $\phi = (c_{\vec{k}\uparrow}, c_{\vec{k}\downarrow}, d_{\vec{k}\uparrow}, d_{\vec{k}\downarrow})^T$. Then

$$H = \sum_{\vec{k}} \phi^\dagger M \phi \tag{5.14}$$

where

$$M = \begin{pmatrix} h_z - 2t_{NN}(\cos(\sqrt{2}k_x a) + \cos(\sqrt{2}k_y a)) & h_x - ih_y \\ h_x + ih_y & -h_z - 2t_{NN}(\cos(\sqrt{2}k_x a) + \cos(\sqrt{2}k_y a)) \\ -4t_N \cos(\frac{k_x a}{\sqrt{2}}) \cos(\frac{k_y a}{\sqrt{2}}) & 2V_{SO}(\sin(\frac{-k_x a + k_y a}{\sqrt{2}}) + i \sin(\frac{k_x a + k_y a}{\sqrt{2}})) \\ 2V_{SO}(\sin(\frac{-k_x a + k_y a}{\sqrt{2}}) - i \sin(\frac{k_x a + k_y a}{\sqrt{2}})) & -4t_N \cos(\frac{k_x a}{\sqrt{2}}) \cos(\frac{k_y a}{\sqrt{2}}) \end{pmatrix}$$

$$\begin{pmatrix} -4t_N \cos(\frac{k_x a}{\sqrt{2}}) \cos(\frac{k_y a}{\sqrt{2}}) & 2V_{SO}(\sin(\frac{-k_x a + k_y a}{\sqrt{2}}) + i \sin(\frac{k_x a + k_y a}{\sqrt{2}})) \\ 2V_{SO}(\sin(\frac{-k_x a + k_y a}{\sqrt{2}}) - i \sin(\frac{k_x a + k_y a}{\sqrt{2}})) & -4t_N \cos(\frac{k_x a}{\sqrt{2}}) \cos(\frac{k_y a}{\sqrt{2}}) \\ -h_z - 2t_{NN}(\cos(\sqrt{2}k_x a) + \cos(\sqrt{2}k_y a)) & -h_x + ih_y \\ -h_x - ih_y & h_z - 2t_{NN}(\cos(\sqrt{2}k_x a) + \cos(\sqrt{2}k_y a)) \end{pmatrix} \tag{5.15}$$

Here, $\vec{h} = J_{sd}\vec{S}/2$. We can obtain the band structure by diagonalizing the 4×4 matrix for different $\vec{k}$.

It can be shown that the finite-size supercell method give the same DOS curve in certain limit. And the advantage of the supercell method is the ability of dealing with disorder more realistically. In the first step, we'll focus on Bloch theory method in the clean limit.

5.3 Numerical simulations

In this section, we'll discuss the details of numerical simulation. First, we'll discuss the matrix elements of spin operator and velocity operator between two eigenvectors and how to get the site resolved values of the spin operator. Then, we'll explicitly work out the results in the four band model.

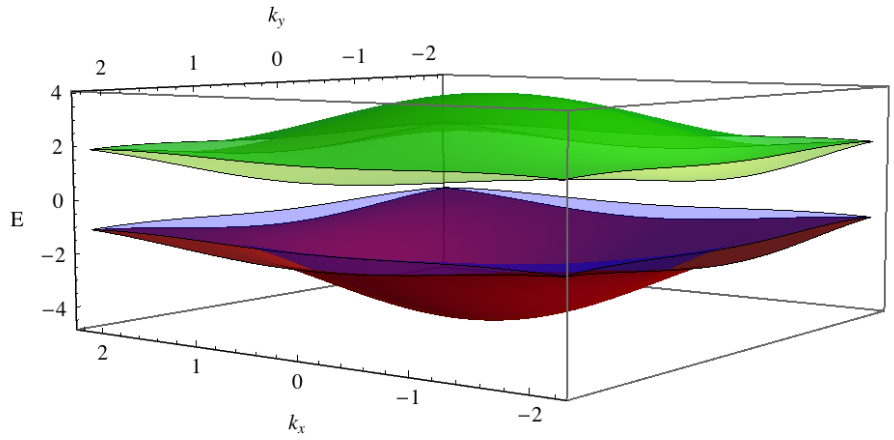

Figure 5.3: Typical 3D plot of the band structures (four bands) with parameters $t_N = 1eV, t_{NN} = 0.1eV, V_{SO} = 0.1eV$ and $h_z = 1.5eV$.

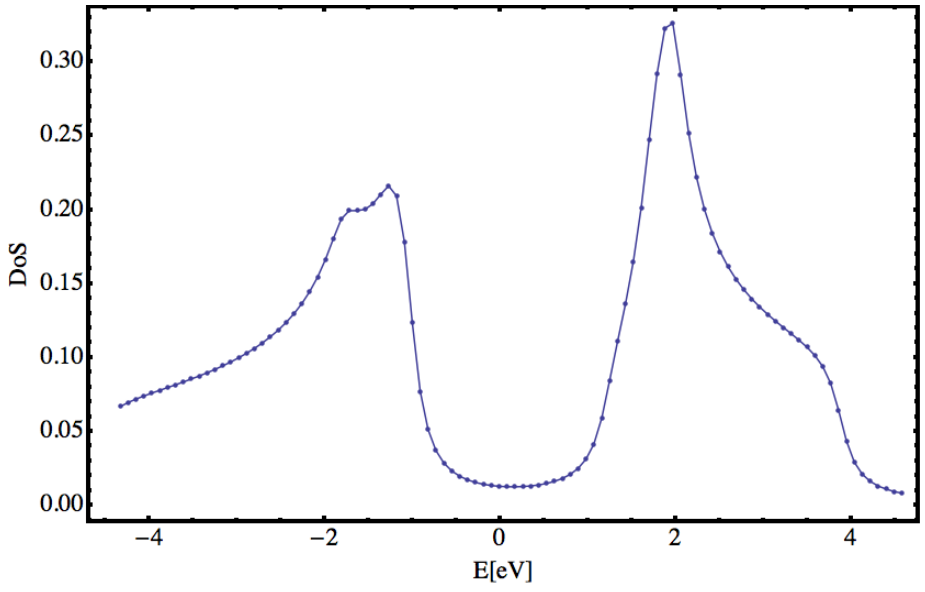

Figure 5.4: Total DOS plot with the parameters in the band structure calculation in Fig. 5.3.

5.3.1 Spin and current operator

In order to use the Kubo formula given in the previous chapter, we need to find out the expectation value of spin operator and current operator within tight-binding scheme. After diagonalizing the Hamiltonian, the eigenvector has form $\Phi^{(\alpha)} = ((\phi^{(\alpha)}_{1\uparrow}, \phi^{(\alpha)}_{1\downarrow}), (\phi^{(\alpha)}_{2\uparrow}, \phi^{(\alpha)}_{2\downarrow}), \cdots, (\phi^{(\alpha)}_{i\uparrow}, \phi^{(\alpha)}_{i\downarrow}), \cdots)^T$. So the expectation value for the spin operator is given by

$$(\vec{s})_{\alpha\beta} = \frac{1}{2}\sum_i ((\phi^{(\alpha)}_{i\uparrow}, \phi^{(\alpha)}_{i\downarrow})^T)^\dagger (\vec{\sigma})(\phi^{(\beta)}_{i\uparrow}, \phi^{(\beta)}_{i\downarrow})^T, \tag{5.16}$$

where the summation is over all lattice sites. When we simulate the non-equilibrium spin polarization in anti-ferromagnets, we need the resolved site results in order to capture the effects of SOT on different sub lattices. This is easy to realize using the linear response formula. Instead of summing over all the sites i, we sum over different sites corresponding to different sub lattices separately.

$$(\vec{s})^A_{\alpha\beta} = \frac{1}{2}\sum_{i\in A} ((\phi^{(\alpha)}_{i\uparrow}, \phi^{(\alpha)}_{i\downarrow})^T)^\dagger (\vec{\sigma})(\phi^{(\beta)}_{i\uparrow}, \phi^{(\beta)}_{i\downarrow})^T \tag{5.17}$$

$$(\vec{s})^B_{\alpha\beta} = \frac{1}{2}\sum_{i\in B} ((\phi^{(\alpha)}_{i\uparrow}, \phi^{(\alpha)}_{i\downarrow})^T)^\dagger (\vec{\sigma})(\phi^{(\beta)}_{i\uparrow}, \phi^{(\beta)}_{i\downarrow})^T, \tag{5.18}$$

where A, B correspond to A, B sub lattices. By doing this, we'll get site resolved non-equilibrium spin polarization.

Then, we'll derive the current operators.

$$v_x = \frac{1}{\hbar}\frac{\partial H}{\partial k_x} = \frac{\hbar k_x}{m} - \frac{\alpha}{\hbar}\sigma_y \tag{5.19}$$

$$v_y = \frac{1}{\hbar}\frac{\partial H}{\partial k_y} = \frac{\hbar k_y}{m} + \frac{\alpha}{\hbar}\sigma_x \tag{5.20}$$

and the current density operator can be written as

$$j_x = -\frac{i\hbar}{2m}(\psi^\dagger \partial_x \psi - \partial_x \psi^\dagger \psi) - \frac{\alpha}{\hbar}\psi^\dagger \sigma_y \psi \tag{5.21}$$

$$j_y = -\frac{i\hbar}{2m}(\psi^\dagger \partial_y \psi - \partial_y \psi^\dagger \psi) + \frac{\alpha}{\hbar}\psi^\dagger \sigma_x \psi. \tag{5.22}$$

Then, we express the corresponding operator in the tight-binding model, and we get the current operator

$$\vec{J} = \vec{J}_0 + \vec{J}_R, \tag{5.23}$$

where

$$\vec{J}_0 = \frac{1}{i\hbar}[-t_N \sum_{<ij>_N \sigma} (\vec{R}_i - \vec{R}_j) c^\dagger_{i\sigma} c_{j\sigma} - t_{NN} \sum_{<ij>_{NN} \sigma} (\vec{R}_i - \vec{R}_j) c^\dagger_{i\sigma} c_{j\sigma}], \tag{5.24}$$

with $\vec{R}_i$ the lattice vectors, and

$$\vec{J}_{Rx} = \frac{i\alpha}{\hbar} \sum_i (c^\dagger_{i\uparrow} c_{i\downarrow} - c^\dagger_{i\downarrow} c_{i\uparrow}) \tag{5.25}$$

$$\vec{J}_{Ry} = \frac{\alpha}{\hbar} \sum_i (c^\dagger_{i\uparrow} c_{i\downarrow} + c^\dagger_{i\downarrow} c_{i\uparrow}). \tag{5.26}$$

So, the expectation value of the current operator (which is the same as velocity operator) is given by the corresponding combination of eigenvector elements. For example:

$$(\vec{J}_{Rx})_{\alpha\beta} = \frac{i\alpha}{\hbar} \sum_i (\phi^{(\alpha)*}_{i\uparrow} \phi^{(\beta)}_{i\downarrow} - \phi^{(\alpha)*}_{i\downarrow} \phi^{(\beta)}_{i\uparrow}); \tag{5.27}$$

$$(\vec{J}_{Ry})_{\alpha\beta} = \frac{\alpha}{\hbar} \sum_i (\phi^{(\alpha)*}_{i\uparrow} \phi^{(\beta)}_{i\downarrow} + \phi^{(\alpha)*}_{i\downarrow} \phi^{(\beta)}_{i\uparrow}). \tag{5.28}$$

These are the relations needed in the numerical simulation using the Kubo formula.

5.3.2 Spin and current operator in four bands model

In the four band model, $\vec{k}$ is a good quantum number, and the Hamiltonian matrix is 4×4. The spin operator is simply given by

$$(\vec{s})_{\alpha\beta} = \frac{1}{2} \sum_{i=A,B} ((\phi_{i\uparrow}^{(\alpha)}, \phi_{i\downarrow}^{(\alpha)})^T)^\dagger (\vec{\sigma}) (\phi_{i\uparrow}^{(\beta)}, \phi_{i\downarrow}^{(\beta)})^T, \tag{5.29}$$

and the site resolved results are

$$(\vec{s})_{\alpha\beta}^A = \frac{1}{2} ((\phi_{A\uparrow}^{(\alpha)}, \phi_{A\downarrow}^{(\alpha)})^T)^\dagger (\vec{\sigma}) (\phi_{A\uparrow}^{(\beta)}, \phi_{A\downarrow}^{(\beta)})^T \tag{5.30}$$

$$(\vec{s})_{\alpha\beta}^B = \frac{1}{2} ((\phi_{B\uparrow}^{(\alpha)}, \phi_{B\downarrow}^{(\alpha)})^T)^\dagger (\vec{\sigma}) (\phi_{B\uparrow}^{(\beta)}, \phi_{B\downarrow}^{(\beta)})^T. \tag{5.31}$$

These results are $\vec{k}$ dependent, and in the last step we'll sum or integrate over the first Brillouin zone.

The current operator is more complicated. But we can follow the same procedure as we derive the four band Hamiltonian by writing:

$$\begin{aligned} \vec{J}_0 &= \frac{1}{i\hbar} [-t_N \sum_{<ij>_N \sigma} (\vec{R}_i - \vec{R}_j)(c_{i\sigma}^\dagger d_{j\sigma} + d_{i\sigma}^\dagger c_{j\sigma}) \\ &\quad -t_{NN} \sum_{<ij>_{NN} \sigma} (\vec{R}_i - \vec{R}_j)(c_{i\sigma}^\dagger c_{j\sigma} + d_{i\sigma}^\dagger d_{j\sigma})], \end{aligned} \tag{5.32}$$

and

$$\vec{J}_{Rx} = \frac{i\alpha}{\hbar} \sum_{i=A,B} [(c_{i\uparrow}^\dagger c_{i\downarrow} - c_{i\downarrow}^\dagger c_{i\uparrow}) + (d_{i\uparrow}^\dagger d_{i\downarrow} - d_{i\downarrow}^\dagger d_{i\uparrow})] \tag{5.33}$$

$$\vec{J}_{Ry} = \frac{\alpha}{\hbar} \sum_{i=A,B} [(c_{i\uparrow}^\dagger c_{i\downarrow} + c_{i\downarrow}^\dagger c_{i\uparrow}) + (d_{i\uparrow}^\dagger d_{i\downarrow} + d_{i\downarrow}^\dagger d_{i\uparrow})]. \tag{5.34}$$

Transform these equations to k-space. We have

$$\begin{aligned} J_x &= \frac{t_N a}{\hbar}\sum_{\vec{k}\sigma} 2\sin\left(\frac{k_x a}{\sqrt{2}}+\frac{k_y a}{\sqrt{2}}\right)(c^\dagger_{\vec{k}\sigma}d_{\vec{k}\sigma}+d^\dagger_{\vec{k}\sigma}c_{\vec{k}\sigma}) \\ &\quad \frac{t_{NN}a}{\hbar}\sum_{\vec{k}\sigma} 2[\sin(\sqrt{2}k_x a)+\sin(\sqrt{2}k_y a)](c^\dagger_{\vec{k}\sigma}c_{\vec{k}\sigma}+d^\dagger_{\vec{k}\sigma}d_{\vec{k}\sigma}) \\ &\quad + \frac{i2aV_{SO}}{\hbar}\sum_{\vec{k}}[(c^\dagger_{\vec{k}\uparrow}c_{\vec{k}\downarrow}+d^\dagger_{\vec{k}\uparrow}d_{\vec{k}\downarrow})+\text{H.c}] \end{aligned} \tag{5.35}$$

and

$$\begin{aligned} J_y &= \frac{t_N a}{\hbar}\sum_{\vec{k}\sigma} 2\sin\left(-\frac{k_x a}{\sqrt{2}}+\frac{k_y a}{\sqrt{2}}\right)(c^\dagger_{\vec{k}\sigma}d_{\vec{k}\sigma}+d^\dagger_{\vec{k}\sigma}c_{\vec{k}\sigma}) \\ &\quad \frac{t_{NN}a}{\hbar}\sum_{\vec{k}\sigma} 2[-\sin(\sqrt{2}k_x a)+\sin(\sqrt{2}k_y a)](c^\dagger_{\vec{k}\sigma}c_{\vec{k}\sigma}+d^\dagger_{\vec{k}\sigma}d_{\vec{k}\sigma}) \\ &\quad + \frac{2aV_{SO}}{\hbar}\sum_{\vec{k}}[(c^\dagger_{\vec{k}\uparrow}c_{\vec{k}\downarrow}+d^\dagger_{\vec{k}\uparrow}d_{\vec{k}\downarrow})+\text{H.c}]. \end{aligned} \tag{5.36}$$

Here, we assume the J_x direction is the same as $\vec{r}_B$ direction in Figure (5.2), not the same as k_x direction. So, when we calculate the value of the current operator sandwiched by two eigenvectors, we have

$$(J_x)_{\alpha\beta} = \phi^\dagger_\alpha \mathbf{J_x} \phi_\beta \tag{5.37}$$

and

$$(J_y)_{\alpha\beta} = \phi^\dagger_\alpha \mathbf{J_y} \phi_\beta \tag{5.38}$$

where the summation over $\vec{k}$ is dropped, and $\mathbf{J_x}$, $\mathbf{J_y}$ are given by matrices

$$\mathbf{J_x} = \frac{a}{\hbar}\begin{pmatrix} 2t_{NN}[\sin(\sqrt{2}k_x a)+\sin(\sqrt{2}k_y a)] & i2V_{SO} \\ -i2V_{SO} & 2t_{NN}[\sin(\sqrt{2}k_x a)+\sin(\sqrt{2}k_y a)] \\ 2t_N \sin\left(\frac{k_x a}{\sqrt{2}}+\frac{k_y a}{\sqrt{2}}\right) & 0 \\ 0 & 2t_N \sin\left(\frac{k_x a}{\sqrt{2}}+\frac{k_y a}{\sqrt{2}}\right) \end{pmatrix}$$

$$\begin{pmatrix} 2t_N \sin\left(\frac{k_x a}{\sqrt{2}}+\frac{k_y a}{\sqrt{2}}\right) & 0 \\ 0 & 2t_N \sin\left(\frac{k_x a}{\sqrt{2}}+\frac{k_y a}{\sqrt{2}}\right) \\ 2t_{NN}[\sin(\sqrt{2}k_x a)+\sin(\sqrt{2}k_y a)] & i2V_{SO} \\ -i2V_{SO} & 2t_{NN}[\sin(\sqrt{2}k_x a)+\sin(\sqrt{2}k_y a)] \end{pmatrix} \tag{5.39}$$

and

$$\mathbf{J_y} = \frac{a}{\hbar}\begin{pmatrix} 2t_{NN}[-\sin(\sqrt{2}k_x a)+\sin(\sqrt{2}k_y a)] & 2V_{SO} \\ 2V_{SO} & 2t_{NN}[-\sin(\sqrt{2}k_x a)+\sin(\sqrt{2}k_y a)] \\ 2t_N \sin\left(-\frac{k_x a}{\sqrt{2}}+\frac{k_y a}{\sqrt{2}}\right) & 0 \\ 0 & 2t_N \sin\left(-\frac{k_x a}{\sqrt{2}}+\frac{k_y a}{\sqrt{2}}\right) \end{pmatrix}$$

$$\begin{pmatrix} 2t_N \sin\left(-\frac{k_x a}{\sqrt{2}}+\frac{k_y a}{\sqrt{2}}\right) & 0 \\ 0 & 2t_N \sin\left(-\frac{k_x a}{\sqrt{2}}+\frac{k_y a}{\sqrt{2}}\right) \\ 2t_{NN}[-\sin(\sqrt{2}k_x a)+\sin(\sqrt{2}k_y a)] & 2V_{SO} \\ 2V_{SO} & 2t_{NN}[-\sin(\sqrt{2}k_x a)+\sin(\sqrt{2}k_y a)] \end{pmatrix} \tag{5.40}$$

Then, we can plug these relations into the Kubo formula and integrate over k-space to get the current induced non-equilibrium spin density.

5.4 Results of the 2D AFM model

5.4.1 Band structures and DOS

First, we'll show the band structures and DOS. The results are obtained from the four band model with parameters $t_N = 3.0eV, t_{NN} = 0.0, J_{sd}|S||s| = 1.0eV, V_{SO} = 0.1eV$. From the band structures, figure 5.5, we see a band gap around zero energy due to the exchange interaction. Near the Γ point, the lower bands are similar to the 2D Rashba electron gas. The splitting is due to Rashba spin-orbit coupling. Compared to the 2D FM system with two bands separated by the large exchange interaction, we have two groups of bands with two nearby bands in each group in the AFM system. The DOS are show in figure 5.6. The total DOS is the sum of all the four curves. The reason we show the DOS this way is that we can clearly show that there are four Von Hove singularities in this system. These singularities play important roles in the inter band contribution of the SOT.

Another useful DOS plot is the spin projected DOS. Like the local density of states, the spin projected DOS is defined as

$$\mathrm{DoS}_\sigma(E) = \sum_n \langle\phi_n|\sigma\rangle \langle\sigma|\phi_n\rangle \delta(E - E_n), \tag{5.41}$$

where $|\sigma\rangle$ is the eigenvectors of the spin operator. The eigenvectors of spin 1/2 electrons with arbitrary quantization direction (θ, ϕ) are given by [4]

$$|\uparrow\rangle = \begin{pmatrix} e^{-i\phi/2}\cos\left(\frac{\theta}{2}\right) \\ e^{i\phi/2}\sin\left(\frac{\theta}{2}\right) \end{pmatrix}, |\downarrow\rangle = \begin{pmatrix} -e^{-i\phi/2}\sin\left(\frac{\theta}{2}\right) \\ e^{i\phi/2}\cos\left(\frac{\theta}{2}\right) \end{pmatrix}. \tag{5.42}$$

For example, when sub lattice magnetization is in-plane and we want to project the spin in the direction of sub lattice magnetization, we need to set $\theta = \pi/2$. By

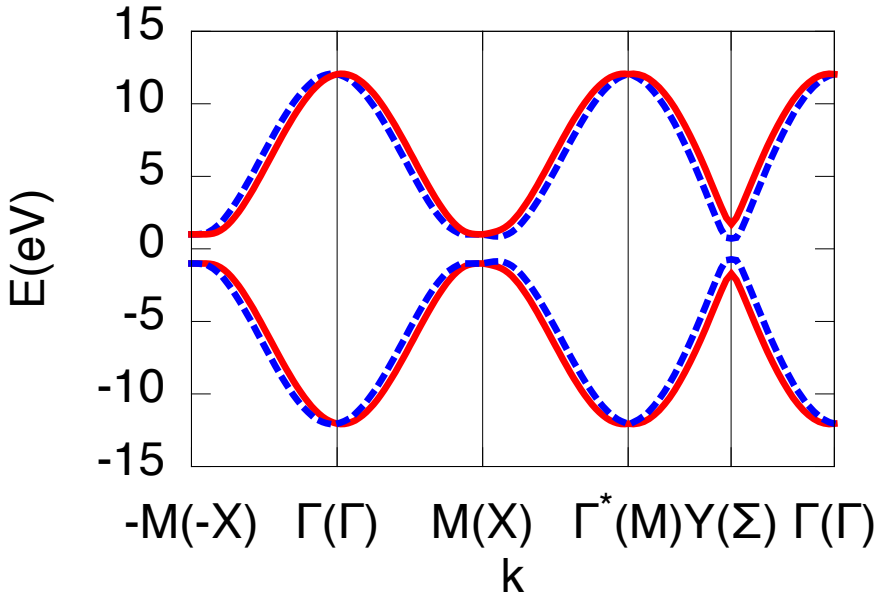

Figure 5.5: Band structures for the four band model with sub lattice magnetizations along the y-direction. Symbols in the bracket of the x-axis labels denote corresponding points in the Brillouin zone of the 2D ferromagnetic system. Different colors correspond to different signs of spin expectations along the y-direction.

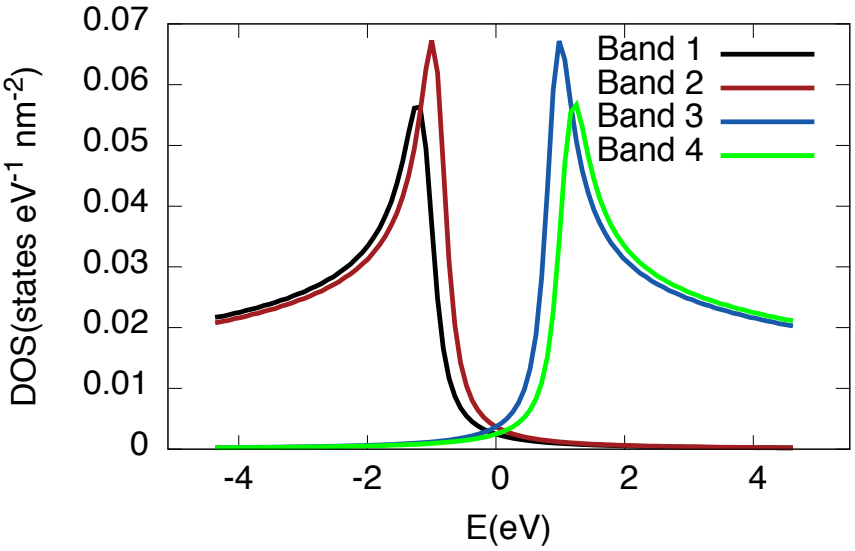

Figure 5.6: DOS plots. We have separated the DOS plots by the energies at each k points. Band 1 is formed by the lowest energy at each k point, and band 2 the second lowest energy, and so on.

doing this projection, the spin projected DOS is shown in figure 5.7. These curves clearly show that there is no net magnetization in equilibrium and the singularities correspond to the saddle points in the band structure curve.

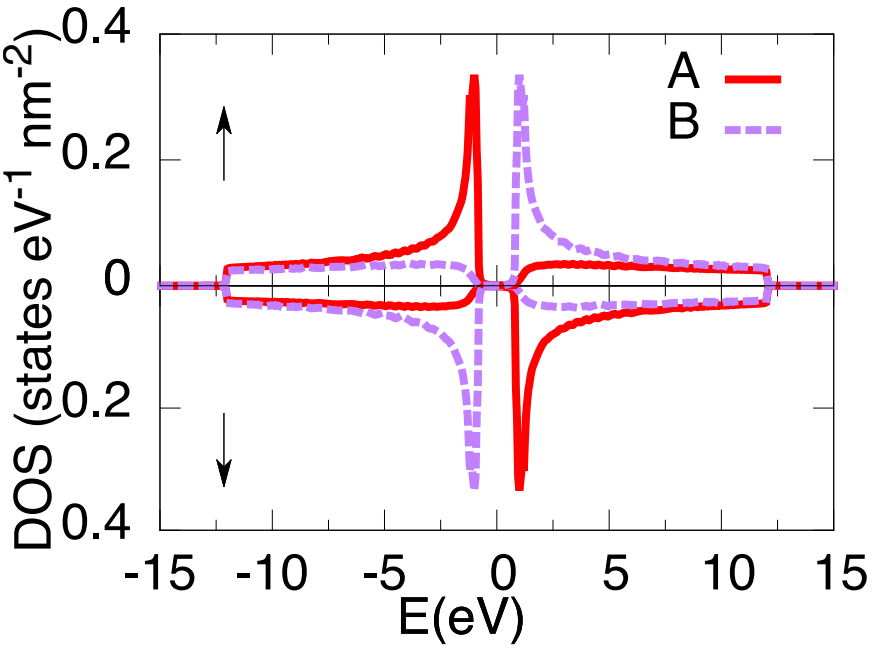

Figure 5.7: Spin projected DOS plots. A and B denote sub lattices.

5.4.2 DC conductivity

Experimentalists usually measure current density and find other quantities as a function of current density. To connect the electric field with current density, we need DC conductivity. Using the same Kubo linear response approach, the DC conductivity can be easily obtain by replacing the s operator with the current operator

or $e\vec{v}$. We have

$$\sigma_{ij} = \frac{\hbar}{2\pi L^2}\mathrm{Re}\sum_{\vec{k}\alpha\beta}(ev_i)_{\alpha\beta}(ev_j)_{\beta\alpha}[G^A_{\vec{k}\alpha}G^R_{\vec{k}\beta} - G^R_{\vec{k}\alpha}G^R_{\vec{k}\beta}]. \tag{5.43}$$

We will ignore the inter band contributions here because they are order of magnitudes smaller than the intra band contributions and we will also ignore the off-diagonal term. Then this formula can be simplified in the small spectral broadening (small Γ) limit as

$$\sigma_0 = \frac{1}{L^2}\sum_{\vec{k}\alpha}\frac{\hbar}{2\Gamma}(ev_x)_\alpha(ev_x)_\alpha\delta(E_{\vec{k}\alpha} - E_F). \tag{5.44}$$

Here, current and sub lattice magnetization are along the x-axis. Figure 5.8 shows the calculated DC conductivity as a function of Fermi energy. Zero results around zero energy corresponds to the gap of the system. Otherwise it is almost constant at other Fermi energies. We do see magneto-resistance in this system. It's of the order of $\sim 1\%$ here.

5.4.3 Spin-orbit torques

In this part, we show the main results of our study, current induced effective field or SOT. Again, we discuss the intra band and inter band contribution separately.

First, we study the in-plane (xy-plane) sub lattice magnetization case. To compare with experiments, we assume a 2D sample with thickness 10 nm in the z-direction and current density $10^5\mathrm{Acm}^{-2}$. The parameters we use are $t_N = 3.0eV, t_{NN} = 0.0eV, J_{sd} = 1.0eV, V_{SO} = 0.1eV, \Gamma = 0.01eV$ and $E_F = -6.0eV$. Figure 5.9 and 5.10 are the effective field projected to A and B sub lattice from intra band and inter band contributions respectively. All these components projected onto the A and B sub lattice have the same sign except the out-of-plane inter term which has opposite signs for A and B sub lattices in the in-plane sub lattice magnetization case. This

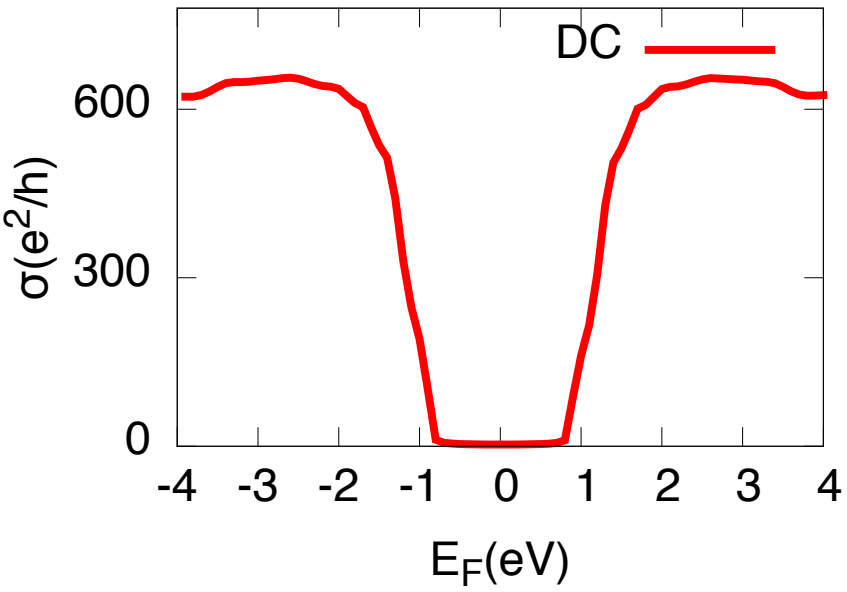

Figure 5.8: DC conductivity as a function of the Fermi energy. The parameters are the same as the previous band structure calculation.

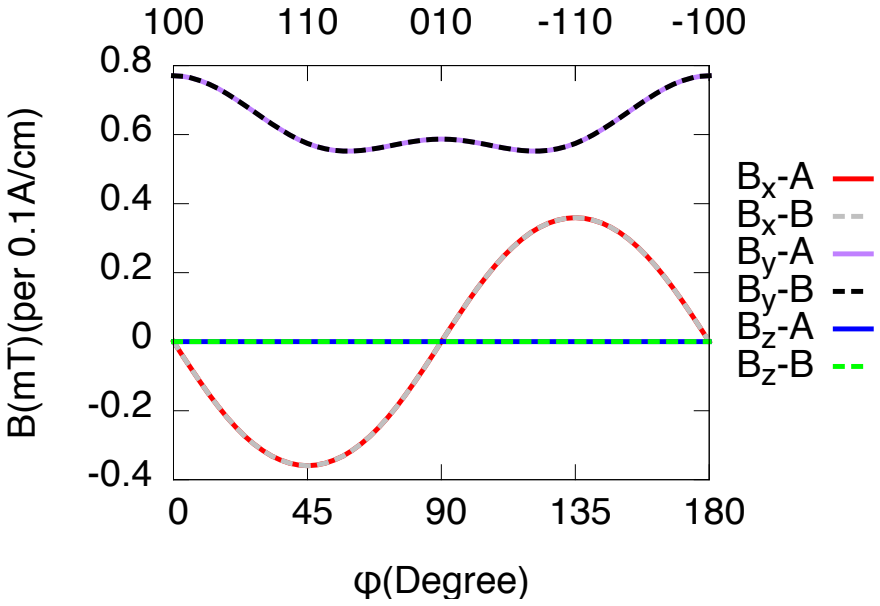

Figure 5.9: SOT projected to A and B sub lattices from the intra band contribution.

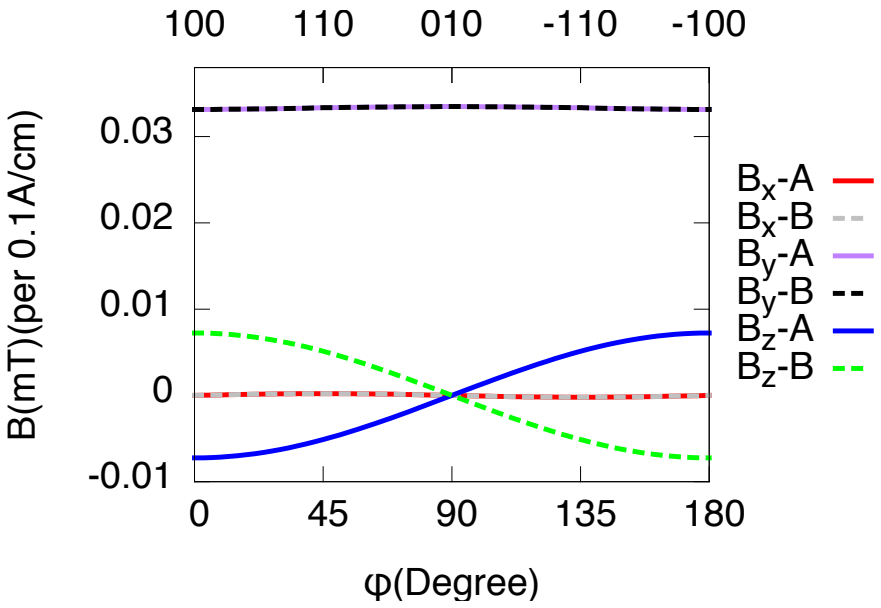

Figure 5.10: SOT projected to A and B sub lattices from the inter band contribution.

sign change following the local magnetic moments can be used to manipulate the Neel parameter which is harder to achieve by other conventional methods.

We'll study the out-of-plane inter term further here. If we change the carrier density or Fermi level, figure 5.11 (which is obtained with a Fermi energy of -2.0eV), shows that the overall angular dependence is the same, but the magnitude is much larger than the E_F=-6.0eV case. From the band resolved DoS curves, we have two peaks close to each other near $\pm 1.0eV$. We expect a great enhancement of the inter band component when the Fermi energy is approaching these regions. Figure 5.12 shows the out-of-plane inter band component for different Fermi energies. Site B has opposite sign. To have a better view of the change in magnitude, we show the same data in figure 5.13 with logarithmic y-scale. It is clearly shown that we have roughly a three order of magnitude enhancement near the singularity points.

When the sub lattice magnetization goes out-of-plane, the results will change.

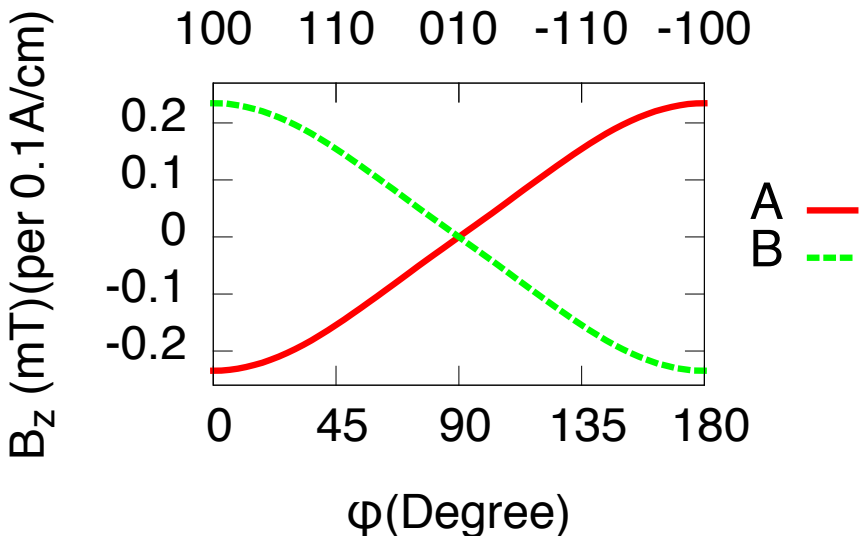

Figure 5.11: SOT projected to A and B sub lattices for the in-plane sub lattice magnetizations with $E_F = -2.0eV$.

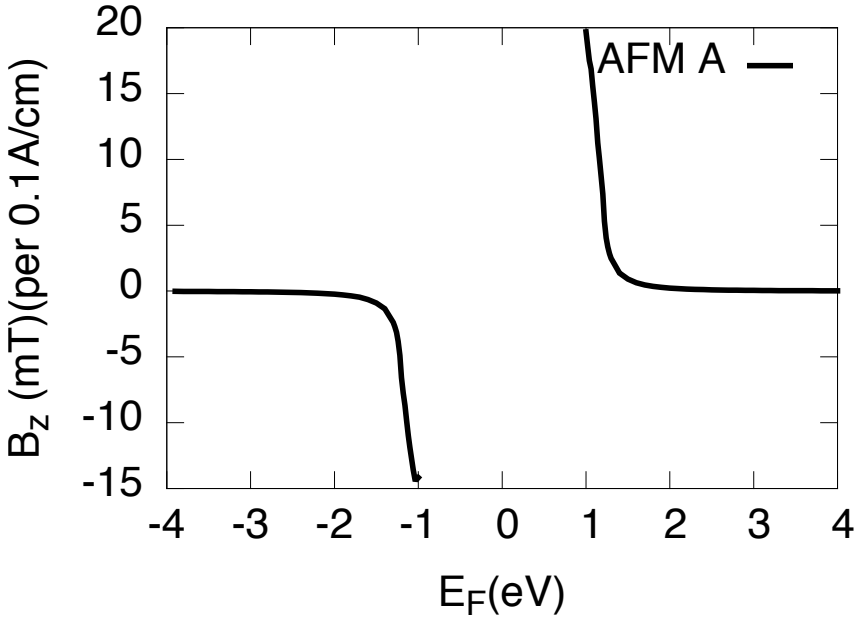

Figure 5.12: Out-of-plane inter band SOT as a function of the Fermi energy with the sub lattice magnetizations along 100 and -100 directions.

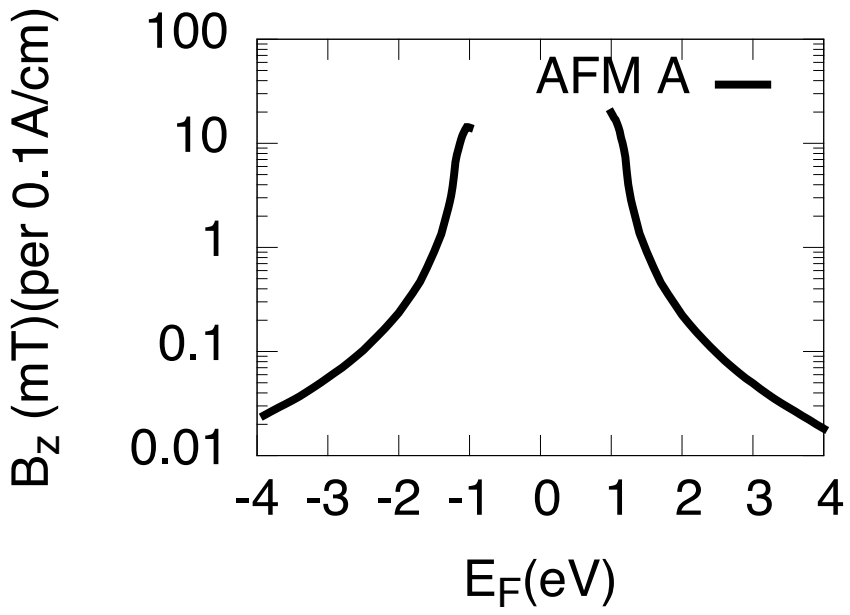

Figure 5.13: Out-of-plane inter band SOT as a function of the Fermi energy with y-axis in logarithmic scale.

Figure 5.14 and 5.15 are the results of rotating the sub lattice magnetizations along the path $(-\hat{z} \to \hat{x} \to \hat{z})$ for intra band and inter band contribution respectively. The only non-zero component from the intra band term is along y-direction. And both the x-component and z-component of the inter band term have different signs for A and B sub lattices.

5.5 Summary

This project is about current induced spin orbit torques in 2D antiferromagnetic system with broken inversion symmetry. The main results we get are i) the effective field (torque) from inter band contribution can have different signs for sub lattices which can be used to manipulate the Neel parameter, ii)when Fermi energy approaches singularity points in the DOS, we get greatly enhanced results. Symmetry

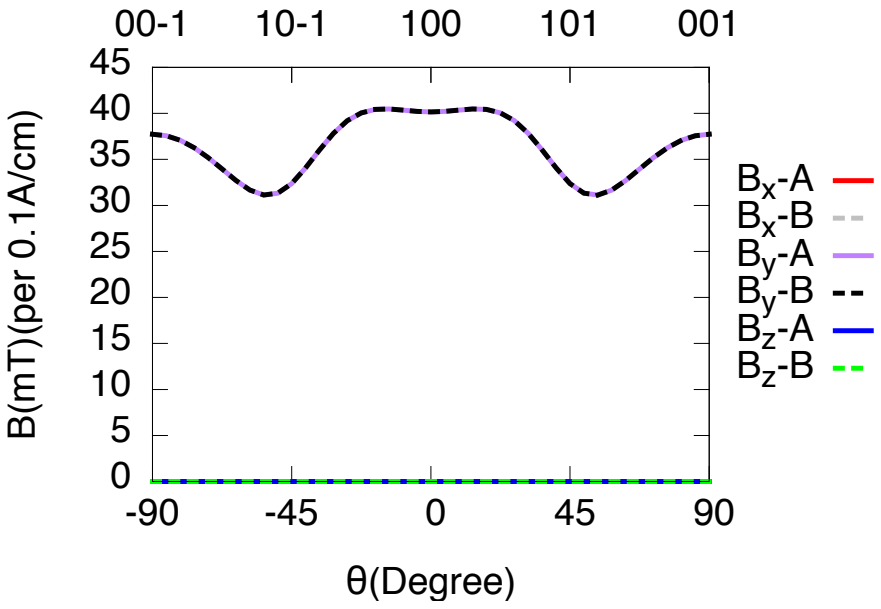

Figure 5.14: SOT projected to A and B sub lattices for the out-of-plane sub lattice magnetizations from the intra band contribution.

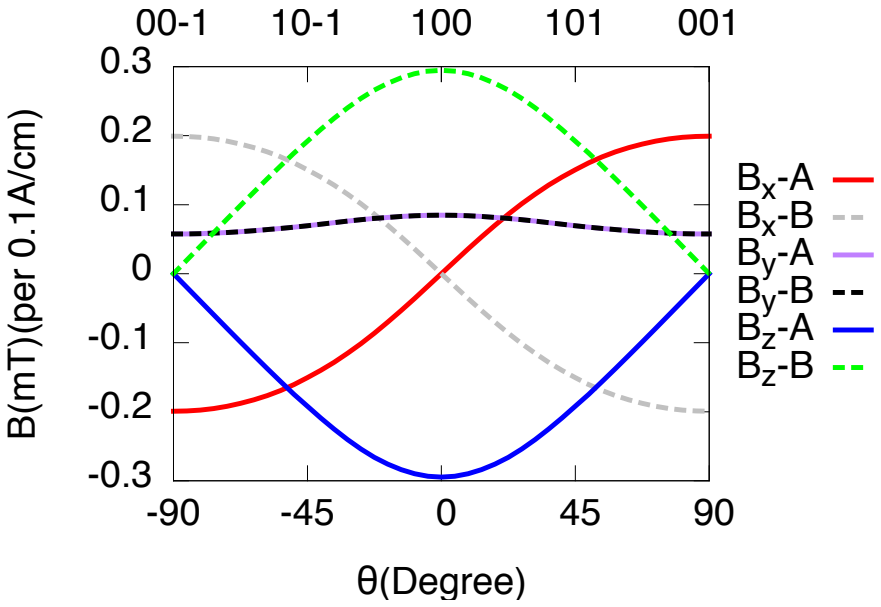

Figure 5.15: SOT projected to A and B sub lattices for the out-of-plane sub lattice magnetizations from the inter band contribution.

plays an important role here which determines the signs of different components. By only symmetry arguments, we may determine which component should be zero and which components should have the same or opposite signs. This will be our next project. Besides this model study, we are also studying this effect in the realistic material Mn_2Au. The details of this study is available in the paper by J. Zelenzy, and H. Gao [55].

6. SPIN-ORBIT TORQUES IN NON-COLLINEAR AFM $IrMn_3$

6.1 Introduction

We have studied the spin-orbit torques (SOT) in collinear antiferromagnetic systems, e.g. 2D AFM with Rashba and Mn_2Au. In this chapter we will extend the study to the non-collinear antiferromagnet $IrMn_3$ [86], which is widely used as an exchange bias in spin-valve devices. This material is also under intensive research due to its complicated magnetic structure, and other structural parameters which will affect the quality and stability of the devices. SOT effects are important in $IrMn_3$ because they can change the configuration of magnetic structures. As shown in figure 6.1, $IrMn_3$ crystal is a face-center-cubic with Mn in the face-center positions forming two kagome lattice planes perpendicular to the 111 direction [86, 87]. This structure has bulk inversion symmetry, meaning that there are no SOT effects in the bulk material. However, if we consider the $IrMn_3$ layer with structural inversion asymmetry, the spin-orbit torques will be non-zero. The dynamics of magnetization in the present of SOT is quite complicated and require further study.

6.2 Tight-binding model of $IrMn_3$

The crystal structure is shown in figure 6.1. We will use a tight-binding approach to study this material. For simplicity, only the nearest neighbors (NN) are considered. The exchange interaction is incorporated by a simple $s-d$ model. We treat the Mn spins as classical magnetic moments. There are four atoms in each unit cell, one Ir atom and three Mn atoms with different spin directions. The relative positions are chosen as:

$$\text{Ir} \qquad (0,0,0) \tag{6.1}$$

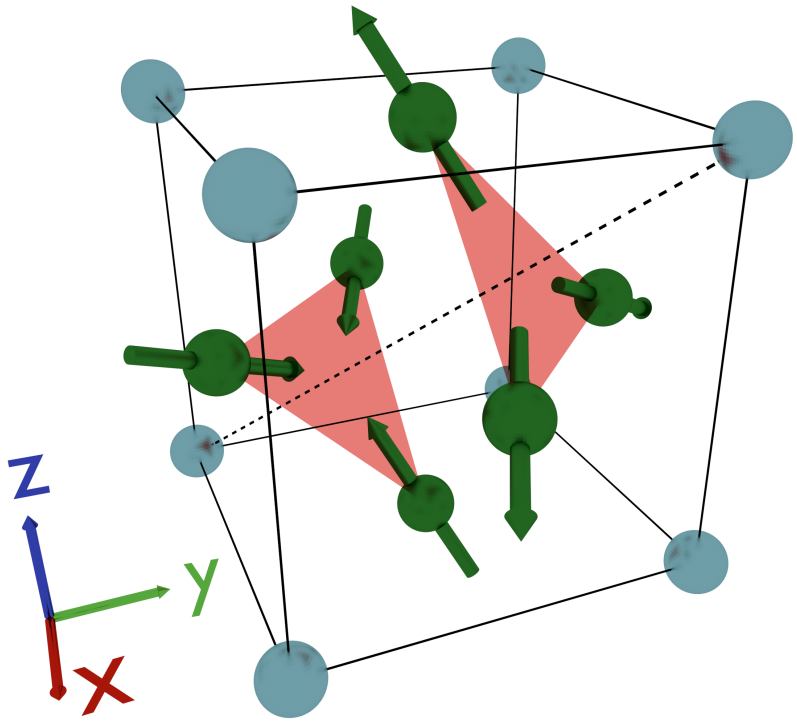

Figure 6.1: $IrMn_3$ lattice structure.

$$\begin{array}{ll} \mathrm{Mn}_A & (a/2, a/2, 0) \\ \mathrm{Mn}_B & (a/2, 0, a/2) \\ \mathrm{Mn}_C & (0, a/2, a/2). \end{array}$$

And the ground state sub lattice magnetizations are:

$$\begin{aligned} \vec{m}_A &= \frac{1}{\sqrt{6}}(-1, -1, 2) \\ \vec{m}_B &= \frac{1}{\sqrt{6}}(-1, 2, -1) \\ \vec{m}_C &= \frac{1}{\sqrt{6}}(2, -1, -1). \end{aligned} \tag{6.2}$$

For later convenience, we list all the NN for each atom in the unit cell here.

Ir-Ir:

$$\begin{array}{ll} (a, 0, 0) & (-a, 0, 0) \\ (0, a, 0) & (0, -a, 0) \\ (0, 0, a) & (0, 0, -a) \end{array} \tag{6.3}$$

Ir-Mn:

$$\begin{array}{llll} (a/2, a/2, 0) & (-a/2, a/2, 0) & (a/2, -a/2, 0) & (-a/2, -a/2, 0) \\ (a/2, 0, a/2) & (-a/2, 0, a/2) & (a/2, 0, -a/2) & (-a/2, 0, -a/2) \\ (0, a/2, a/2) & (0, -a/2, a/2) & (0, a/2, -a/2) & (0, -a/2, -a/2) \end{array} \tag{6.4}$$

Mn_A-Ir:

$$(0, 0, 0) \quad (a, 0, 0) \quad (0, a, 0) \quad (a, a, 0) \tag{6.5}$$

Mn_B-Ir:

$$(0,0,0) \quad (a,0,0) \quad (0,0,a) \quad (a,0,a) \tag{6.6}$$

Mn_C-Ir:

$$(0,0,0) \quad (0,a,0) \quad (0,0,a) \quad (0,a,a) \tag{6.7}$$

Mn_A-Mn:

$$\begin{array}{cccc} (a/2,0,a/2) & (a/2,0,-a/2) & (a/2,a,a/2) & (a/2,a,-a/2) \\ (0,a/2,a/2) & (0,a/2,-a/2) & (a,a/2,a/2) & (a,a/2,-a/2) \end{array} \tag{6.8}$$

Mn_B-Mn:

$$\begin{array}{cccc} (a/2,a/2,0) & (a/2,-a/2,0) & (a/2,a/2,a) & (a/2,-a/2,a) \\ (0,a/2,a/2) & (0,-a/2,a/2) & (a,a/2,a/2) & (a,-a/2,a/2) \end{array} \tag{6.9}$$

Mn_C-Mn:

$$\begin{array}{cccc} (a/2,a/2,0) & (-a/2,a/2,0) & (a/2,a/2,a) & (-a/2,a/2,a) \\ (a/2,0,a/2) & (-a/2,0,a/2) & (a/2,a/2,a) & (-a/2,a/2,a) \end{array} \tag{6.10}$$

Here, we need several different hopping parameters. To be simple, we assume the hopping parameters between different Mn sub lattices are the same. So, we have hopping between Ir and Ir t_1, hopping between Ir and Mn t_2, and hopping between Mn and Mn t_3. We need one more parameter to describe the onsite energy. Here

only the energy difference matters. $\Delta\epsilon = \epsilon_{Ir} - \epsilon_{Mn}$. The Hamiltonian can be written as

$$H_0 = \sum_{\alpha i\sigma\sigma'} J_{sd}\vec{S}_i \cdot (\vec{\sigma})_{\sigma\sigma'} c^\dagger_{\alpha i\sigma} c_{\alpha i\sigma'} + \sum_{\alpha i\sigma} \Delta\epsilon c^\dagger_{\alpha i\sigma} c_{\alpha i\sigma} - \sum_{\alpha\beta<ij>\sigma} t_{\alpha\beta} c^\dagger_{\alpha i\sigma} c_{\beta j\sigma}, \tag{6.11}$$

where $t_{\alpha\beta}$ are the hopping parameters, the summations over i, j in the third term are limited to nearest neighbors, and $(c^\dagger_\alpha, c_\alpha)$ denote the creation and annihilation operators of an α-kind of atom in the unit cell. Then we change to k-space by using relations

$$c_{\alpha i\sigma} = \frac{1}{\sqrt{N}} \sum_{\vec{k}} e^{i\vec{k}\cdot(\vec{R}_i + \vec{r}_\alpha)} c_{\alpha\vec{k}\sigma}, \tag{6.12}$$

where $\vec{r}_\alpha$ are the relative positions of atoms in the unit cell, and

$$\frac{1}{N} \sum_{\vec{R}_i} e^{i(\vec{k}-\vec{k}')\cdot\vec{R}_i} = \delta_{\vec{k}\vec{k}'}. \tag{6.13}$$

The first two terms in equation (6.11) are straight forward. The third term needs to be calculated carefully. We will list the results here.

Ir-Ir:

$$-t_1 \sum_{\vec{k}\sigma} 2(\cos k_x a + \cos k_y a + \cos k_z a) c^\dagger_{\mathrm{Ir}\vec{k}\sigma} c_{\mathrm{Ir}\vec{k}\sigma}. \tag{6.14}$$

Ir-Mn:

$$\begin{aligned} &-t_2 \sum_{\vec{k}\sigma} 4\cos\frac{k_x a}{2}\cos\frac{k_y a}{2} c^\dagger_{\mathrm{Ir}\vec{k}\sigma} c_{\mathrm{Mn}_A\vec{k}\sigma} \\ &-t_2 \sum_{\vec{k}\sigma} 4\cos\frac{k_x a}{2}\cos\frac{k_z a}{2} c^\dagger_{\mathrm{Ir}\vec{k}\sigma} c_{\mathrm{Mn}_B\vec{k}\sigma} \\ &-t_2 \sum_{\vec{k}\sigma} 4\cos\frac{k_y a}{2}\cos\frac{k_z a}{2} c^\dagger_{\mathrm{Ir}\vec{k}\sigma} c_{\mathrm{Mn}_C\vec{k}\sigma}. \end{aligned} \tag{6.15}$$

Mn-Ir:

$$
\begin{aligned}
&-t_2 \sum_{\vec{k}\sigma} 4 \cos \frac{k_x a}{2} \cos \frac{k_y a}{2} c^{\dagger}_{\mathrm{Mn}_A \vec{k}\sigma} c_{\mathrm{Ir}\vec{k}\sigma} \\
&-t_2 \sum_{\vec{k}\sigma} 4 \cos \frac{k_x a}{2} \cos \frac{k_z a}{2} c^{\dagger}_{\mathrm{Mn}_B \vec{k}\sigma} c_{\mathrm{Ir}\vec{k}\sigma} \\
&-t_2 \sum_{\vec{k}\sigma} 4 \cos \frac{k_y a}{2} \cos \frac{k_z a}{2} c^{\dagger}_{\mathrm{Mn}_C \vec{k}\sigma} c_{\mathrm{Ir}\vec{k}\sigma}.
\end{aligned} \tag{6.16}
$$

Mn_A-Mn:

$$
\begin{aligned}
&-t_3 \sum_{\vec{k}\sigma} 4 \cos \frac{k_y a}{2} \cos \frac{k_z a}{2} c^{\dagger}_{\mathrm{Mn}_A \vec{k}\sigma} c_{\mathrm{Mn}_B \vec{k}\sigma} \\
&-t_3 \sum_{\vec{k}\sigma} 4 \cos \frac{k_x a}{2} \cos \frac{k_z a}{2} c^{\dagger}_{\mathrm{Mn}_A \vec{k}\sigma} c_{\mathrm{Mn}_C \vec{k}\sigma}.
\end{aligned} \tag{6.17}
$$

Mn_B-Mn:

$$
\begin{aligned}
&-t_3 \sum_{\vec{k}\sigma} 4 \cos \frac{k_y a}{2} \cos \frac{k_z a}{2} c^{\dagger}_{\mathrm{Mn}_B \vec{k}\sigma} c_{\mathrm{Mn}_A \vec{k}\sigma} \\
&-t_3 \sum_{\vec{k}\sigma} 4 \cos \frac{k_x a}{2} \cos \frac{k_y a}{2} c^{\dagger}_{\mathrm{Mn}_B \vec{k}\sigma} c_{\mathrm{Mn}_C \vec{k}\sigma}.
\end{aligned} \tag{6.18}
$$

Mn_C-Mn:

$$
\begin{aligned}
&-t_3 \sum_{\vec{k}\sigma} 4 \cos \frac{k_x a}{2} \cos \frac{k_z a}{2} c^{\dagger}_{\mathrm{Mn}_C \vec{k}\sigma} c_{\mathrm{Mn}_A \vec{k}\sigma} \\
&-t_3 \sum_{\vec{k}\sigma} 4 \cos \frac{k_x a}{2} \cos \frac{k_y a}{2} c^{\dagger}_{\mathrm{Mn}_C \vec{k}\sigma} c_{\mathrm{Mn}_B \vec{k}\sigma}.
\end{aligned} \tag{6.19}
$$

By diagonalizing the Hamiltonian in k-space, we will obtain the band structures.

In order to break the inversion symmetry, we consider a Rashba type spin-orbit coupling which introduces the structural inversion asymmetry. Experimentally, the

growth direction of $L1_2$ type $IrMn_3$ is 001 direction. So, we add the spin orbit coupling within 001 plane.

$$H_{SO} = \alpha(\vec{\sigma} \times \vec{k}) \cdot \hat{z}, \tag{6.20}$$

where α is the strength of the spin-orbit coupling. In 001 plane, the lattice structure is square lattice. We can use the same $\vec{k}$ from the 3D lattice and keep only k_x, k_y. Following the same procedure as in previous notes, we write the spin-orbit coupling in the tight-binding basis. We have two terms

$$\begin{aligned}
H_{SO}^{(1)} &= V_{SO} \sum_i \{(c^\dagger_{\mathrm{Ir}i\uparrow} c_{\mathrm{Mn}_A i\downarrow} - c^\dagger_{\mathrm{Ir}i\downarrow} c_{\mathrm{Mn}_A i\uparrow}) \\
&\quad -i(c^\dagger_{\mathrm{Ir}i\uparrow} c_{\mathrm{Mn}_A i-\delta_x\downarrow} + c^\dagger_{\mathrm{Ir}i\downarrow} c_{\mathrm{Mn}_A i-\delta_x\uparrow}) \\
&\quad + (-c^\dagger_{\mathrm{Ir}i\uparrow} c_{\mathrm{Mn}_A i-\delta_x-\delta_y\downarrow} + c^\dagger_{\mathrm{Ir}i\downarrow} c_{\mathrm{Mn}_A i-\delta_x-\delta_y\uparrow}) \\
&\quad +i(c^\dagger_{\mathrm{Ir}i\uparrow} c_{\mathrm{Mn}_A i-\delta_y\downarrow} + c^\dagger_{\mathrm{Ir}i\downarrow} c_{\mathrm{Mn}_A i-\delta_y\uparrow})\} \\
&\quad +\{\mathrm{Ir} \leftrightarrow \mathrm{Mn}_A\} \\
H_{SO}^{(2)} &= V_{SO} \sum_i \{(c^\dagger_{\mathrm{Mn}_B i\uparrow} c_{\mathrm{Mn}_C i\downarrow} - c^\dagger_{\mathrm{Mn}_B i\downarrow} c_{\mathrm{Mn}_C i\uparrow}) \\
&\quad -i(c^\dagger_{\mathrm{Mn}_B i\uparrow} c_{\mathrm{Mn}_C i-\delta_y\downarrow} + c^\dagger_{\mathrm{Mn}_B i\downarrow} c_{\mathrm{Mn}_C i-\delta_y\uparrow}) \\
&\quad + (-c^\dagger_{\mathrm{Mn}_B i\uparrow} c_{\mathrm{Mn}_C i+\delta_x-\delta_y\downarrow} + c^\dagger_{\mathrm{Mn}_B i\downarrow} c_{\mathrm{Mn}_C i+\delta_x-\delta_y\uparrow}) \\
&\quad +i(c^\dagger_{\mathrm{Mn}_B i\uparrow} c_{\mathrm{Mn}_C i+\delta_x\downarrow} + c^\dagger_{\mathrm{Mn}_B i\downarrow} c_{\mathrm{Mn}_C i+\delta_x\uparrow})\} \\
&\quad +\{\mathrm{Mn}_B \leftrightarrow \mathrm{Mn}_C\}
\end{aligned} \tag{6.21}$$

Here the summation i is over 2D square lattice unit cells, $V_{SO} = \alpha/2a$, and $\leftrightarrow$ means exchanging the positions of the left and right components in the previous bracket. If we only keep k_x, k_y, we have similar orthogonal relations as in equation (6.12) and (6.13). And k_x, k_y have the same values as in the 3D case. In the 2D case, $\vec{r}_\alpha$ will be

also two dimensional.

$$\vec{r}_A = (a/2, a/2); \vec{r}_B = (a/2, 0); \vec{r}_C = (0, a/2). \tag{6.22}$$

Transforming to k space, we get

$$\begin{aligned} H_{SO}^{(1)} &= V_{SO} \sum_{\vec{k}} \{2[\sin(-\frac{k_x a}{2} + \frac{k_y a}{2}) + i \sin(\frac{k_x a}{2} + \frac{k_y a}{2})] c^{\dagger}_{\mathrm{Ir}\vec{k}\uparrow} c_{\mathrm{Mn}_A \vec{k}\downarrow} \\ &\quad + 2[\sin(-\frac{k_x a}{2} + \frac{k_y a}{2}) - i \sin(\frac{k_x a}{2} + \frac{k_y a}{2})] c^{\dagger}_{\mathrm{Ir}\vec{k}\downarrow} c_{\mathrm{Mn}_A \vec{k}\uparrow} + \mathrm{H.c.}\} \\ H_{SO}^{(2)} &= V_{SO} \sum_{\vec{k}} \{2[\sin(-\frac{k_x a}{2} - \frac{k_y a}{2}) + i \sin(-\frac{k_x a}{2} + \frac{k_y a}{2})] c^{\dagger}_{\mathrm{Mn}_B \vec{k}\uparrow} c_{\mathrm{Mn}_C \vec{k}\downarrow} \\ &\quad + 2[\sin(-\frac{k_x a}{2} - \frac{k_y a}{2}) - i \sin(-\frac{k_x a}{2} + \frac{k_y a}{2})] c^{\dagger}_{\mathrm{Mn}_B \vec{k}\downarrow} c_{\mathrm{Mn}_C \vec{k}\uparrow} + \mathrm{H.c.}\} \end{aligned} \tag{6.23}$$

These are the two terms we should include in our Hamiltonian matrix to break the inversion symmetry.

6.3 Numerical simulations

In this part, we discuss the numerical simulation details. Basically, the procedures of simulation are similar to the 2D AFM model. Since it is more complicated for $IrMn_3$, we write out the spin and velocity operators explicitly. Here we also need the sub lattice projected spin operator. Since there is no magnetic moment on the Ir sub lattice, we only consider the three Mn sub lattices which are denoted by A, B and C.

6.3.1 Spin operator

The Hamiltonian matrix is 8×8. The eigenvector has form

$$\Phi^{(\alpha)} = ((\phi^{(\alpha)}_{Ir\uparrow}, \phi^{(\alpha)}_{Ir\downarrow}), (\phi^{(\alpha)}_{A\uparrow}, \phi^{(\alpha)}_{A\downarrow}), (\phi^{(\alpha)}_{B\uparrow}, \phi^{(\alpha)}_{B\downarrow}), (\phi^{(\alpha)}_{C\uparrow}, \phi^{(\alpha)}_{C\downarrow}))^T. \tag{6.24}$$

The spin operator is simply given by

$$(\vec{s})_{\alpha\beta} = \frac{1}{2} \sum_{i=Ir,A,B,C} ((\phi^{(\alpha)}_{i\uparrow}, \phi^{(\alpha)}_{i\downarrow})^T)^\dagger (\vec{\sigma}) (\phi^{(\beta)}_{i\uparrow}, \phi^{(\beta)}_{i\downarrow})^T, \tag{6.25}$$

and the site resolved results are

$$(\vec{s})^A_{\alpha\beta} = \frac{1}{2}((\phi^{(\alpha)}_{A\uparrow}, \phi^{(\alpha)}_{A\downarrow})^T)^\dagger (\vec{\sigma}) (\phi^{(\beta)}_{A\uparrow}, \phi^{(\beta)}_{A\downarrow})^T \tag{6.26}$$

$$(\vec{s})^B_{\alpha\beta} = \frac{1}{2}((\phi^{(\alpha)}_{B\uparrow}, \phi^{(\alpha)}_{B\downarrow})^T)^\dagger (\vec{\sigma}) (\phi^{(\beta)}_{B\uparrow}, \phi^{(\beta)}_{B\downarrow})^T \tag{6.27}$$

$$(\vec{s})^C_{\alpha\beta} = \frac{1}{2}((\phi^{(\alpha)}_{C\uparrow}, \phi^{(\alpha)}_{C\downarrow})^T)^\dagger (\vec{\sigma}) (\phi^{(\beta)}_{C\uparrow}, \phi^{(\beta)}_{C\downarrow})^T. \tag{6.28}$$

We only list the projected results on sites with magnetic moments. These results are $\vec{k}$ dependent, and in the last step we sum or integrate over the first Brillouin zone.

6.3.2 Velocity operator

The velocity operator can be obtained by calculating the k-derivatives of the Hamiltonian matrix, or by computing the commutator between the displacement operator and Hamiltonian following Mahan's textbook [56]. The velocity operator can be written as

$$\vec{v} = -\frac{1}{i\hbar} \sum_{\alpha\beta<ij>\sigma} t_{\alpha\beta}(\vec{R}_i - \vec{R}_j) c^\dagger_{\alpha i\sigma} c_{\beta j\sigma}, \tag{6.29}$$

where $\vec{R}_i$ denote the lattice vectors, and we only consider nearest neighbors here. By transforming to k space, we will obtain the same results as direct k-derivatives of the Hamiltonian matrix. The results can be easily read off from the Hamiltonian. We don't list them here.

After adding spin orbit coupling, there is another term we should include. Following same procedure in the 2D AFM notes, we have

$$\begin{aligned} v_x^R &= \frac{i2aV_{SO}}{\hbar}\sum_{\vec{k}}(c^\dagger_{\mathrm{Ir}\vec{k}\uparrow}c_{\mathrm{Ir}\vec{k}\downarrow}+c^\dagger_{\mathrm{Mn}_A\vec{k}\uparrow}c_{\mathrm{Mn}_A\vec{k}\downarrow})+\mathrm{H.c} \\ &+\frac{i2aV_{SO}}{\hbar}\sum_{\vec{k}}(c^\dagger_{\mathrm{Mn}_B\vec{k}\uparrow}c_{\mathrm{Mn}_B\vec{k}\downarrow}+c^\dagger_{\mathrm{Mn}_C\vec{k}\uparrow}c_{\mathrm{Mn}_C\vec{k}\downarrow})+\mathrm{H.c} \end{aligned} \tag{6.30}$$

$$\begin{aligned} v_y^R &= \frac{2aV_{SO}}{\hbar}\sum_{\vec{k}}(c^\dagger_{\mathrm{Ir}\vec{k}\uparrow}c_{\mathrm{Ir}\vec{k}\downarrow}+c^\dagger_{\mathrm{Mn}_A\vec{k}\uparrow}c_{\mathrm{Mn}_A\vec{k}\downarrow})+\mathrm{H.c} \\ &+\frac{2aV_{SO}}{\hbar}\sum_{\vec{k}}(c^\dagger_{\mathrm{Mn}_B\vec{k}\uparrow}c_{\mathrm{Mn}_B\vec{k}\downarrow}+c^\dagger_{\mathrm{Mn}_C\vec{k}\uparrow}c_{\mathrm{Mn}_C\vec{k}\downarrow})+\mathrm{H.c} \end{aligned} \tag{6.31}$$

and

$$v_z^R = 0. \tag{6.32}$$

6.4 Results and discussion

By diagonalizing the Hamiltonian, we are able to calculate the SOT effective fields. The results are hard to show because of the complicated magnetic structure. We show a sample calculation here with underlying magnetic structure as the equilibrium configuration. Figure 6.2 shows the results for the projected effective magnetic fields on different sub lattices. Blue arrows show the intra band contributions and green arrows show the inter band contributions. The actual lengths of the arrows do not represent the magnitude of the effective fields. Inter band contributions are

overall one order of magnitude smaller than the intra band contributions. Our results confirm that structure inversion asymmetry gives rise to nonzero SOT effects, which enable us to manipulate the magnetic structures using electric current. Further study involves the parameter dependence and magnetization dynamics which will be studied later.

6.5 Summary

We have simulated the SOT effects in $IrMn_3$ non-collinear antiferromagnet using tight-binding approach. Rashba type spin-orbit coupling is added to break the inversion symmetry. The nonzero results of SOT show that electric currents have effects on the magnetic structure. Later study of this project includes the magnetization dynamics in the presence of SOT. Once the dynamics is known, we can extract the information of magnetization changes and compare with experiments.

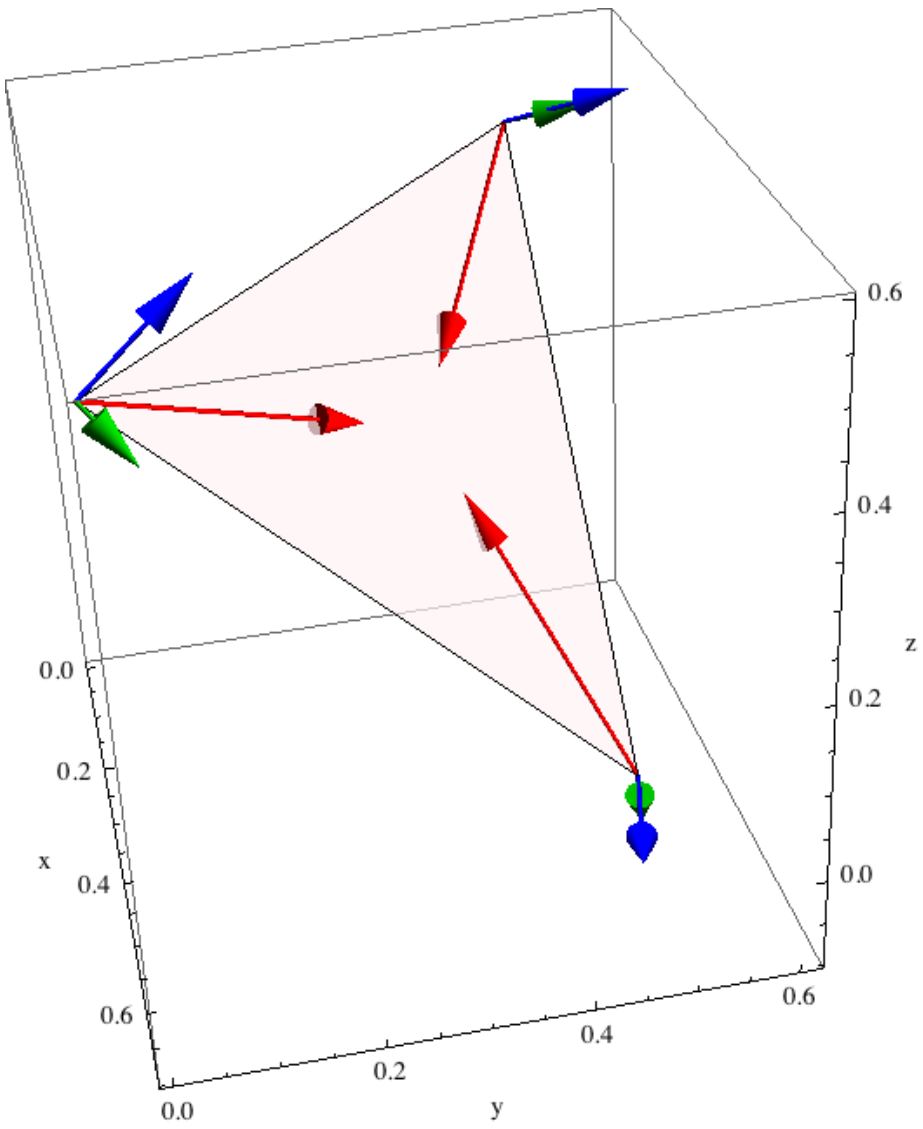

Figure 6.2: Projected SOT effective fields from the intra and inter band contributions. Red arrows denote the sub lattice magnetization directions, blue and green arrows denote the intra and inter band SOT respectively.

7. CONCLUSIONS

In this report, we study the SOT effects in ferromagnets systematically to understand the underlying physics, symmetry, parameter dependence, as well as these effects in collinear and non-collinear antiferromagnets. The methods we use include the tight-binding electronic structure calculation, the $\vec{k}\cdot\vec{p}$ band structure calculation, and the Kubo linear response formula.

In ferromagnets, the SOT effects are easier to understand. From the simple 2D ferromagnetic model, we can analytically study the symmetry and the parameter dependence. Intra band contribution is inverse proportion to the disorder broadening, while inter band is proportion to this parameter. A special intrinsic component exists for the inter band term which is independent of disorder broadening. In the study of the more realistic material $Ga_{1-x}Mn_xAs$, we see the same parameter dependence which indicates the nature of these torques. The complex band structures of $Ga_{1-x}Mn_xAs$ add higher harmonics in the magnetization dependence of SOT and change the overall magnitude, which show the competition of the different symmetry and asymmetry terms in the Hamiltonian.

Comparing with the ferromagnets, SOT in antiferromagnets are more complicated and interesting. We need to project the non-equilibrium spin density onto sub lattices to study the effects of SOT on the magnetic orders. An interesting result is that a lateral electrical current in antiferromagnets can induce non-equilibrium Neel-order fields, i.e., fields whose sign alternates between the spin sub lattice, which can trigger ultrafast spin-axis reorientation. In the 2D AFM model, due to the 2D nature, the spin-orbit torques can have very large magnitudes if we tune the Fermi energy to certain level. The study of 3D non collinear antiferromagnet $IrMn_3$ show that SOT

can exist in this material and may play important role in the magnetization dynamics.

All of our simulations assume a static magnetic configuration. We can easily generalize SOT to the study of magnetization dynamics if we know the equation governing the dynamics, e.g. LLG equation in ferromagnets. This is a very interesting project because the results from dynamics study can be compared with experimental observations directly. However, the magnetization dynamics in complex AFM (for example $IrMn_3$) is very complicated. This area is still under intensive research.

To conclude, our results provide us a nonvolatile approach of manipulating the magnetic orders in the spin-based devices, which is the future trend in the novel memory devices. The parameter dependence studies enable us to optimize these devices using doping control and structural design. Compared with the ferromagnetic material based devices, SOT effects make the antiferromagnetic material based devices even better candidates with faster spin switching, lower switching current density, and better stability in the presence of external magnetic fields. In addition to these future applications, SOT effects are also important for unveiling the rich underlying physics and symmetry of various complex electric magnetic coupled systems.

REFERENCES

[1] Igor Zutic, Jaroslav Fabian, S. Das Sarma, Rev. Mod. Phys. **76,** 323 (2014).

[2] S. Blundell, *Magnetism in Condensed Matter* (Oxford University Press, New York, 2001).

[3] Eugen Merzbacher, *Quantum Mechanics*, 3rd Ed. (John Wiley & Sons, New York, 1998).

[4] J. J. Sakurai, *Modern Quantum Mechanics, Revised Edition* (Addison-Wesley, Massachusetts, 1993).

[5] Albert Fert, Rev. Mod. Phys. **80,** 1517 (2008).

[6] M. N. Baibich, J. M. Broto, A. Fert, F. Nguyen Van Dau, F. Petroff et al., Phys. Rev. Lett. **61,** 2472 (1988).

[7] C. Chappert, A. Fert, and F. N. V. Dau, Nat. Mater. **6,** 813 (2007).

[8] J. Slonczewski, J. Magn. Magn. Mater. **159,** L1 (1996).

[9] L. Berger, Phys. Rev. B **54,** 9353 (1996).

[10] E. B. Myers, D. C. Ralph, J. A. Katine, R. N. Louie, and R. A. Buhrman, Science **285,** 867 (1999).

[11] J. Z. Sun, Phys. Rev. B **62,** 570 (2000).

[12] D. Ralph, M. Stiles and S. Bader, J. Magn. Magn. Mater. **320,** 1189 (2008).

[13] E. V. Gomonay, and V. M. Loktev, Low Temp. Phys. **40,** 17 (2014).

[14] B. A. Bernevig, and O. Vafek, Phys. Rev. B **72,** 033203 (2005).

[15] K. Obata, and G. Tatara, Phys. Rev. B **77,** 214429 (2008).

[16] E. van der Bijl, and R. A. Duine, Phys. Rev. B **86,** 094406 (2012).

[17] H. Li, X. Wang, F. Dogan, and A. Manchon, Appl. Phys. Lett. **102,** 192411 (2013).

[18] I. M. Miron, Kevin Garello, Gilles Gaudin, Pierre-Jean Zermatten, Marius V. Costache et al., Nature **476,** 189 (2011).

[19] L. Liu, Chi-Feng Pai, Y. Li, H. W. Tseng, D. C. Ralph and R. A. Buhrman, Science **336,** 555 (2012).

[20] L. D. Landau and E. M. Lifshitz, Phys. Z. Sowjetunion, **8,** 153 (1935).

[21] T. L. Gilbert, IEEE Trans. Mag. **40** (6): 3443-3449 (2004).

[22] Arne Brataas, Andrew D. Kent and Hideo Ohno, Nat. Mater. **11,** 372 (2012).

[23] A. Brataas, Y. Tserkovnyak, and G. E. Bauer, Phys. Rev. Lett. **101,** 037207 (2008).

[24] A. A. Starikov, P. J. Kelly, A. Brataas, Y. Tserkovnyak, and G. E. Bauer, Phys. Rev. Lett. **105,** 236601 (2010).

[25] V. M. Edelstein, Solid State Commun. **73,** 233 (1990).

[26] V. V. Belkov and S. D. Ganichev, Semicond. Sci. Technol. **23,** 114003 (2008).

[27] K. -W. Kim, S. -M. Seo et al., Phys. Rev. B **85,** 180404(R) (2012).

[28] D. A. Pesin and A. H. MacDonald, Phys. Rev. B **86,** 014416 (2012).

[29] X. Wang, and A. Manchon, Phys. Rev. Lett. **108,** 117201 (2012).

[30] A. Manchon and S. Zhang, Phys. Rev. B **78,** 212405 (2008).

[31] A. Manchon and S. Zhang, Phys. Rev. B **79,** 094422 (2009).

[32] I. Garate and A. H. MacDonald, Phys. Rev. B **80,** 134403 (2009).

[33] D. Fang, H. Kurebayashi, J. Wunderlich, K. Vyborny, L. P. Zarbo et al., Nat. Nanotech. **6,** 413 (2011).

[34] H. Kurebayashi, J. Sinova, D. Fang, A. C. Irvine, J. Wunderlich et al., Nat. Nanotech. **9,** 211 (2014).

[35] Jairo Sinova, Dimitrie Culcer, Q. Niu, N. A. Sinitsyn, T. Jungwirth, and A. H. MacDonald, Phys. Rev. Lett. **92,** 126603 (2004).

[36] S. Murakami, M. Nagaosa, and S. -C. Zhang, Science **301,** 1348 (2003).

[37] Y. K. Kato, R. C. Myers, A. C. Gossard, and D. D. Awschalom, Science **306,** 1910 (2004).

[38] J. Wunderlich, B. Kaestner, J. Sinova, T. Jungwirth, Phys. Rev. Lett. **94,** 047204 (2005).

[39] P. M. Haney, H. W. Lee, K. -J. Lee, A. Manchon, and M. D. Stiles, Phys. Rev. B **87,** 174411 (2013).

[40] A. Chernyshov, M. Overby, X. Liu, J. K. Furdyna, Y. Lyanda-Geller, and L. P. Pokhinson, Nat. Phys. **5,** 656 (2009).

[41] M. Endo, F. Matsukura, and H. Ohno, Appl. Phys. Lett. **97,** 222501 (2010).

[42] I. M. Miron, G. Gaudin, S. Auffret, B. Rodmacq, A. Schuhl et al., Nat. Mater. **9,** 230 (2010).

[43] L. Liu, O. J. Lee, T. J. Gudmundsen, D. C. Ralph, and R. A. Buhrman, Phys. Rev. Lett. **109,** 096602 (2012).

[44] J. Kim, J. Sinha, M. Hayashi, M. Yamanouchi, S. Fukami et al., Nat. Mater. **12,** 240 (2013).

[45] K. Garello, I. M. Mron, C. O. Avci, F. Freimuth, Y. Mokrousov et al., Nat. Nanotechnol. **8,** 587 (2013).

[46] C. O. Avci, K. Garello, M. Gabureac, A. Ghosh, A. Fuhrer et al., Phys. Rev. B **90,** 224427 (2014).

[47] X. Fan, J. Wu, Y. Chen, M. J. Jerry, H. Zhang, and J. Q. Xiao, Nat. Commun. **4,** 1799 (2013).

[48] M. Jamali, K. Narayanapillai, X. Qiu, L. M. Loong, A. Manchon, and H. Yang, Phys. Rev. Lett. **111,** 246602 (2013).

[49] H. -R. Lee, K. Lee, J. Cho, Y. -H. Choi, C. -Y. You, M, -H, Jung. F. Bonell et al., Sci. Rep. **4,** 6548 (2014).

[50] A. R. Mellnik, J. S. Lee, A. Richardella. J. L. Grab, P. J. Mintun et al., Nature **511,** 449 (2014).

[51] Y. Fan, P. Upadhyaya, X. Kou, M. Lang, S. Takei,Z. Wang et al., Nat. Mater. **13,** 699 (2014).

[52] G. Dresselhaus, Phys. Rev. **100**(2), 580 (1955).

[53] E. I. Rashba, Sov. Phys. Solid State **1,** 368 (1959).

[54] Hang Li, H. Gao, Liviu P. Zarbo, K. Vyborny, Xuhui Wang et al., Phys. Rev. B **91,** 134402 (2015).

[55] J. Zelezny, H. Gao, K. Vyborny, J. Zemen. J. Masek, et al., Phys. Rev. Lett. **113,** 157201 (2014).

[56] Gerald D. Mahan, *Many-Particle Phsics*, 3rd Ed. (Kluwer Academic/Plenum, New York, 2000).

[57] Michael P. Marder, *Condensed Matter Physics*, 2nd Ed. (John Wiley & Sons, New York, 2010).

[58] Giuseppe Grosso and Giuseppe Pastori Parravicini, *Solid State Physics* (Academic Press, San Diego, California, 2000).

[59] L. P. Zarbo, K. Vyborny, Ion Garate, E. K. Vehstedt, A. Cejchan et. al, unpublished.

[60] Peter Y. Yu, Manuel Cardona, *Fundamentals of Semiconductors, Physics and Materials Properties*, 4th Ed. (Springer-Verlag, Berlin, Heidelberg, 2010).

[61] Weng W. Chow, Stephan W. Koch, *Semiconductor-Laser Fundamentals, Physics of the Gain Materials* (Springer-Verlag, Berlin, Heidelberg, 1999).

[62] T. Jungwirth, Jairo Sinova, J. Mesek, J. Kucera and A. H. MacDonald, Rev. Mod. Phys. **78,** 809 (2006).

[63] M. Silver, W. Batty, A. Ghiti, and E. P. OReilly, Physica B **46,** 6781 (1992).

[64] R. Winkler, *Spin-Orbit Coupling Effects in Two-Dimensional Electron and Hole Systems* (Springer-Verlag, Berlin, Heidelberg, 2010).

[65] Lok C. Lew Yan Voon, Morten Willatzen, *The k·p Method, Electronics Properties of Semiconductors* (Springer-Verlag, Berlin, Heidelberg, 2010).

[66] J. M. Luttinger and W. Kohn, Phys. Rev. **97,** 869 (1955).

[67] J. M. Luttinger, Phys. Rev. **102,** 1030 (1956).

[68] M. Abolfath, T. Jungwirth, J. Brum, and A. H. MacDonald, Phys. Rev. B **63,** 054418 (2001).

[69] S. -R. Eric Yang, J. Sinova, T. Jungwirth, Y. P. Shim, and A. H. MacDonald, Phys. Rev. B **67,** 045205 (2003).

[70] M. Birowska, C. Sliwa, J. A. Majewski, and T. Dietl, Phys. Rev. Lett. **108,** 237203 (2012).

[71] G. L. Bir and G. E. Pikus, *Symmetry and Strain-Induced Effects in Semiconductors* (John Wiley & Sons, New York, 1974).

[72] Y. A. Bychkov and E. I. Rashba, J. Phys. C: Solid State Phys. **17,** 6039 (1984).

[73] I. V. Shvets, A. N. Grigorenko, K. S. Novoselov, and D. J. Mapps, Appl. Phys. Lett. **86,** 212501 (2005).

[74] B. G. Park, J. Wunderlich, X. Marti, V. Holy, Y. Kurosaki, M. Yamada et al., Nat. Mater. **10,** 347 (2011).

[75] I. Fina, X. Marti, D. Yi, J. Liu, J. H. Chu, C. Rayan-Serrao et al., Nat. Commun. **5,** 4671 (2014).

[76] X. Marti, I. Fina, C. Frontera, Jian Liu, P. Wadley, Q. He et al., Nat. Mater. **13,** 367 (2014).

[77] H. Wu, Z. -M. Liao, R. G. Sumesh Sofin, G. Feng, X. -M. Ma, A. B. Shick et al., Adv. Mater. **24,** 6374 (2012).

[78] V. M. T. S. Barthem, C. V. Colin, H. Mayaffre, M. Julien, and D. Givord, Nat. Commun. **4,** 2892 (2013).

[79] A. S. Sunez, R. A. Duine, P. Haney, and A. H. MacDonald, Phys. Rev. B **73,** 214426 (2006).

[80] A. B. Shick, S. Khmelevskyi, O. N. Mryasov, J.Wunderlich, and T. Jungwirth, Phys. Rev. B **81,** 212409 (2010).

[81] T. Jungwirth, V. Novak, X. Marti, M. Cukr, F. Maca et al., Phys. Rev. B **83,** 035321 (2011).

[82] Kjetil M. D. Hals, Yaroslav Tserkovnyak, and Arne Brataas, Phys. Rev. Lett. **106,** 107206 (2011).

[83] E. Fullerton, S. Maat, and J. U. Thiele, U.S. patent No. 20050281081 (2005).

[84] B. Dieny, R. C. Sousa, J. Herault, C. Papusoi, G. Prenat, U. Ebels et al., Int. J. Nanotechnology **7,** 591 (2010).

[85] L. Sheng, D. N. Sheng, and C. S. Ting, Phys. Rev. Lett. **94,** 016602 (2005).

[86] A. Kohn, A. Kovacs et el., Sci. Rep. **3,** 2412 (2013).

[87] Hua Chen, Qian Niu, and A. H. MacDonald, Phys. Rev. Lett. **112,** 017205 (2014).

APPENDIX A

EQUIVALENCE BETWEEN KUBO AND GRGA-GRGR

The Green's function formula is

$$\delta\vec{s} = \frac{\hbar}{2\pi L^2}\mathrm{Re}\sum_{\vec{k}a,b}(\vec{s})_{ab}(e\vec{E}\cdot\vec{v})_{ba}[G^A_{\vec{k}a}G^R_{\vec{k}b} - G^R_{\vec{k}a}G^R_{\vec{k}b}], \tag{1}$$

where the Green's functions are $G^R_{\vec{k}\alpha}(E)|_{E=E_F} \equiv G^R_{\vec{k}\alpha} = 1/(E_F - E_{\vec{k}\alpha} + i\Gamma)$, with the property $G^A = (G^R)^*$. Here, L is the dimension of the 2D sample, e is the charge of electrons (negative), and Γ is the spectral broadening. For small Γ, we have Kubo formula for intra band contribution

$$\delta\vec{s}^{intra} = \frac{1}{L^2}\sum_{\vec{k}a}\frac{\hbar}{2\Gamma}(\vec{s})_{\vec{k}a}(e\vec{E}\cdot\vec{v})_{\vec{k}a}\delta(E_{\vec{k}a} - E_F). \tag{2}$$

And inter band contribution is given by two terms

$$\delta\vec{s}^{inter} = \delta\vec{s}^{(1)} + \delta\vec{s}^{(2)}, \tag{3}$$

with

$$\begin{aligned}
\delta\vec{s}^{(1)} &= -\frac{\hbar}{L^2}\sum_{\vec{k}a\neq b} 2\mathrm{Re}[(\vec{s})_{ab}(e\vec{E}\cdot\vec{v})_{ba}]\frac{\Gamma(E_{\vec{k}a} - E_{\vec{k}b})}{[(E_{\vec{k}a} - E_{\vec{k}b})^2 + \Gamma^2]^2}(f_{\vec{k}a} - f_{\vec{k}b}) \\
\delta\vec{s}^{(2)} &= -\frac{\hbar}{L^2}\sum_{\vec{k}a\neq b} \mathrm{Im}[(\vec{s})_{ab}(e\vec{E}\cdot\vec{v})_{ba}]\frac{\Gamma^2 - (E_{\vec{k}a} - E_{\vec{k}b})^2}{[(E_{\vec{k}a} - E_{\vec{k}b})^2 + \Gamma^2]^2}(f_{\vec{k}a} - f_{\vec{k}b}).
\end{aligned} \tag{4}$$

We compare these two sets of formulae numerically in the 2D FM system with the parabolic band description of the kinetic term ($\frac{\hbar^2}{2m^*} = 3.0eV, J_{sd} = 1.0eV, V_{SO} =$

$0.1eV$). Figure A.1, A.2, A.3 show that these two sets of formulae match quite well at small Γ.

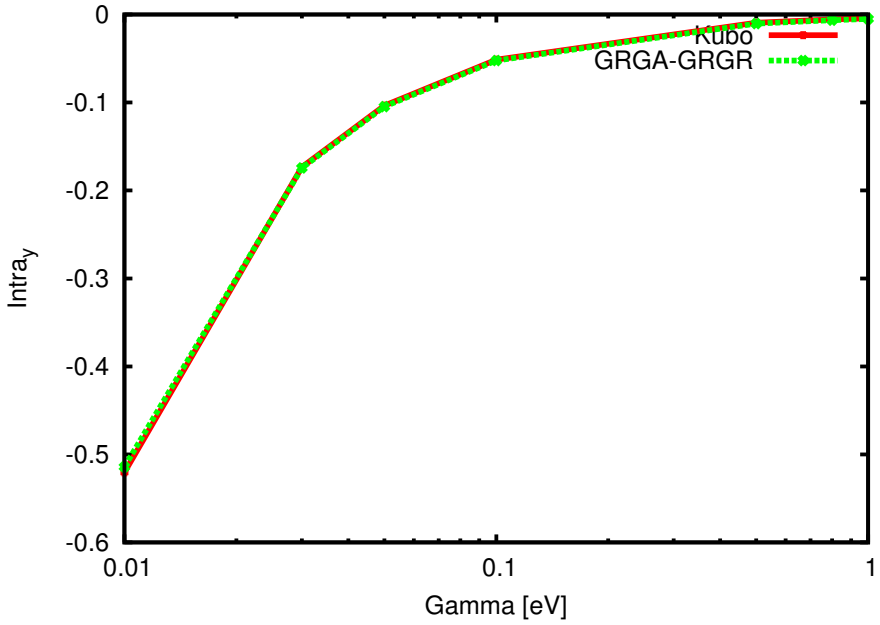

Figure A.1: y component of the intra band SOT.

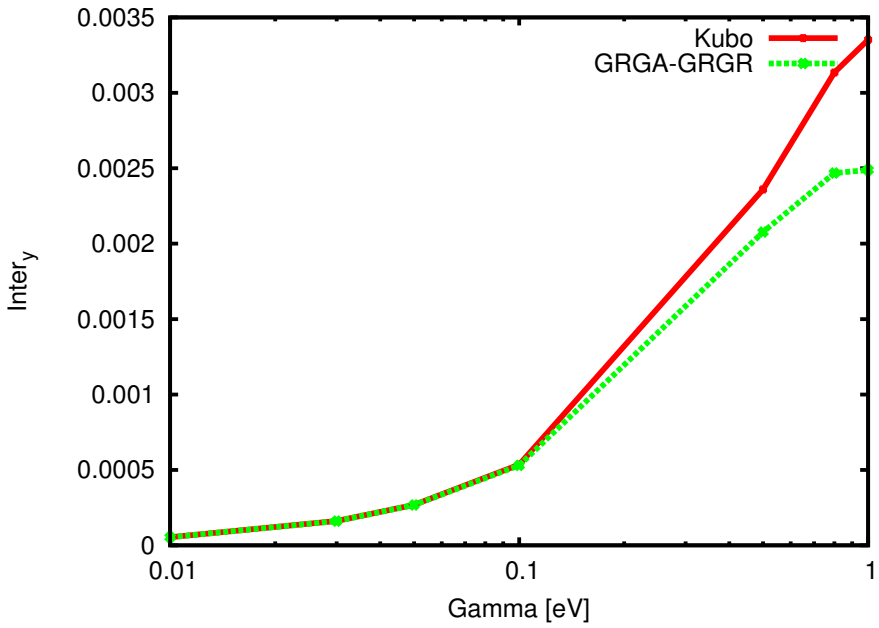

Figure A.2: y component of the inter band SOT.

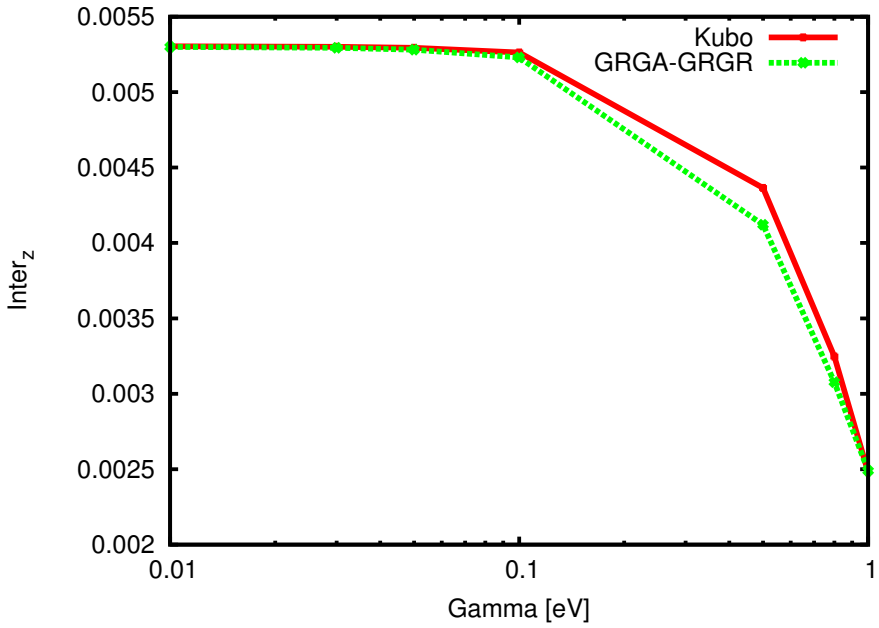

Figure A.3: z component of the inter band SOT.

APPENDIX B

RASHBA SPIN-ORBIT COUPLING IN SECOND QUANTIZATION

Rashba spin-orbit coupling is given by

$$H_R = \frac{\alpha}{\hbar}(\sigma_x p_y - \sigma_y p_x) \tag{5}$$

or

$$H_R = \alpha(\sigma_x k_y - \sigma_y k_x) \tag{6}$$

where α is the strength of the Rashba spin-orbit coupling. In second quantization we have

$$H_R = \int d^2x(-i\alpha)\psi^\dagger(\sigma_x\partial_y - \sigma_y\partial_x)\psi. \tag{7}$$

Transforming to the atomic-like basis using

$$\begin{aligned} \psi(\vec{r}) &= \sum_{i\sigma} w_\sigma(\vec{r} - \vec{R}_i)c_{i\sigma} \\ \psi^\dagger(\vec{r}) &= \sum_{i\sigma} w^*_\sigma(\vec{r} - \vec{R}_i)c^\dagger_{i\sigma}, \end{aligned} \tag{8}$$

where σ is spin index. We replace the derivative by the difference

$$\partial_x w_\sigma(\vec{r}) = \frac{w_\sigma(\vec{r} + \vec{\delta_x}) - w_\sigma(\vec{r} - \vec{\delta_x})}{2a}; \tag{9}$$

$$\partial_y w_\sigma(\vec{r}) = \frac{w_\sigma(\vec{r} + \vec{\delta_y}) - w_\sigma(\vec{r} - \vec{\delta_y})}{2a}. \tag{10}$$

For the nearest neighbor approximation, we have

$$\begin{aligned} H_R &= -i\alpha \int d^2x \sum_{ij\sigma\sigma'} [w^*_\sigma(\vec{r}-\vec{R}_i)c^\dagger_{i\sigma}(\sigma_x\partial_y)w_{\sigma'}(\vec{r}-\vec{R}_i)c_{j\sigma'} \\ &\quad -w^*_\sigma(\vec{r}-\vec{R}_i)c^\dagger_{i\sigma}(\sigma_y\partial_x)w_{\sigma'}(\vec{r}-\vec{R}_i)c_{j\sigma'}] \\ &= \frac{-i\alpha}{2a}\sum_{ij\sigma\sigma'}\int d^2x\{w^*_\sigma(\vec{r}-\vec{R}_i)(\sigma_x)[w_{\sigma'}(\vec{r}-\vec{R}_i+\vec{\delta_y})-w_{\sigma'}(\vec{r}-\vec{R}_i-\vec{\delta_y})]c^\dagger_{i\sigma}c_{j\sigma'} \\ &\quad -w^*_\sigma(\vec{r}-\vec{R}_i)(\sigma_y)[w_{\sigma'}(\vec{r}-\vec{R}_i+\vec{\delta_x})-w_{\sigma'}(\vec{r}-\vec{R}_i-\vec{\delta_x})]c^\dagger_{i\sigma}c_{j\sigma'}\} \end{aligned} \tag{11}$$

Using the orthogonal relation of the basis, we get the results

$$H_R = \frac{\alpha}{2a}\sum_i[(c^\dagger_{i\uparrow}c_{i+\delta_x\downarrow}-c^\dagger_{i\downarrow}c_{i+\delta_x\uparrow})-i(c^\dagger_{i\uparrow}c_{i+\delta_y\downarrow}+c^\dagger_{i\downarrow}c_{i+\delta_y\uparrow})+\text{H.c.}]. \tag{12}$$

And $V_{SO} = \alpha/2a$ in the previous formula.